# Authors Response to Reviewer 1 comments

The Authors present an extensive work (reinforced by experimental data) aimed to assess the operational use of the Soil Plant Atmosphere and Remote Sensing Evapotraspiration (SPARSE) model and its accuracy by a comparison to the Scintillometric technique. I think that Authors address relevant scientific questions within the scope of HESS. Furthermore the paper is generally well organized and well written and there-fore the paper could be taken into account for the final publication after a moderate revision. Particularly, The Authors should improve the part of "Results and discussion" (pag. 16-20) with a better description of the validation of SPARSE model carried out with by comparing H and AE estimations with flux station and XLAS scintillometer (see comments n 7, 11 and 12). My comments and questions are as follow:

1. Lines 33-44: The Authors corroborated "the good correspondence between instantaneous H estimates and large aperture scintillometer H measurements" reporting RMSE values expressed in W m-2. As stated by the Authors (Line 418) "For hydrological applications, daily ET is usually required: : :." and in my opinion this means that for hydrological purposes the accuracy of daily evapotranspiration should be expressed in millimeters for day (mmd-1). Therefore in the abstract and through the paper this aspect should be considered and also critically analyzed. From my calculations the accuracy obtained by SPARSE model application should be around 1.6 mmd-1. Is this value "acceptable" ?

*Response:*

*Indeed, we agree with Reviewer 1 that for hydrological purposes the accuracy of daily evapotranspiration (ET) should be expressed in millimeters per day, however, the RMSE values mentioned in the abstract and throughout the paper are instantaneous sensible and latent heat fluxes estimates at the satellite overpass time and are not daily values, therefore, they are expressed in W.m-2. Since, they are instantaneous data, it should not be converted using this formula:*
*47.2 W.m-2*0.0864/2.45= 1.66 mm/day*
*43.2 W.m-2*0.0864/2.45= 1.52 mm/day*
*Therefore, we get an instantaneous LE error of about 0.1 mm/0.5.hour around the satellite overpass (around midday, at the max. ET rate)*
*In the revised version of the manuscript (section 6.4), when dealing with daily ET, all values are expressed in mm.day$^{-1}$; following the reviewer's suggestion, we added the model daily ET estimates accuracy (RMSE= 0.7 mm/day) similarly to what as been done for instantaneous results.*

2. Lines 87-88: Is "irrigation requirements" (generally expressed in mmd-1) a prerogative only "of RS-based SWB models" ? Please, clarify.

*Response:*

*Irrigation requirements are mainly estimated using RS-based SWB models, since irrigation is a component of the water balance equation on which is based SWB models. Indeed, the*

*crop coefficient method (FAO56 method) is currently the main method used for scheduling irrigations around the world (Glenn et al., 2007).*
*Irrigation requirement was rarely directly estimated using SEB models. Indeed, SEB outputs are generally actual evapotranspiration (its energy equivalent LE) and if Irrigation is estimated, it should be computed as a residual term of the water balance equation. Exception exists, for example, (Courault et al., 1998) used surface temperature derived from NOAA data and a SVAT model called MAGRET to find parameters linked to the irrigation over the agricultural region "la Crau" in South-Eastern France ; the predicted parameters were the beginning and the end of irrigation, frequency and water quantity diverted.*

3. Line 108: ": : :at the beginning of the process". Please clarify.

*Response:*

*This was corrected before review, and we did not find this expression in line 108 of the last article manuscript version "hess-2017-454-manuscript-version3_discussion" to which we refer. Indeed, in this last version, the mentioned sentence was written as follows: "at the beginning of the dry down".*

4. Lines 111-112: ": : :the lack of information about the actual irrigation scheduling adopted by the farmers is the critical limitation for SWB modeling". I believe that var-ious SWB models (Swap, Cropsyst, FAO56, AcquaCrop) are able to consider both scheduled by farmer irrigation (as input) or predicted irrigation (as output). Please, clarify or modify.

*Response:*

*Indeed, several SWB models such as Swap, Cropsyst, FAO56, AcquaCrop and also the SAMIR model that we have already used (Saadi et al., 2015) are able to consider both methods to take irrigation into account: either an estimated amount provided by the farmer (as an input) or a predicted irrigation with a module to trigger irrigation according to, say, critical soil moisture levels (as an output). We clarify this part in the revised version by saying that the lack of actual irrigation scheduling information does not impact the irrigation estimation by these models, since irrigation could be simulated by SWB models, but rather the validation protocol of irrigation requirements estimates (irrigation data is usually unavailable).*

5. Line 123: Insert ". . ." in dual-source models.

*Response:*

*In the version to which we refer this expression is already put in inverted commas (line 116): "However, separate estimates of evaporation and transpiration makes the "dual-source" models more useful for agrohydrological applications*

6. Lines 152-154: Clarify that the "layer" approach of SPARSE is essentially a "dual-source" scheme.

*Response:*

*In the revised version of the manuscript, the paragraph is simplified accordingly (line 180):*

*"In this study, (…) were obtained by the SEB method, using the Soil Plant Atmosphere and Remote Sensing Evapotranspiration (SPARSE) (...)."*

*We specify in the "model" section (section 4 line 465) that we use the "layer" approach and define it: "The SPARSE dual-source model solves the energy budgets of the soil and the vegetation. Here we use the "layer approach", for which the resistance network relating the soil and vegetation heat sources to a main reference level through a common aerodynamic level use a series electrical branching"*

7. Line 187: The Authors should explain (also under a theoretical point of view) the choice to install Scintillometer at a 20 m height. About the experimental setup it is strange the absence of a "net radiometer" that, on the basis of the footprint analysis, could be installed in the average prevalent source area of footprint. The Authors could explain this fact.

*Response:*

*The choice to install Scintillometer at a 20 m height was based on the XLAS installation principle detailed in the "Kipp & Zonen LAS and XLAS instruction manual", indeed, the minimum installation height of the XLAS as function of the path length and for different surface conditions is graphically explained and shows that for a path length of 4km, the XLAS height of 20m is an adequate height since the XLAS is high enough to minimize measurement saturation and not too high to be representative of the 4km path Boundary Layer.*

*The absence of a "net radiometer" is explained by the high heterogeneity of the study area, especially in terms of vegetation cover; therefore, it is not possible to measure the net radiation (Rn) of all plots or even the Rn of "typical" plots (with similar land cover and irrigation practice).*
*This is clarified in the revised version (line 2014).*

8. Line 280: The terms "incoming solar radiation" and "incoming atmospheric radiation" are correct but could generate a misunderstanding. Please use the more classical "shortwave" and "longwave" terminology in eq. (9) and explain how RS data are generally used to solve balance equation of radiation (eq.9).

*Response:*

*In the revised version of the manuscript, the terms "incoming shortwave radiation" and "incoming longwave radiation" are used. This terminology is also used all along the manuscript.. The following paragraph is added accordingly (line 392):*
*"The Ben Salem meteorological station was used to provide $Rg_t$ and $R_{atm\text{-}t}$. Remote sensing variables α, LST, $\varepsilon_s$ and NDVI came from MODIS products"*

9. Line 367: About the "Temporal interpolation of albedo and NDVI" some brief details could be considered.

*Response:*

*Albedo MODIS products (MCD43) are available every 8 days and come from different satellite overpasses over a period of 16 days, the day of interest is central date. Both Terra and Aqua data are used in the generation of this product, providing the highest probability for quality input data and designating it as the acronym MCD, which means Combined product.*

*NDVI MODIS products (MOD13A2/MYD13A2 for Terra and Aqua, respectively) come from different satellite overpasses over a period of 16 days, and they are available every 16 days and separately for Terra and Aqua. Indeed, algorithms generating this product operate on a per-pixel basis and requires multiple daily observations to generate a composite NDVI value that will represent the full period (16 days), the 1km/16days MOD13A2 (respectively MYD13A2) product is an aggregated 250m/16 days MOD13Q1 (respectively MYD13Q1) product..*

*For both products, the data is linearly interpolated over the available dates in order to get daily data. For each pixel, the best data is taken into account (based on the quality index supplied with the product). Therefore, the temporal interpolation was done pixel by pixel.*

*This explanation is inserted in the revised version (line 248).*

10. Line 455: Which method has been used to evaluate the "potential conditions", please clarify.

*The half hourly potential latent heat flux is computed using the prescribed mode of the SPARSE model (see (Boulet et al., 2015)): " The system of equation can also be solved for Ts and Tv only if the efficiencies representing stress levels (dependent on surface soil moisture for the evaporation, and root zone soil moisture for the transpiration) are known. In that case the sole first four equations are solved. This prescribed mode allows computing all the fluxes in known limiting soil moisture levels (very dry, e.g. fully stressed, and wet enough, e.g. potential). (…) The potential evaporation and transpiration rates used later on are computed using this prescribed mode with minimum surface resistance to evaporation and transpiration, respectively."*

*The above paragraph is added to the SPARSE model description in the revised version of the manuscript (line 482).*

11. Lines 491-492: The Authors reported that . . .."An overestimation of about 15% is found between estimated and measured daily available energy. . ..and the coefficients . . .. . .were applied to remove this bias". If I well understand the above procedure (re- move of bias) is a sort of calibration of the output of modeled on the basis of observed flux station. Please clarify.

*Response: see response to comment 12.*

12. Lines 526-527: About the estimation of sensible heat flux the authors reported that "This result is of great interest considering that the SPARSE model was run with no prior calibration", but I feel a sort of contradiction with the bias removing procedure described in the above comment. Please clarify. Moreover I think that the Authors should describe the accuracy of model prior and after the bias correction.

*Responses to comments 11 and 12:*

*In fact, bias removal does concern neither the SPARSE model which was run with no prior calibration nor its estimates. Since the model provide a single instantaneous estimate of energy budget components, the global solar incoming radiation Rg was used to scale modeled AE and H from instantaneous to daily values (see section 4.2.3), the same applies to instantaneous available energy (see sections 3.3.1 and 3.3.2) computed using remote sensing and meteorological data (equation 9 ) and measured H by the XLAS.*

*Indeed, the extrapolation from an instantaneous flux estimate to a daytime flux assumes that the surface energy budget is "self-preserving" i.e. the relative partitioning among components of the budget remains constant throughout the day. However, many studies (Brutsaert and Sugita, 1992; Gurney and Hsu, 1990; Sugita and Brutsaert, 1990) showed that the self-preservation method gives day- time latent heat estimates that are smaller than observed values by 5-10%. Moreover, (Anderson et al., 1997) found that the evaporative fraction computed from instantaneous measured fluxes tends to underestimate the daytime average by about 10%, hence, corrected parameterization was used and a coefficient=1.1 was applied. Similarly, (Delogu et al., 2012) founded an overestimation of about 10% between estimated and measured daily component of the available energy thus, a coefficient =0.9 was applied. The (Delogu et al., 2012) corrected parameterization were tested, since, in our study case also an overestimation between estimated and measured AE was found, but this coefficient did not give consistent results, therefore, we had to calibrate the extrapolation relationship in order to get accurate daily results of AE and H*
*Thereby, the applied extrapolation method was tested using in situ Ben Salem flux station measurements. Indeed, Daily measured available energy $AE_{BS\text{-}day}$ (all the same for $H_{BS}$) computed as the average of half-hourly measured $AE_{BS\text{-}30}$, was compared to daily available energy ($AE_{BS\text{-}day\text{-}Terra}$ and $AE_{BS\text{-}day\text{-}Aqua}$) computed using the extrapolation method from instantaneous measured $AE_{BS\text{-}t\text{-}Terra}$ and $AE_{BS\text{-}t\text{-}Aqua}$ at Terra and Aqua overpass time, respectively (Equation 14). Results gave an overestimation of about 15 %. The corrected parameterizations of AE (Table 1), needed to remove the bias between measured ($AE_{BS\text{-}day}$) and computed AE ($AE_{BS\text{-}day\text{-}Terra}$ and $AE_{BS\text{-}day\text{-}Aqua}$), were applied to compute daily remotely sensed AE ($AE_{day}$) from instantaneous AE ($AE_t$) following the extrapolation method shown in equation 14.*

*This explanation is inserted in the revised version (lines 419 to 450 and lines 542 to 554).*

13. Line 545: (Figure 7). Looking at the scatterplot it is clear a more dispersion for H value greater than 150. Is there an explanation of this?

*Response:*

*Possible explanations of the scatter observed or high H values are (revised version line):*

- *i) the XLAS measurement saturation; according to the "Kipp & Zonen Las and XLAS instruction manual", for a path length of 4km and a scintillometer high of 20 m, saturation measurement problem might be present from H values of about 300 $W.m^{-2}$*
- *ii) Uncertainties on the correction of stability using the universal stability function*
- *iii) Potential inconsistencies between the area average MODIS radiative temperature and the air temperature measured locally at the meteorological station.*

14. Line 604: The Authors reported that "Daily observed and modeled ET over the whole study period were both in the range of 0-4 mm mm.day-1 which is consistent with the land use present in the XLAS pat". In my opinion this is a prosy comment, Trouble if not.

*Response:*

*We agree with the reviewer 1, and the composition of the vegetation cover over the study area (above the scintillometer) with detailed land use percentage is added (section 3.2), in order to show that this area is almost covered by fruit trees spaced by a lot of bare soil, with less herbaceous soil-covering crops; which lead to this range of daily ET. These ET values range was also found in (Saadi et al., 2015) dealing with the same study area. This is precised in the revised version (Figure 4).*

15. Line 616-617: The Authors reported that “Some points with little to null ET were recorded from May to July 2013 which can be explained by the very dry conditions and scattered vegetation cover with a considerable amount of bare soil”. Why this behavior was not observed in the same period of 2014 ?

*Response:*

*This behavior was not observed in the same period of 2014, because 2014 was a rainy year in comparison to 2013 (more rainfall peaks), so, even supposing that the farmers have the same attitude and cultivate the same crop types between the two years (which is not true in the context of our study area and farmers always change crop types), precipitations favor the growth of spontaneous vegetation over fallows which contribute to ET rise. On the other hand, since the year experiences more rain, farmers cultivate a larger part of the land diversify the crop types and the vegetation cover is denser, this contributes to an overall increase in ET.*
*This explanation is inserted in the revised version (line 693).*

16. Line 863: Please check the (Minacapilli and Ciraolo, 2007) reference.

*Response:*

*This reference should be corrected as follows:*

*Minacapilli, M., Ciraolo, G., D Urso, G., and Cammalleri, C.: Evaluating actual evapotranspiration by means of multi-platform remote sensing data: a case study in Sicily, IAHS PUBLICATION, 316, 207., 2007.*

## *References*


*Anderson, M., Norman, J., Diak, G., Kustas, W., Mecikalski, J., 1997. A two-source time-integrated model for estimating surface fluxes using thermal infrared remote sensing. Remote sensing of environment 60, 195-216.*

*Boulet, G., Mougenot, B., Lhomme, J.P., Fanise, P., Lili-Chabaane, Z., Olioso, A., Bahir, M., Rivalland, V., Jarlan, L., Merlin, O., Coudert, B., Er-Raki, S., Lagouarde, J.P., 2015. The SPARSE model for the prediction of water stress and evapotranspiration components from thermal infra-red data and its evaluation over irrigated and rainfed wheat. Hydrol. Earth Syst. Sci. 19, 4653-4672.*

*Brutsaert, W., Sugita, M., 1992. Application of self-preservation in the diurnal evolution of the surface energy budget to determine daily evaporation. Journal of Geophysical Research: Atmospheres 97, 18377-18382.*

*Courault, D., Clastre, P., Cauchi, P., Delécolle, R., 1998. Analysis of spatial variability of air temperature at regional scale using remote sensing data and a SVAT model, Proceedings of the First International Conference on Geospatial Information in Agriculture and Forestry.*

*Delogu, E., Boulet, G., Olioso, A., Coudert, B., Chirouze, J., Ceschia, E., Le Dantec, V., Marloie, O., Chehbouni, G., Lagouarde, J.P., 2012. Reconstruction of temporal variations of evapotranspiration using instantaneous estimates at the time of satellite overpass. Hydrol. Earth Syst. Sci. 16, 2995-3010.*

*Glenn, E.P., Huete, A.R., Nagler, P.L., Hirschboeck, K.K., Brown, P., 2007. Integrating remote sensing and ground methods to estimate evapotranspiration. Critical Reviews in Plant Sciences 26, 139-168.*

*Gurney, R., Hsu, A., 1990. Relating evaporative fraction to remotely sensed data at the FIFE site.*

*Saadi, S., Simonneaux, V., Boulet, G., Raimbault, B., Mougenot, B., Fanise, P., Ayari, H., Lili-Chabaane, Z., 2015. Monitoring Irrigation Consumption Using High Resolution NDVI Image Time Series: Calibration and Validation in the Kairouan Plain (Tunisia). Remote Sensing 7, 13005.*

*Sugita, M., Brutsaert, W., 1990. Regional surface fluxes from remotely sensed skin temperature and lower boundary layer measurements. Water Resources Research 26, 2937-2944.*

# Authors Response to Reviewer 2 comments

| | **General comments** | Authors response |
|---|---|---|
| 1 | Depending upon editor's decision I would like to see further:<br>1) Figures with better accuracy in their representation. For example, some of them seems to have been the result of quick spreadsheet plots but without including accurate axis ticks, grids, labels, etc. | All figures are improved in the revised version. Particular attention is paid to axis ticks, grid and labels. |
| 2 | 2) Same as for the description of the figure captions and legends. The reader needs to understand a given figure by analyzing the figure and reading the information on the figure caption and legends. | Figures captions and legends are enhanced in the revised version of the article in order to provide complete information. |
| 3 | 3) A better explanation of the SPARSE methodology is needed, steps and the set of equations in the ET and H estimates. What the assumptions are and what is the physical framework? All of that is missing and therefore theoretically this paper is very weak.<br><br>For example, from where the authors got a threshold value of 30 W/m2 to start the iteration? How convergence is achieved is a mystery here and how many iterations and how signal-to-noise ratio of RS data plays a role in that convergence? Which equation provides convergence we don't know. | This article deals with an assessment of the SPARSE model accuracy and operational use in a semi arid context over a heterogeneous landscape; the theoretical framework of SPARSE is only summarized since it has been detailed in (Boulet et al., 2015) as well as in the online documentation (Boulet, 2017); since it is critical to have a self-understandable methodology section in the revised version of this article, we extend the explanation of the SPARSE methodology and add a diagram showing the flowchart of the SPARSE algorithm (Figure 5).<br><br>There is no iteration till convergence in the SPARSE algorithm, only a decision tree with decisions made upon the sign of the retrieved soil latent heat flux component: if negative, the assumption of unstressed vegetation is considered as invalid and the stress of the vegetation is retrieved. This is detailed in the added figure.<br><br>The $30Wm^{-2}$ is not a threshold to start iteration since there is not a convergence in SPARSE model, but it is a minimum positive threshold for vegetation stress detection which accounts for the small but non negligible vapor flow reaching the surface (Boulet et al., 1997). (Revised version line 492) |

| | | |
|---|---|---|
| 4 | 4) I would like the authors to provide adequate justification to the use of formulas to deduce H based on LAS or XLAS. Particularly since the indicated formulas are valid only under the similarity hypothesis of Monin-Obukhov which implies homogenous surface and stationary flows. No justification was provided as for how these conditions were tested to render valid the resulting HLAS flux. | In our study area topography is flat, and landscape is heterogeneous only from an agronomic point of view since we find different land uses (cereals, vegetables and fruit trees mainly small olive trees with considerable spacing of bare soil); however, this heterogeneity in landscape features at field scale is randomly distributed and there is no drastic change in height and density of the vegetation at the scale of the XLAS transect (i.e. little heterogeneity at the km scale, most MODIS pixels have similar NDVI values for instance). In these conditions, considering the size of the surface changes in roughness (mean vegetation height ~1.5m), we assumed that the XLAS measurement height was close to the blending height, or either higher. Thus, the fluxes measured by scintillometry are area-averaged and MOST theory can be applied in the flux algorithm computation. In addition, support for the MOST theory was assessed by looking at non-dimensional diagrams of normalized $Ct^2$ and most points are aligned on the theoretical curves of Andreas and (De Bruin et al., 1993). On that basis, we believe that MOST is valid. |
| 5 | 5) when the authors discuss about uncertainties it is not clear what kind of uncertainties we are talking about and how have those been calculated? Moreover, uncertainties in heterogeneous terrain based on pure observations XLAS have not been computed. | Uncertainties concern mainly:<br>i/ the instantaneous remote sensing data: there is indeed an issue with the MODIS pixel heterogeneity and notably the distribution of components at the intersection between the square pixel and the XLAS footprint. Also, MODIS products, and mainly LST which is paramount in stress coefficient computation, are assumed to be reliable since we do not have means to reprocess them; however, results could be checked using Landsat high resolution TIR data.<br>ii/ half hourly forcing and XLAS data (meteorological and flux data);<br>iii/ the extrapolation method from instantaneous to daily results ;<br>iv) unlike temperate areas in which sensible hat flux H is relatively low, in our semi-arid study area, H is mostly high leading to important difference between H and LE (which approaches zero) requiring more data postchecking in the residual derivation of LE from XLAS.<br>v/ the empirical estimation methods of soil heat flux G (3 methods were tested) as well as the possible |

| | | |
|---|---|---|
| | A reference is provided so that the authors can check on that.<br>Bai, et al., 2015. "Characterizing the Footprint of Eddy Covariance System and Large Aperture Scintillometer Measurements to Validate Satellite-Based Surface Fluxes. *Geoscience and Remote Sensing Letters, IEEE,* 12(5), 943-947, 2015. doi: 10.1109/LGRS.2014.2368580. | daily heat accumulation can lead to possible errors in available energy estimation and in turn in residual LE estimation, hence, both minimum and maximum daily observed LE were presented, the same for the modeled daily LE presented by error bars.<br>Despite all these possible uncertainty sources, our findings are reasonable compared to previous published results (SAMIR model,(Saadi et al., 2015).<br><br>Thank you for this interesting reference on which we draw on to add a paragraph in the revised version discussing the uncertainties in heterogeneous terrain based on pure XLAS observations. |
| 6 | 6) Not clear where the EC flux comes into play. Also footprint functions for the scintillometers need to be accounted for. Reference on this element is provided below. | There are two EC stations located at the top of the towers (on the side of the XLAS emitter and receiver, respectively), which are used to process the XLAS data (initialization of friction velocity u* values and the Obukhov length Lo) and one EC station on the ground. This is detailed in the revised manuscript:<br>*i)Line 218: "two automatic Campbell Scientific (Logan, USA) eddy covariance (EC) flux stations were also positioned at the same level on the two water tower top platforms. Half hourly turbulent fluxes in the western and the eastern EC stations were measured used a sonic anemometer CSAT3 (Campbell Scientific, USA) at a rate of 20 Hz and a sonic anemometer RM 81000 (Young, USA) at a rate of 10 Hz, respectively. The western station data were more reliable with less measurement errors and gaps, hence, the western EC set-up was used initialise friction velocity u* values and the Obukhov length Lo in the scintillometer flux computation".*<br>*ii) Line 232: "In addition, an EC flux station, referred as the Ben Salem flux station (few tens of meters away from the meteorological station) was installed from November 2012 to June 2013 in an irrigated wheat field (Figure 2) measuring half hourly convective fluxes exchanged between the* |

| | | |
|---|---|---|
| | | *surface and the atmosphere ($H_{BS-30}$ and $LE_{BS-30}$) combined with measurements of the net radiation $Rn_{BS-30}$ and the soil heat flux $G_{BS-30}$. Net radiation and soil heat flux measurements were transferred to the meteorological station from June 2013 till June 2015. Since, there are no Rn and G measurements in the two water towers EC stations, $Rn_{BS}$ and $G_{BS}$ measurements were among the inputs data to derive sensible and latent heat fluxes from the XLAS measurements. In addition, measured available energy ($AE_{BS}=Rn_{BS}—G_{BS}$) and $H_{BS}$ were used to calibrate the extrapolation relationship of the available energy and the sensible heat flux, respectively"* |
| 7 | 7) I would like the authors to provide an in-depth description of physical processes explaining the results in the final figures. Description of what is being presented in the figures is fine but we need more science here. | In the revised version, more physically-based explanation dealing mainly with the outliers is added to describe the final figures. |
| 8 | As an aside note the use of XLAS is not unique in this problem. A LAS can do 5 km max. Optical beam path and resolve the same situation. What is critical with using XLAS is beyond 5 km optical path. | |

| | **Detailed comments** | Authors response |
|---|---|---|
| 1 | Line 45 –off : please put references in chronologic order. This is the proper way to recognize previous work; unless specific discussions are provided which in those cases the trail of references needs to be broken down. This note is valid through the entire paper. | References are put in chronologic order in the revised version. |
| 2 | Line 50: About the claims about water scarcity related to climate change. -or better say climate variability: I wonder how compelling are these claims? – Can the authors substantiate in more details about this problem in this area? This is an important claim and need to be fully addressed by the authors to build context to this research and the methodologies being used. | The paragraph below is added in the revised version (line 50):<br>*"Indeed, the Mediterranean region is one of the most prominent "hot spots" in future climate change projections (Giorgi and Lionello, 2008) due to an expected larger warming than the global average and to a pronounced increase in precipitation inter-annual variability. The major part of the southern Mediterranean countries, among others Tunisia, already suffer from water scarcity, and show a growing water deficit, due to the combined effect of the water needs growth (soaring demography and irrigated areas extension), and the reduction of resources (temporary drought and/or climate change)"* |
| 3 | Line 53: the use of "greatest" here tries to indicate what? "the larger" or "the most important"? This needs to be clearly understood without ambiguity and therefore we need to bring more specificity. | "*greatest*" is replaced by "*the largest*" in the revised version (line 59) |
| 4 | Line 56: I'll add complexity in. As we move from ecosystem scale to landscape scales surface heterogeneity but also dynamic of the flow, cloudiness, precipitation come into play more aggressively. This also bring more context to the need of this study. | We have already mentioned the impact of land cover heterogeneity at large scale on the land atmosphere exchange:<br>*"Moreover, at these scales, land cover is usually heterogeneous and this affects the land-atmosphere exchanges of heat, water and other constituents (Giorgi and Avissar, 1997)."*<br>However, to develop this idea further, in the revised version, we provide some more explanation about the hydro-meteorological processes complexity and its impact on climate variables (line 61):<br>*"(…)it is much more difficult at larger scales (irrigated perimeter or watershed) due to the complexity not only of the hydrological processes* |

| | | |
|---|---|---|
| | | *(Minacapilli et al., 2007) but also of the hydro-meteorological processes. Indeed, at landscape scale, surface heterogeneity influences regional and local climate, inducing for example cloudiness, precipitation and temperature patterns differences between areas of higher elevation (hills and mountains surrounding the Kairouan plain) and the plain downstream. Moreover, at these scales, land cover is usually heterogeneous and this affects the land-atmosphere exchanges of heat, water and other constituents (Giorgi and Avissar, 1997).* |
| 5 | Line 61: I would disagree that "RS techniques becomes essential". Basically it has been demonstrated that plot (or ecosystem) exchanges within same complex canopies do verify consistent differences in sensible heat fluxes (the simplest and ubiquitous flux on earth) over distances that are much smaller than the RS footprint in particular MODIS. See Starkenburg et al., (2015). Starkenburg et al. 2015: "Temperature regimes and turbulent heat fluxes across a heterogeneous canopy in an Alaskan boreal forest". J. Geophys. Res. Atmos., 120: 1348–1360. doi: 10.1002/2014JD022338<br><br>Now, I do agree that RS brings a mean to deduce, within certain ranges, an approximation of fluxes. What about mesoscale models? Or perhaps you wanted to indicated physical models using RS data as input? In any case, I think you should open this perspective here since there are other disciplines other than Remote Sensing Researchers that can also provide the same product. | Remote sensing (RS) can provide estimates of large area fluxes in remote locations, but those estimates are based on the spatial and temporal scales of the measuring systems and thus vary one from another. Hence, one solution is to upscale local micrometeorological measurements to larger spatial scales in order to acquire an optimum representation of land-atmosphere interactions (Samain et al., 2012). However, such upscaling is not always possible and results might not be reliable in comparison to the RS distributed products.<br>In order to keep the introduction as short as possible, in the revised version, two examples of complex physically based LSMs using RS data as inputs to derive ET are mentioned (line 76) |
| 6 | Line 63: vegetation physical properties or characteristics? | In the revised version:<br>"*vegetation's physical properties*" is replaced by "*vegetation physical characteristics*" (line 72) |

| | | |
|---|---|---|
| 7 | Line 65: Authors use "plot" as one of the scales in which I assume results would be obtained. However, at no point plot-scale was defined. Please whenever plot is used for the first time in the Introduction section for example please clarify that. (excluding the abstract). | We agree with Reviewer 2 and the word "plot" induces ambiguity. "*plot*" is replaced by "*field*" in the revised version. (line 75) |
| 8 | Line 87: please rephrase the text between parenthesis. | In the revised version:<br>*"(mostly derived from, say, actual water content in the root zone, wilting point and field capacity)"*<br>is replaced by:<br>"*mostly derived from the soil moisture characteristics: actual available water content in the root zone, wilting point and field capacity "*(line 107) |
| 9 | Line 93: Spell out FAO. If it is not being used anymore in the text, then no need to define an acronym. | In the revised version:<br>*"FAO guidelines"* is replaced by<br>*"Food and Agriculture Organization-FAO guidelines"* (line 113) |
| 10 | Line 98-99: get rid of parenthesis here. What is inside is part of the phrase. | Parentheses are removed in the revised version. |
| 11 | Line 102: FAO-56 put a reference here. Or make a short phrase explanation. | The Allen et al. (1998) reference is added in the revised version. |
| 12 | Line 103: what is "dry down"? please make sure you check consistency in all phrases. | *"Dry-down period is the period after rain or irrigation where the soil moisture is decreasing due to evapotranspiration and drainage. It is of great interest, because soil moisture has such a strong effect on nearly every aspect of the land surface (heat distribution, albedo, carbon uptake… etc.)."*<br><br>This short explanation is added to the revised version (line 123). |
| 13 | Line 114: What's the meaning of adding quotes here? If single-source means single source, then no need for quotes. Quotes are used when you use a word or combination of words but you would like to indicate a different meaning. | Quotes are removed for *single-source models* and *dual-source models*. |

| | | |
|---|---|---|
| | Line 116: same as 114. | |
| 14 | Line 117: comma missing before etc. | It is rectified in the revised version. |
| 15 | Line 128: add "they provide area-averaged sensible heat flux" | "*average sensible heat estimates*" is replaced by "*area-averaged sensible heat flux*" in the revised version (line 154). |
| 16 | Line 130-131: incomplete phrase. And, can you elaborate a little bit more here? | This phrase is rectified in the revised version as follows (line 156):<br>"*Scintillometry can provide sensible heat using different wavelengths (optical wavelength and microwave wavelength ranges), aperture sizes (15-30 cm) and configurations (long-path and short-path scintillometry )"* . |
| 17 | Line 132: delete space before comma. | This is rectified in the revised version. |
| 18 | Line 133: representative of the pixel? It may be the case that for a particular MODIS data your scintillometer data intersects several pixels. Then we are talking about several pixels. | Indeed, the issue of the representativity of the heterogeneity (land use and irrigation practice) at the intersection between the MODIS pixels considered as homogeneous and the XLAS footprint was not discussed in the submitted version of the article. We add the suggested reference and discuss the relative percentages of Land Use classes within each MODIS pixel to provide a first guess on these relative heterogeneities. (line 329) |
| 19 | Line 140: **large-scale area-average** this is the proper measurement that one obtains from a scintillometer. | In the revised version:<br>*"Since the scintillometer only provides spatially averaged sensible heat flux (…)"*<br>is replaced by<br>*"Since the scintillometer only provides large-scale area-average sensible heat flux (…)"* |
| 20 | Lines 140-143: Here I need help. Are you indicating that to get ET large-scale area-average you use XLAS? But you need to assume a closure fraction or assume is 100% Energy Balance closure. As we increase surface heterogeneity and the atmospheric flow acquires an increased space-time variability then it is difficult to assume 100% energy balance closure. How you do then? Please explain how you treat and eventually circumvent this problem. See for example Foken et al., (2006; 2010) and Foken (2008).<br>Foken, T., F. Wimmer, M. Mauder, C. Thomas, and C. Liebethal, 2006. Some aspects of the energy balance | Please see authors' response to the general comment N°4. |

| | | |
|---|---|---|
| | closure problem. *Atmos. Chem. Phys.*, 6, 4395–4402.<br>Foken, T., 2008: "The energy balance closure problem: An overview", *Ecol. Appl*., 18(6), 1351– 1367.<br>Foken, T., M. Mauder, C. Liebethal, F. Wimmer, F. Beyrich, J.-P. Leps, S. Raasch, H. A. R. DeBruin, W. M. L. Meijninger, and J. Bange, 2010: "Energy balance closure for the LITFASS- 2003 experiment", *Theor. Appl. Climatol.*, *101*(1-2), 149-160, doi: 10.1007/s00704-009-0216-8. | |
| 21 | Line 146: what is the "layer" approach? Can you be more explicit and detailed? If layer is the name of the approach, then no need to use quotes. | Indeed "*layer*" is the name of the approach, hence, the quote are removed in the revised version. More details about this approach is given in (Boulet et al., 2015) |
| 21 | Line 147: when authors normally explain the use of electrical resistance as equivalent models really are not paying attention to the details. So then now you need to explain how you transform an electrical element such as a Resistor, which is a concentrated parameter into a distributed vegetation or soil representation. What are the assumption? Hypothesis? Regions where this approximation is valid and where it fails, etc. I'll give you a hint R=V/I where V(electrical voltage: what is imposed the potential) and I(electrical current, what flows between the boundaries). Then when you say you use Rsoil and Rveg. What are the analogs of V and I here? What R actually means? And how you walk out from the Ohm's Law for concentrated electrical parameters and transition to our problem where these parameters are distributed?<br>This comes from Norman and Kustas TSEB- way before SPARSE.<br>For example, here it is important to remark that vegetation information has to be at much higher resolution | The resistance scheme is detailed in Boulet et al. (2015) and is similar to that used in (Kustas and Norman, 1999), cf. (Monteith and Unsworth, 2007). V is either a temperature difference (soil-aerodynamic level or vegetation-aerodynamic level) or the corresponding vapour pressure difference. I is the flux component (sensible or latent) and R is the resistance to transfer (aerodynamic resistances within and above the vegetation, stomatal resistance). There is no need of specifying a soil resistance to evaporation because the evaporation rate is directly retrieved. The Series description of the electrical analogy used here is that of most LSMs following (Shuttleworth and Wallace, 1985) which describes the interactions within the soil-plant-atmosphere interface for sparse crops. The radiation interception by sparse crops might be difficult to represent with a layer approach, this will be further commented in the text. |

| | | |
|---|---|---|
| | than the radiometric information to account for vegetation/forest variations for example the existence of clear areas within the forest or cultivars. How the authors account for that needs better explanations. And, what assumptions underlain these approximations? | |
| 22 | Line 150: I wanted to be clear here that XLAS ONLY can deduce sensible heat not LE. Please make sure this thread is conveyed all the way through your work. | In the revised version (line 183):<br>*"The main objective of this paper is to compare H and LE obtained using the SPARSE model and XLAS (…)"*<br>is replaced by:<br>*"The main objective of this paper is to compare the modeled H and LE simulated by the SPARSE model with, respectively, the H measured by the XLAS and the LE reconstructed from the XLAS measurements acquired during two years over a large, heterogeneous area."* |
| 23 | Line 158: put "(" to indicate the reference the cultivars are within the phrase. | This is rectified in the revised version. |
| 24 | Line 173: what "double device" means for you. Please be specific. | This phrase is simplified in the revised version and "*double device*" is removed.<br>(line 205) |
| 25 | Figure 2: it is not clear where the XLAS emitter and receiver are specifically located. Put a dot or a symbol to indicate that. Photos actually say nothing here. Now I see that the CSAT is close to the XLAS receiver. I would caution the authors here that any interpretation between XLAS fluxes and EC-CSAT fluxes would not be representative since the EC system is closer to the XLAS receiver and/or transmitter for that matter is the same.<br>More importantly what is not clear here is what are the green contours indicating the footprint? And if these are EC footprint more likely are wrong.<br>Please specify what SPOT5 bands 1,2,3 are in terms of wavelengths and they are used in this work. | Green contours are half-hourly XLAS footprints for selected typical wind conditions.<br>High resolution SPOT5 image of 9$^{th}$ April 2013 was only used as background image to illustrate the land cover under the XLAS transect.<br>Hence, figure 2 caption is modified in the revised version as follows:<br>*"XLAS set up: XLAS transect (white), for which the emitter and the receiver are located at the extremity of each white arrow, half-hourly XLAS footprint for selected typical wind conditions (green), MODIS grid (black), orchards (blue) and the location of the Ben Salem meteorological and flux stations. Background is a three colour (red, green, blue) composite of SPOT5 bands 3 (NIR), 2 (VIS-red) and 1(VIS-green) acquired on 9th April 2013 and showing in red the cereal plots".*<br><br>On the other hand, EC station flux measurements are not compared to XLAS fluxes along the article. This EC station utility has been already explained in the above responses (general comment N°6). |

| | | |
|---|---|---|
| 26 | Line 196: I would write Extra Large Aperture Scintillometer (XLAS) | This is rectified in the revised version. |
| 27 | Line 198: Phrase: "Scintillometer is based on the scintillation method" what is this? | This is rectified in the revised version. |
| 28 | Line 198-200: What is the cause and what is the effect? This phrase is wrong please think about a little bit. | This is rectified in the revised version as follows (line 269): *"Scintillometer measurements are based on the scintillation theory; fluxes of sensible heat and momentum cause atmospheric turbulence close to the ground, and create, with surface evaporation, refractive index fluctuations due mainly to air temperature and humidity fluctuations (Hill et al., 1980)""* |
| 29 | Line 205: replace "bean" by "beam" | This is rectified in the revised version (line) |
| 30 | Line 204: The reference that links scintillations and Cn2 is given by Tatarskii. We need to give the proper reference here. The fact that those references have been using it doesn't mean they were the ones given the foundation for this relationship. We need to make sure we give proper value to the actual references. | (Tatarskii, 1961) reference is added to the revised version (line 275) |
| 31 | Line 206: symmetrical to what? What is that symmetry you are talking about? | *This sentence is corrected (line 275): "The sensitivity of the scintillometer to $C_{n^2}$ along the beam is not uniform and follows a bell-shape curve due to the symmetry of the devices. This means that the measured flux is more sensitive to sources located towards the transect centre and is less affected by those close to the transect extremities."* |
| 32 | Line 208: get rid of an extra space in the phrase.<br>Same line: "structure parameter of temperature" by structure parameter of temperature turbulence (refractive index in the case of CN2). | This is corrected in the revised version (line). |
| 33 | Line 210-212: here the authors mentions very cursory a very important problem which is the variation of Cn2 because of the beam height variation across the landscape. It seems this is one point you should be more cautious in bring some | The terrain is very flat; therefore there is little beam height variation across the landscape, except for what is induced by the various roughness heights of the individual fields. Since the interspace between trees is large, the effective roughness of the orchard is not significantly different from that of cereal fields, and far below |

| | | |
|---|---|---|
| | references and eventually limit your study on the basis of this sensitivity parameter. | the measurement height. |
| 34 | Line 213: only sensitive to temperatures. Add a period in the phrase. | This is corrected in the revised version. |
| 35 | Eq. [1] you introduce here an approximation that then you'll use as an equality. Please explain and substantiate or directly correct the equation. Also, I wonder how much beta introduce error, in this case, a semi-arid environment. | This is corrected; an equality sign is used in Eq. 1. The sensible heat flux dominates the energy balance in most cases; therefore the Bowen ratio is mostly above one. The influence of the beta correction has been analyzed in (Solignac et al., 2009) which shows that since the beta closure method does not rely on an exact locally observed beta it is far less sensitive to the precision on beta. |
| 36 | Line 217: iterative methods have intrinsic convergence and resolution errors. You have to specify the convergence error and also how the average of Cn2 gives you a signal with enough SNR to keep the specific convergence factor. Now recently analytical methods have been developed that integrate the set of nonlinear equations in this casa Tatarskii and Monin-Obukhov similarity hypothesis set. See Gruber and Fochesatto, (2013).<br>Gruber M. A. and G. J. Fochesatto. 2013: "A New Sensitivity Analysis and Solution Method for Scintillometer Measurements of Area-Average Turbulent Fluxes" *Boundary-Layer Meteorology*, 149:65– 83 DOI 10.1007/s10546-013-9835-9 | I'm not sure to fully understand the reviewer's remark. Actually, as shown by (Gruber and Fochesatto, 2013), the height z at which $C_T^2$ is sampled can substantially affect the sensible heat flux (20%), but in our study, the *in situ* G measurement (used to initialize the energy budget closure) has also an impact on the estimate of H_XLAS throughout the convergence algorithm. Since XLAS measurements were processed at the beginning of the project, no sensitivity analysis of theses variables, *e.g.* effective height z, initial guess of the iterative algorithm (local *vs* integrated *via* remote sensing or modeling) was performed. As it is not the scope of the paper, we didn't achieve any sensitivity analysis on XLAS fluxes computation to determine which parameter has the strongest influence on the flux uncertainty. |
| 37 | Line 220: Zlas is a function where is that?<br><br>Andreas parameterization might not be valid for your site.- Can you justify here?<br><br>Zv: is the average canopy height but | $Z_{LAS}$ is not a function, since the XLAS experiment took place over a flat surface, $Z_{LAS}$ is the XLAS height; the word "*effective*" is therefore removed because it induces confusion.<br><br>We indeed test the De Bruin (De Bruin et al., 1993) parameterization in the revised version (cf. Figure above). |

| | | |
|---|---|---|
| | weighted by the extension of the plots? | Zv estimation method is detailed by the end of section 4.1. It accounts for the various heights within the footprint selected using angular zones originating from the centre of the transect, and supported by high resolution remote sensing data. |
| 37 | Eq.4 contains u* but it is not clarified here from where this is taken.<br>Here we can conclude that XLAS ONLY measures T* as a large-scale area-average variable but u* is a local variable or at least a variable measured at the scale of the EC system which is not the same as the XLAS. Explain please? | u* is not taken from EC system, it is computed based on an iteration approach in the beta closure method, only the initialization value of u* was taken from the EC station positioned on the western water tower. |
| 38 | Line 225: rho is the air density and cp here are considered constants. Do they vary across the experiment? | Indeed, air density, pressure and temperature depend on the location on the earth, on altitude and on the season of the year. However, in our study, standard values of air density (ρ) and air specific heat at constant pressure (cp) were used without verifying their variation across the experiment since our study concerns a limited extent (10 km*8 km, same earth location) with flat terrain (no altitude variation) and without a considerable temperature difference between the hot and cold seasons (average monthly temperature oscillates between 10°C and 28°C). |
| 39 | Line 227: nomenclature is Number[space]unit. please correct all the way your text. | This is rectified in the revised version. |
| 40 | Line 228: change “circa” by “near”. The correct use of “circa” in English is to indicate something that happened in the past (circa, 1000 AD) for example. | This is rectified in the revised version. |
| 41 | Line 230: how many “aberrant” values you have in the entire dataset. Please give more precision to the signal processing so that researchers can compare their work with yours in the future. | The following paragraph is added to the revised version (line 306):<br>*“Furthermore, half hourly H_XLAS aberrant values due to measurement errors and values higher than 400 $Wm^{-2}$, arising from measurement saturation, were ruled out (3% of the total measurement throughout the experiment duration)”* |
| 42 | Line 247: and also gives the major sensitivity to H. See also (Gruber et | Again, the terrain here is very flat and does not induce any disturbance linked to topography. |

| | | |
|---|---|---|
| | al., 2014) for the specific analytic derivation of the sensitivity to the topography height.<br>Gruber, M. A., G.J. Fochesatto, O.K. Hartogensis, and M. Lysy. 2014: "Functional derivatives applied to error propagation of uncertainties in topography to large-aperture scintillometer-derived heat fluxes".<br>*Atmos. Meas. Tech.*, 7, 2361-2371, doi:10.5194/amt-7-2361-2014, 2014. | |
| 43 | Equations 7 and 8: assume closure of energy balance at 100% please explain how this is possible. And what are your assumptions that lead to this approximation and what is the uncertainty in this assumption. | Please see authors' response to the general comment N°4. There is no large scale advection of heat and the XLAS is located above the blending height, therefore we expect that the 100% energy closure assumption is valid. |
| 44 | Line 271: Here the authors give an estimation of G/Rn energy partition that is known to be variable not only across a given landscape but also across landscapes. This needs to be carefully estimated. This goes from 31% to very low values in dense canopies. Please be more specific and give values of this factors across all your landscapes. | Indeed G estimation was the most uncertain variable in this study, and that's why we tested three methods to compute it since based on in situ data, we generally found an accumulation of G and the daily G is rarely zero.<br>This part is discussed in the revised version (line 365). |
| 45 | Line 284: change "meteo" by "meteorological station". | This is rectified in the revised version |
| 46 | Lines 280-290: Here the authors bring parameterizations of G. And certainly it is appreciated this compilation. However, it would be best to have a discussion of how one of these parameterization is or may result more optimal for this work. It seems all the formulas were found and then tossed in this article to see what happens. – So compare your environment with the environment in which those | We used standard relationships used in models such as SEBS (Su et al., 2001). An overview of the validity of the relationship for the sole Ben Salem EC station (cereal) is illustrated in the revision (line 384). |

| | | |
|---|---|---|
| | parameterizations were developed and then decide or make some arguments about how to best use or adapt any of these parameterizations. | |
| 47 | Line 294: basically with the current satellite technology we cannot estimate diurnal cycles. However, you must know that at higher latitudes Aqua and Terra have at least six-passages a day. | We agree with Reviewer 2. |
| 48 | Line 300: I don't understand why the authors propose a=1 and b=0 and then find motivation on finding that actually these are not zero. The approximation of Rn by SW (Short Wave Downwelling) is known in micrometeorology and only works to some extent in clear skies when Rn is dominated by SW downwelling. I mean Rn can be negative but never SWdown. So, the way this paragraph is written possess a problem since it is not physically correct. | This paragraph as well as the associated result section (6.1) is rephrased in the revised version (lines 419 to 450 and lines 542 to 554) |
| 49 | Line 304: How you weigh the 10x8 km images data by the footprint? What kind of functions are used here to compute the footprint. Please explain. | Daily footprints were computed as a weighted sum of the half hourly footprints by the XLAS sensible heat flux.<br>Weighing the 10x8 km images data by the footprint means multiplying the 10x8 km result grid by the footprint (weight coefficients ranging from zero and one). |
| 50 | Line 310: replace the "temperature of soil" by "soil temperature". | This is rectified in the revised version |
| 51 | Here you mention a "reference height" and simultaneously we are talking about a heterogeneous canopy and soil and canopy. Where is that reference height? And what are the assumptions and approximations you are taking by taking this assumption. For example, you are considering some variables at soil level but others at canopy level. How the reference height represents | Reference height here is the measurement height of the meteorological forcing (2.32 m). This is precised in the revision. |

| | | |
|---|---|---|
| | both? And what are the assumptions in terms of physical processes? | |
| 52 | Eq. [15] you have here a radiative balance equation where it is assumed (without indication) that emissivity (on the left hand side ) is =1. Also this equation needs a reference level and a specific condition for the fluxes to be added and represented at the reference level. Please make sure you are accounting for all these so that the reader can fully understand what your assumptions are and where and under what conditions your analysis is valid. | Details are added to the revised version (line 467). |
| 53 | Line 319-320: is SPARSE better than TSEB? Can you give a little bit more explanation here? TSEB has modes to trait vegetation ALEXI and DIS-ALEXI. Are you saying that by incorporating aerodynamic functions makes SPARSE better than TSEB? Please clarify here what's the extent and implication of your comment on the paper. | A detailed intercomparison study between TSEB and SPARSE based on several flux stations is underway, first results indicate that bounding the fluxes simulated by both models by the potential rates given by SPARSE improves the performance of both models which have otherwise similar performances, though constrasted for the various cover types. In SPARSE the aerodynamic functions are those used in almost all Land Surface Models. ALEXI and DIS-ALEXI rely on coarse scale (few km) MSG data, and intercomparison of the ALEXI ET product and the scintillometer will also be carried out in the next future. |
| 54 | Line 325: from where you got the 30W/m2 minimum value? In some environments this will be three times G. Please justify this value. | Please see authors' response to the general comment N°3. |
| 55 | Line 334:335: Here we need to be more specific. What data is from bibliography and what data comes from RS? Please be specific. | After this sentence, bibliography, remote sensing and in situ data are detailed in the following paragraphs, however, in order to be more clear, this section will be rephrased in the revised version. |
| 56 | Line 343: Why you define an acronym MRT that is not used anymore? Acronyms that are not mentioned in the text anymore are unnecessary. | Rectified in the revised version |

| | | |
|---|---|---|
| 57 | Line 343-347: this phrase is too long and badly constructed. | This paragraph is reworded in the revised version. |
| 58 | Line 349: We need more detail here. How many days or cases have been excluded from the entire dataset. We need to know how critical is this problem. Because if it is critical then it renders the method useless. | 360 daily data were excluded from the total daily data (1033 days), the following sentence is inserted in the revised version:<br>*"(…) hence, days with missing data in MODIS pixels regarding the scintillometer footprint (35% of the acquired data) were excluded"* |
| 59 | Line 355: k1.15 need space. | Rectified in the revised version |
| 60 | Line 357: explain clump-LAI measurements. | Clump LAI is the value of the LAI of an isolated element of vegetation (tree, shrub...); if this element occupies a fraction cover f and is surrounded by bare soil, then the clump LAI value is simply equal to the area average LAI divided by f. This is specified in the revised version (Line 402). |
| 61 | Delete the word "Bibliography" from Table 1. That column is for sources and a journal peer review is a source. | Rectified in the revised version |
| 62 | Line 379: "overpasses" | Rectified in the revised version |
| 63 | Line 383: The second step need a more substance. How come you are running a 30 min fluxes based on a single TIR input? This will result in diurnal cycle of fluxes that are totally biased. I would say that this approximation is only valid for time-intervals in which the turbulence conditions are not too different form the TIR observations. | Indeed, the SPARSE model was run at a half hourly time step using the half hourly meteorological measurements ; assuming that either the stress factor or the evaporative fraction are invariant during the same day, the diurnal modelled fluxes are accounted for by recovering the diurnal course of either potential ET or available energy AE.<br>Running the SPARSE model at half hourly time step is only done to get half hourly latent heat flux in potential conditions LEpot which is equivalent to a reference evapotranspiration whose calculation depends only on half hourly climatic data. This LEpot is used later when computing daily LE based on the stress factor method (section 4.2).<br>This is better explained and more detailed in the revised version (line 508). |
| 64 | Line 396: please revise the following | Rephrased in the revised version. |

| | | |
|---|---|---|
| | wording "…complementary part to 1…" | |
| 65 | Section 4.2 seems to go around and around the subject without going down to the specifics. I think is necessary to simplify the description of methods. | Rephrased in the revised version. |
| 66 | Line 407: how you define the wet conditions here? Rain through the day, a specific amount of mm? please be more specific here. | Wet conditions are defined on the basis of a significant amount of rain recorded in the previous day (more than 5 mm). This is clarified. |
| 67 | Eq. [21] assume 100% energy balance closure. You need to justify the use of this condition. | Please see authors' response to the general comment N°4. |
| 68 | Line 429: "deduce" instead of "deduct". | Rectified in the revised version |
| 69 | Fig. 5. This figure is a very low quality without precision in the axis. Also we see only RS data here while it is announced XLAS data. | Please see authors' response to the general comment N°1. |
| 70 | Line 475: "convolving" Convolution has a very specific meaning in mathematics. Please verify the use of this term here. | In the revised version:<br>*"By convolving the XLAS footprint with the SPARSE derived H, we were able to compare the modelled values ($H\_SPARSE_{t\text{-}FP}$ ) with the XLAS measurements ($H\_XLAS_t$ )."*<br>is replaced by<br>"*SPARSE derived H was weighted by the XLAS footprint in order to be able to compare the modeled values ($H\_SPARSE_{t\text{-}FP}$) with the XLAS measurements ($H\_XLAS_t$)"* |
| 71 | Same for the use of modelled or modeled. Both expressions are fine however if your choice is to use words in British English (in this case | Rectified in the revised version |

| | | |
|---|---|---|
| | modelled) you have to be consistent all the way through your paper. | |
| 72 | Line 477: “dots”? seriously? | Rectified in the revised version |
| 73 | Line 478: Why these two days? Please give the reasons why you are specifically using those days. This is important because when scientist reading your paper would like to reproduce your results they will find no framework to produce such comparisons. | Selection criteria are added to the revised version (line 578):<br>- Day 2013-86 (24 March 2013) is in the cold season and day 185-2014 (4th July 2014) is in the warm season in order to highlight the land cover impact on LST and thus on modelled H (trees and rainfed and irrigated cereals in winter vs. only irrigated trees and vegetables in summer).<br>- Day 2013-86 (24 March 2013) shows footprint of strong south wind while the footprint of day 185-2014 is of a light north wind |
| 74 | Figure 6. I don’t understand the coordinates (Y-axis and X-axis). Also the contours of XLAS footprint have no indications. | Figure 6 as well as its caption is improved in the revised version |
| 75 | Line 482: what you mean by “hot pixel”? Please avoid jargon in the writing. | Hot pixel systematically means a pixel with high LST and low NDVI.<br>A short explanation is added to the revised version. |
| 76 | Line 489: In general models are calibrated based on EC systems and thus the deduced large-scale area-average fluxes derived from satellite remote sensing is controlled by LAS observations. | Indeed in this study, SPARSE model was run in an operational way at landscape scale without parameters calibration, since in our study area, we do not have EC station for each crop type. However, SPARSE results at field scale were already compared to EC measurement in an irrigated wheat field and a rainfed wheat field in (Boulet et al., 2015) |
| 77 | Line 490-500: In general, as the heterogeneity in vegetation, soil and eventually in topography leading to variables flows increases the divergence increases. There though cases in which even EC systems that are placed together at distance shorter than the convective ABL development verify more than 50/m2 differences (Starkenburg et al, 2015). So then results expressed here are within the range of reasonable values.<br>The only one physical explanation | Please see authors’ response to the general comment N°4. |

| | | |
|---|---|---|
| | why the LAS path by being longer would give different results is when the heterogeneity is such that the BL that develops integrates patches of different thermodynamic and turbulent properties. Then, the mention of issue is interesting but without a correct explanation is useless. | |
| 78 | Figure 7. contains features that are important to discuss since there is a change in the bias as function of the flux level. I wonder the authors to discuss this aspect from the physical aspects of the processes dominating this scale integration. | This part is improved in the revised version.<br>Indeed, possible explanations are:<br>- the XLAS measurement saturation; according to the "Kipp & Zonen LAS and XLAS instruction manual", for a path length of 4km and a scintillometer height of 20 m, saturation measurement problem starts from H values of about 300 $W.m^{-2}$<br>- Uncertainties on the correction of stability using the universal stability function<br>- Potential inconsistencies between the area average MODIS radiative temperature and the air temperature measured locally at the meteorological station. |
| 79 | Figure 10. display several cases where there is a huge divergence in stress index particularly in April and July for both spacecraft. | These individual dates are discussed in the revised version. |
| 80 | Line 562: here the authors mentioned –uncertainties- but at no point in the paper we are discussing about this. As previously mentioned uncertainties come not only in EC and XLAS observations but also in the approximation used based on 100% closure in the energy balance. It is confusing and not clear definitively. | Please see authors' response to the general comment N°4. |
| 81 | Line 565-570: give some explanation but actually is a description of the time-series. Can you provide a real-actual-explanation about what is the physical processes underlining this divergences and convergences. | The discussion part relating to Figure 11 is improved in the revised version. |
| 82 | Same from 570 to 575 | Same as comment 80. |

| | | |
|---|---|---|
| 83 | Line 588: is this the actual explanation of why there is such divergence or is this another speculation? | Same as comment 80. |
| 84 | Line 590-592: the error indicated here is extremely low now can you please indicate all- conditions in which this is valid and please circumvent this result to the specific interval of conditions in which this is actually valid. | Same as comment 80. |
| 85 | Figure 11. From where and how you got errorbars in blue trace? Figure caption is not clear. We need a accurate description of the contents in the figure. | Figure 11 caption is improved in the revised version.<br><br>Error bars for the SPARSE results show the minimum and the maximum daily evapotranspiration (ET) resulting from the three methods used to compute daily ET from instantaneous modeled ET at the time of Terra and Aqua overpasses: evaporative fraction, stress factor and residual methods, hence, six estimates of the daily modelled ET are produced. |
| 86 | Line 610: “valorize” I wonder what the authors wanted to indicate here? | This word is rather vague indeed, we precise the perspectives of this work, notably using a LSM applied at the field scale (Etchanchu et al., 2017) to analyse the scaling properties from the field to the footprint of the XLAS and the MODIS pixels similarly to the reference provided by Reviewer 2 (Bai et al., 2015). |
| 87 | SVAT seems not to have been defined earlier. | Rectified in the revised version. |

References:


Bai, J., Jia, L., Liu, S., Xu, Z., Hu, G., Zhu, M., and Song, L.: Characterizing the footprint of eddy covariance system and large aperture scintillometer measurements to validate satellite-based surface fluxes, IEEE Geoscience and Remote Sensing Letters, 12, 943-947, 2015.

Boulet, G., Braud, I., and Vauclin, M.: Study of the mechanisms of evaporation under arid conditions using a detailed model of the soil–atmosphere continuum. Application to the EFEDA I experiment, Journal of Hydrology, 193, 114-141, https://doi.org/10.1016/S0022-1694(96)03148-4, 1997.

Boulet, G., Mougenot, B., Lhomme, J. P., Fanise, P., Lili-Chabaane, Z., Olioso, A., Bahir, M., Rivalland, V., Jarlan, L., Merlin, O., Coudert, B., Er-Raki, S., and Lagouarde, J. P.: The SPARSE model for the prediction of water stress and evapotranspiration components from thermal infra-red data and its evaluation over irrigated and rainfed wheat, Hydrol. Earth Syst. Sci., 19, 4653-4672, 10.5194/hess-19-4653-2015, 2015.

Boulet, G.: SPARSE online documentation, http://tully.ups-tlse.fr/gilles.boulet/sparse 2017.

De Bruin, H., Kohsiek, W., and Van den Hurk, B.: A verification of some methods to determine the fluxes of momentum, sensible heat, and water vapour using standard deviation and structure parameter of scalar meteorological quantities, Boundary-Layer Meteorology, 63, 231-257, 1993.

Etchanchu, J., Rivalland, V., Gascoin, S., Cros, J., Brut, A., and Boulet, G.: Effects of multi-temporal high-resolution remote sensing products on simulated hydrometeorological variables in a cultivated area (southwestern France), Hydrol. Earth Syst. Sci. Discuss., 2017, 1-23, 10.5194/hess-2016-661, 2017.

Giorgi, F., and Avissar, R.: Representation of heterogeneity effects in earth system modeling: Experience from land surface modeling, Reviews of Geophysics, 35, 413-437, 1997.

Giorgi, F., and Lionello, P.: Climate change projections for the Mediterranean region, Global and planetary change, 63, 90-104, 2008.

Gruber, M., and Fochesatto, G. J.: A new sensitivity analysis and solution method for scintillometer measurements of area-averaged turbulent fluxes, Boundary-layer meteorology, 149, 65-83, 2013.

Kustas, W. P., and Norman, J. M.: Evaluation of soil and vegetation heat flux predictions using a simple two-source model with radiometric temperatures for partial canopy cover, Agricultural and Forest Meteorology, 94, 13-29, https://doi.org/10.1016/S0168-1923(99)00005-2, 1999.

Minacapilli, M., Ciraolo, G., D Urso, G., and Cammalleri, C.: Evaluating actual evapotranspiration by means of multi-platform remote sensing data: a case study in Sicily, IAHS PUBLICATION, 316, 207., 2007.

Monteith, J., and Unsworth, M.: Principles of environmental physics, Academic Press, 2007.

Saadi, S., Simonneaux, V., Boulet, G., Raimbault, B., Mougenot, B., Fanise, P., Ayari, H., and Lili-Chabaane, Z.: Monitoring Irrigation Consumption Using High Resolution NDVI Image Time Series: Calibration and Validation in the Kairouan Plain (Tunisia),

Remote Sensing, 7, 13005, 2015.

Samain, B., Simons, G. W., Voogt, M. P., Defloor, W., Bink, N.-J., and Pauwels, V.: Consistency between hydrological model, large aperture scintillometer and remote sensing based evapotranspiration estimates for a heterogeneous catchment, Hydrology and Earth System Sciences, 16, 2095-2107, 2012.

Shuttleworth, W. J., and Wallace, J.: Evaporation from sparse crops an energy combination theory, Quarterly Journal of the Royal Meteorological Society, 111, 839-855, 1985.

Solignac, P. A., Brut, A., Selves, J. L., Béteille, J. P., Gastellu-Etchegorry, J. P., Keravec, P., Béziat, P., and Ceschia, E.: Uncertainty analysis of computational methods for deriving sensible heat flux values from scintillometer measurements, Atmos. Meas. Tech., 2, 741-753, 10.5194/amt-2-741-2009, 2009.

Su, Z., Schmugge, T., Kustas, W. P., and Massman, W. J.: An Evaluation of Two Models for Estimation of the Roughness Height for Heat Transfer between the Land Surface and the Atmosphere, Journal of Applied Meteorology, 40, 1933-1951, 10.1175/1520-0450(2001)040<1933:aeotmf>2.0.co;2, 2001.

Tatarskii, V. I.: Wave propagation in turbulent medium, Wave Propagation in Turbulent Medium, by Valerian Ilich Tatarskii. Translated by RA Silverman. 285pp. Published by McGraw-Hill, 1961., 1961.

# Assessment of actual evapotranspiration over a semi-arid heterogeneous land surface by means of coupled low resolution remote sensing data with energy balance model: comparison to extra Large Aperture Scintillometer measurements

Sameh Saadi[1,2], Gilles Boulet[1], Malik Bahir[1], Aurore Brut[1], Bernard Mougenot[1], Pascal Fanise[1], Vincent Simonneaux[1], and Zohra Lili Chabaane[2]

[1]Centre d'Etudes Spatiales de la Biosphère, Université de Toulouse, CNRS, CNES, IRD, UPS, Toulouse, France

[2] Université de Carthage / Institut National Agronomique de Tunisie/ LR17AGR01-GREEN-TEAM, Tunis, Tunisie;

*Correspondence to*: Sameh Saadi (saadi_sameh@hotmail.fr)

**Abstract.**

In semi-arid areas, agricultural production is restricted by water availability; hence efficient agricultural water management is a major issue. The design of tools providing regional estimates of evapotranspiration (ET), one of the most relevant water balance fluxes, may help the sustainable management of water resources.
Remote sensing provides periodic data about actual vegetation temporal dynamics (through the Normalized Difference Vegetation Index NDVI) and water availability under water stress (through the land surface temperature LST) which are crucial factors controlling ET.
In this study, spatially distributed estimates of ET (or its energy equivalent, the latent heat ~~fluxes~~flux LE) in the Kairouan plain (Central Tunisia) were computed by applying the Soil Plant Atmosphere and Remote Sensing ~~Evapotraspiration~~Evapotranspiration (SPARSE) model fed by low resolution remote sensing data (Terra and Aqua MODIS). The work goal was to assess the operational use of the SPARSE model and the accuracy of the ~~modelled~~modeled i) sensible heat flux (H) and ii) daily ET over a heterogeneous semi-arid landscape with a complex land cover (*i.e.* trees, winter cereals, summer vegetables).
~~The SPARSE's layer approach~~SPARSE was run to compute instantaneous estimates of H and LE fluxes at the satellite overpass time. The good correspondence ($R^2$= 0.60 and 0.63 and RMSE=57.89 ~~W/m~~$Wm^{-2}$ and 53.85 ~~W/m~~$Wm^{-2}$; for Terra and Aqua, respectively) between instantaneous H estimates and large aperture scintillometer (XLAS)~~'s~~ H measurements along a ~~pathlength~~path length of 4 km over the study area showed that the SPARSE model presents satisfactory accuracy. Results showed that, despite the fairly large scatter, the instantaneous LE can be suitably estimated at large scale (RMSE=47.20 ~~W/m~~$Wm^{-2}$ and 43.20 ~~W/m~~$Wm^{-2}$; for Terra and Aqua, respectively and $R^2$= 0.55 for both satellites). Additionally, water stress was investigated by comparing ~~modelled~~modeled (SPARSE~~-derived) to~~) and observed (XLAS~~-derived~~) water stress values; we found that most points were located within a 0.2 confidence interval, thus the general tendencies are well reproduced.~~.~~
Even though extrapolation of instantaneous latent heat flux values to daily totals was less obvious, daily ET estimates are deemed acceptable.

KEYWORDS: Evapotranspiration, Remote sensing, SPARSE model, scintillometer, water stress.

Mis en forme : Gauche

Mis en forme : Couleur de police : Automatique

Mis en forme : Police :Italique, Non souligné, Couleur de police : Automatique

Mis en forme : Non souligné, Couleur de police : Automatique

Mis en forme : Couleur de police : Automatique

## 1 Introduction

In water scarce regions, especially arid and semi-arid areas, the sustainable use of water by resource conservation as well as the use of appropriate technologies to do so is a priority for agriculture (Amri et al., 2014; Pereira et al., 2002).

Water use rationalization is needed especially for countries actually suffering from water scarcity, or for countries that probably would suffer from water restrictions according to climate change scenarios. Indeed, the Mediterranean region is one of the most prominent "hot spots" in future climate change projections (Giorgi and Lionello, 2008) due to an expected larger warming than the global average and to a pronounced increase in precipitation inter-annual variability. The major part of the southern Mediterranean countries, among others Tunisia, already suffer from water scarcity and show a growing water deficit, due to the combined effect of the water needs growth (soaring demography and irrigated areas extension), and the reduction of resources (temporary drought and/or climate change). This implies that closely monitoring the water budget components is a major issue (Oki and Kanae, 2006).

The estimation of evapotranspiration (ET) is of paramount importance since it represents the preponderant component of the terrestrial water balance; it is the second ~~greatest~~largest component after precipitation (Glenn et al., 2007); hence ET quantification is a key factor for scarce water resources management. Direct measurement of ET is only possible at local scale (single ~~plot~~field) using the eddy~~-~~ covariance method for example; whereas, it is much more difficult at larger scales (irrigated perimeter or watershed) due to the complexity not only of the hydrological processes (Minacapilli ~~and Ciraolo,~~et al., 2007)~~.~~ but also of the hydro-meteorological processes. Indeed, at landscape scale, surface heterogeneity influences regional and local climate, inducing for example cloudiness, precipitation and temperature patterns differences between areas of higher elevation (hills and mountains surrounding the Kairouan plain) and the plain downstream. Moreover, at these scales, land cover is usually heterogeneous and this affects the land-atmosphere exchanges of heat, water and other constituents (Giorgi and Avissar, 1997). ET estimates for various temporal and spatial scales, from hourly to monthly to seasonal time steps, and from field to global scales, are required for hydrologic applications in water resource management (Anderson et al., 2011). Techniques using remote sensing (RS) information are therefore essential when dealing with processes that cannot be represented by point measurements only (Su, 2002).

In fact, the contribution of RS in vegetation's physical ~~properties~~characteristics monitoring on large areas have been identified for years (Tucker, 1978); RS provides periodic data about some major ET drivers, amongst others, land surface temperature and vegetation properties (e.g. Normalized Difference Vegetation Index NDVI and Leaf Area Index LAI) from ~~plot~~field to regional scales (Li et al., 2009; Mauser and Schädlich, 1998). Many methods using remotely-sensed data to estimate ET are reviewed in Courault et al~~.~~ ~~(2005).~~ (2005). ICARE (Gentine et al., 2007) and SiSPAT (Braud et al., 1995) are examples of complex physically based Land Surface Models (LSM) using RS data. They include a detailed description of the vegetation water uptake in the root zone, the interactions between groundwater, root zone and surface water. However, the lateral surface and subsurface flows are neglected. This can lead to inaccurate results when applied in areas where such interactions are important (Overgaard et al., 2006).

Mis en forme : Non souligné, Couleur de police : Automatique

Mis en forme : Couleur de police : Automatique

Code de champ modifié

Moreover, RS can provide estimates of large area fluxes in remote locations, but those estimates are based on the spatial and temporal scales of the measuring systems and thus vary one from another. Hence, one solution is to upscale local micrometeorological measurements to larger spatial scales in order to acquire an optimum representation of land-atmosphere interactions (Samain et al., 2012). However, such up-scaling process is not always possible and results might not be reliable in comparison to the RS distributed products.

Water and energy exchange in the soil-plant-atmosphere continuum have been simulated through several land surface models (Bastiaanssen et al., 2007; Feddes et al., 1978). Among them, two different approaches use remote sensing data to estimate spatially distributed ET (Minacapilli et al., 2009): one is based on the soil water balance (SWB) and ~~on~~one that solves the surface energy budget (SEB). The SWB approach exploits only visible-near-infrared (VIS-NIR) observations to perceive the spatial variability of crop parameters. The SEB ~~modelling~~modeling approach uses visible (VIS), near-infrared (NIR) and thermal (TIR) data to solve the SEB equation by forcing remotely-sensed estimates of the SEB components (mainly the land surface temperature LST). In fact, there is a strong link between water availability in the soil and surface temperature under water stress, hence, in order to estimate soil moisture status as well as actual ET at relevant space and timescales, information in the TIR domain (3–15 µm) is frequently used (Boulet et al., 2007). The SWB approach has the advantage of high resolution and frequency VIS-NIR remote sensing data availability against limited availability of high resolution thermal imagery for the SEB approach. Indeed, satellite data such as Landsat or Advanced Spaceborne Thermal Emission and Reflection Radiometer (ASTER) provide ~~accurate~~ field scale (30–100 m) estimates of ET (Allen et al., 2011), but they have a low temporal resolution (16 day-monthly) (Anderson et al., 2011).

Code de champ modifié

Code de champ modifié

The RS-based SWB models provide ~~estimation~~estimates of ET, soil water content, and irrigation requirements in a continuous way. For instance, at ~~plot~~field scale, ~~accurate~~ estimates of seasonal ET and irrigation can be obtained by SWB modeling using high resolution remote sensing forcing as done in the study with the SAtellite Monitoring of IRrigation (SAMIR) model by Saadi et al ~~(~~, (2015) over the Kairouan plain. However, for an appropriate estimation of ET, the SWB model requires knowledge of the water inputs (precipitation and irrigation) and an assessment of the extractable water from the soil (mostly derived from ~~, say,~~ the soil moisture characteristics: actual available water content in the root zone, wilting point and field capacity ~~–~~), whereas, significant ~~bias~~biases are found mainly when dealing with large areas and long periods, due to the spatial variability of the water inputs uncertainties as well as the inaccuracy in estimating other flux components such as the deep drainage (Calera et al., 2017). Hence, the major limitation of the SWB method is the high number of needed inputs whose ~~estimations are likely~~estimation is highly uncertain especially over a heterogeneous land surface due to hydrologic processes complexity. Moreover, spatially distributed SWB models ~~(~~, typically those using the Food and Agriculture Organization-FAO guidelines (Allen et al., 1998) for crop ET estimation~~),~~ generally parameterize the vegetation characteristics on the basis of land use maps (Bounoua et al., 2015; Xie et al., 2008), and different parameters are used for different land use classes. Nevertheless, SWB modelers generally do not have the possibility to carry out remote sensing-based land use change mapping due to time, budget, or capacity constraints and use often very generic classes potentially leading to modeling errors (Hunink et al., 2017). In addition, the lack of data about the soil properties (controlling field capacity, wilting point and the water retention) as well as the actual root depths ~~for heterogeneous areas crops~~, lead to limited practical use of the SWB models (Calera et al., 2017). The same apply to the soil evaporation whose estimation generally rely

on the FAO guidelines approach (Allen et al., 1998). ~~Although, it was shown that under high evaporation conditions, the FAO-56~~Although, it was shown that under high evaporation conditions, the FAO-56 (Allen et al., 1998) daily evaporation computed on the basis of the readily evaporable water (REW) is overestimated at the beginning of the dry down phase (*i.e.* the period after rain or irrigation where the soil moisture is decreasing due to evapotranspiration and drainage, ~~(~~Mutziger et al., 2005; Torres and Calera, 2010). Hence, to improve its estimation a reduction factor proposed by Torres and Calera (2010) was applied to deal with this problem in several studies (e.g. Odi-Lara et al., 2016; Saadi et al., 2015). ~~Furthermore, since actual ET is computed based on actual soil moisture status, the limited knowledge of the actual farmers' irrigation scheduling is a further critical limitation for SWB modeling.~~Furthermore, SWB models such as SWAP (Kroes, 2017), Cropsyst (Stöckle et al., 2003), AquaCrop (Steduto et al., 2009) and SAMIR (Simonneaux et al., 2009) are able to take irrigation into account, either as an estimated amount provided by the farmer (as an input if available) or a predicted amount through a module triggering irrigation according to, say, critical soil moisture levels (as an output). However, the limited knowledge of the actual irrigation scheduling is a critical limitation for the validation protocol of irrigation requirements estimates by SWB modeling. Therefore, SWB modelers must deal with the lack of information about real irrigation which induces unreliable estimations.

Consequently, ET estimation at regional scale is often achieved using SEB approaches, by combining surface temperature from medium to low resolution (kilometer scale) remote sensing data with vegetation parameters and meteorological variables (Liou and Kar, 2014). Recently, many efforts have been made to feed remotely sensed surface temperature into ET ~~modelling~~modeling platforms in combination with other critical variables, e.g., NDVI and albedo (Kalma et al., 2008; Kustas and Anderson, 2009). A wide range of satellite-based ET models were developed, and these methods are reviewed in (Liou and Kar ~~(~~, 2014). The majority of SEB-based models are ~~"~~single-source models~~",~~; their algorithms compute a total latent heat flux as the sum of the evaporation and the transpiration components using a remotely sensed surface temperature. However, separate estimates of evaporation and transpiration makes the ~~"~~dual-source models" more useful for agrohydrological applications (water stress detection, irrigation monitoring etc.) (Boulet et al., 2015).

Contrarily to SWB models, most SEB models are run in their most standardized version, using observed remote sensing-based parameters such as albedo in conjunction with a set of input parameters taken from literature or *in situ* data. On the other hand, the SEB model validation with enough data in space and time is difficult to achieve, due to the limited availability of high resolution thermal images (Chirouze et al., 2014). Therefore, it is usually possible to evaluate SEB models results only at similar scale (km) to medium or low resolution images. Indeed, the pixel size of thermal remote sensing images, except for the scarce Landsat7 images (60 m), covers a range of 1000 m (Moderate Sensors Resolution Imaging Spectroradiometer MODIS), to the order of 4000 m (Geostationary Operational Environmental Satellite GOES). However, direct methods measuring sensible heat fluxes (eddy covariance ~~EC~~ for example) only provide point measurements with a footprint considerably smaller than a satellite pixel ~~(except for Landsat).~~ Therefore, scintillometry techniques have emerged as one of the best tools aiming to quantify averaged fluxes over heterogeneous land surfaces (Brunsell et al., 2011). They provide ~~average~~area-averaged sensible heat ~~estimates~~flux over areas comparable to those observed by satellites (Hemakumara et al., 2003; Lagouarde et al., ~~2002b~~2002). Scintillometry can provide sensible heat using different wavelengths~~,~~ (optical and microwave wavelength ranges), aperture sizes (15-30 cm) and configurations (long-path and short-path scintillometry) (Meijninger et al., 2002). The upwind area contributing to the flux (*i.e.*

**Code de champ modifié**

**Mis en forme :** Police :(Par défaut) Arial, Italique

**Mis en forme :** Police :Italique, Non souligné, Couleur de police : Automatique

the flux footprint) varies as wind direction and atmospheric stability~~ -~~, and must be estimated for the surface measurements in order to compare them to SEB estimates of the flux which are representative of the pixel (Brunsell et al., 2011). Assessing the upwind area contributing to the flux can be done using several footprint models (Schmid, 2002). ~~The LAS technique has been validated over heterogeneous landscapes against EC~~Although footprint analysis ensures ad hoc spatial intersecting area between ground measurements and satellite-based surface fluxes, the spatial heterogeneity at subpixel scale should be further considered in validating low resolution satellite data (Bai et al., 2015). The LAS technique has been validated over heterogeneous landscapes against eddy covariance measurements (Bai et al., 2009; Chehbouni et al., 2000; Ezzahar et al., 2009) and also against ~~modelled~~modeled fluxes (Marx et al., 2008; Samain et al., 2012; Watts et al., 2000). Few studies dealt with ~~extra large aperture scintillometer~~eXtra Large Aperture Scintillometer (XLAS) data (Kohsiek et al., 2006; Kohsiek et al., 2002; Moene et al., 2006). Historical survey, theoretical background as well as recent works in applied research concerning scintillometry are reviewed in De Bruin and Wang (2017). Since the scintillometer ~~only~~ provides ~~spatially averaged~~large-scale area-average sensible heat flux (H_XLAS), the corresponding latent heat flux (LE_XLAS) can then be computed as the energy balance residual term (LE_XLAS =Rn-G-H_XLAS), hence, the estimation of a representative value for the available energy (AE =Rn-G) is always crucial for the accuracy of the retrieved values of LE_XLAS. This assumption is valid only under the similarity hypothesis of Monin-Obukhov (MOST) (Monin and Obukhov, 1954), *i.e.* surface homogeneity and stationary flows. These hypothesis are verified in our study area where topography is flat, and landscape is heterogeneous only from an agronomic point of view since we find different land uses (cereals, market gardening and fruit trees mainly olive trees with considerable spacing of bare soil); however, this heterogeneity in landscape features at field scale is randomly distributed and there is no drastic change in height and density of the vegetation at the scale of the XLAS transect (*i.e.* little heterogeneity at the km scale, most MODIS pixels have similar NDVI values for instance).

In this study, spatially distributed estimates of surface energy fluxes (sensible heat H and latent heat fluxes LE) over an irrigated area located in the Kairouan plain (Central Tunisia) were obtained by the SEB method, using the ~~"layer" approach (a resistance network that relates the soil and vegetation heat sources to a main reference level using a series-electrical branching) of the~~ Soil Plant Atmosphere and Remote Sensing Evapotraspiration (SPARSE) model (Boulet et al., 2015) fed by 1-km thermal data and 1-km NDVI data from MODIS sensors on Terra and Aqua satellites.

The main objective of this paper is to compare the modeled H and LE ~~obtained using~~simulated by the SPARSE model with, respectively, the H measured by the XLAS and the LE reconstructed from the XLAS measurements acquired during two years over a large, heterogeneous area. We explore the consistency between the instantaneous H and LE estimates at the satellite overpass time, the water stress estimates and also ET derived at daily time step from both approaches.

## 2 Experimental site and datasets

### 2.1 Study area

The study site is a semi-arid region located in central Tunisia, the Kairouan plain (9°23′−10°17′E, 35°1′−35°55′N, (Figure 1). The landscape is mainly flat, and the vegetation is dominated by agricultural

**Mis en forme :** Non souligné, Couleur de police : Automatique

**Mis en forme :** Police :+Titres CS, Non souligné, Couleur de police : Automatique

**Mis en forme :** Police :+Titres CS, Non souligné, Couleur de police : Automatique

**Mis en forme :** Police :+Corps

**Mis en forme :** Non souligné, Couleur de police : Automatique

**Mis en forme :** Couleur de police : Automatique

production (cereals, olive groves, fruit trees, market ~~gardens~~gardening, Zribi et al., 2011). Water management in the study area is typical of semi-arid regions with an upstream sub-catchment that transfers surface and subsurface flows collected by a dam (the El Haouareb dam), and a downstream plain (Kairouan plain) supporting irrigated agriculture (Figure 1). Agriculture consumes more than 80% of the total amount of water extracted each year from the Kairouan aquifer (Poussin et al., 2008). Most farmers in the plain uses their own wells to extract water for irrigation (Pradeleix et al., 2015), while a few depends on public irrigation schemes based on collective networks of water distribution pipelines all linked to a main borehole. The crop intensification in the last decades, associated to increasing irrigation, has led to growing water demand, and an overexploitation of the groundwater (Leduc et al., 2004).

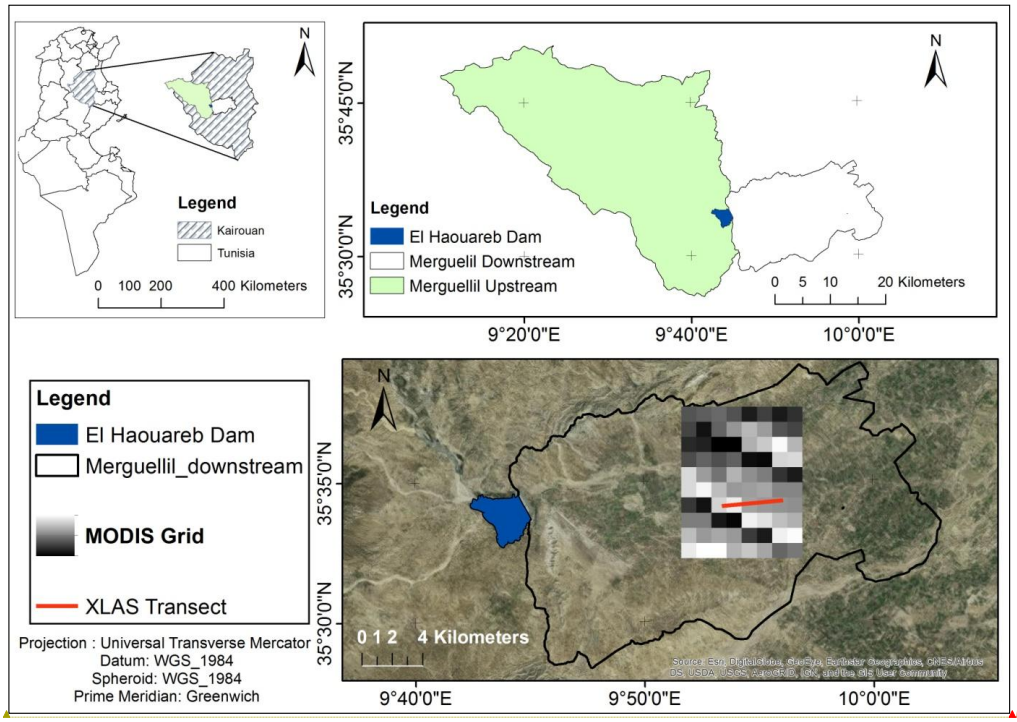


**Figure 1 : The study area: the downstream Merguellil sub-basin is the so called Kairouan plain; MODIS grid is the extracted 10 km × 8 km MODIS sub-image and in red the scintillomter XLAS transect**

## 2.2 Experimental ~~Setup~~ set-up and remote sensing data

An optical Kipp and Zonen Extra Large Aperture Scintillometer (XLAS) was operated continuously for more than two years (1 March 2013 to 3 June 2015) over a relatively flat terrain~~.~~ (maximum difference in elevation of about 18 m). The scintillometer consists in a ~~double device, with a~~ transmitter and a receiver both with an aperture diameter of 0.3 m, which allows longer path length. The wavelength of the light beam emitted by the transmitter is 940 nm. The transmitter was located on ~~the~~an eastern water tower (coordinates: 35° 34' 0.7" N; 9° 53' 25.19" E; 127 m above sea level) and the receiver on ~~the~~a western water tower (coordinates: 35° 34' 17.22" N; 9° 56' 7.30"E; 145 m above sea level) separated by a path length of 4 km (Figure 2). ~~Both instruments were installed at 20 m height.~~

**Mis en forme :** Non souligné, Couleur de police : Automatique

**Mis en forme :** Couleur de police : Automatique

**Mis en forme :** Police par défaut

The scintillometer transect was above mixed vegetation canopy: trees (mainly olive orchards) with some annual crops (cereals and market gardening~~).~~) and the mean vegetation height is estimated about 1.17m along the transect. Both instruments were installed at 20 m height as recommended in the Kipp & Zonen instruction manual for LAS & XLAS (KIPP&ZONEN, 2007). At this height and for a 4-km path length, the devices are high enough to minimize measurement saturation and assumed to be above or close to the blending height where MOST applied.

Furthermore, two ~~similar~~automatic Campbell Scientific (Logan, USA) eddy covariance (EC) ~~systems~~flux stations were also positioned at the same level on the two water tower top platforms. Half hourly ~~sensible heat flux, wind speed components~~turbulent fluxes in the western and ~~wind direction~~ the eastern EC stations were measured used a sonic anemometer ~~CSAT 3D~~CSAT3 (Campbell Scientific, USA) at a rate of 20 Hz and a sonic anemometer ~~RM81000~~RM 81000 (Young, USA) at a rate of 10 Hz, respectively. ~~These EC set ups (~~The western station data were more reliable with less measurement errors and gaps, hence, the western EC set-up was used to initialise friction velocity u* ~~and wind direction measurements) were used to compute~~values and the Obukhov length Lo in the scintillometer ~~derived fluxes as well as footprints.~~ flux computation (sect.3.1).

Half hourly standard meteorological measurements including incoming long wave radiation *i.e.* global incoming radiation~~, wind speed,~~ ($Rg_{30}$), the incoming longwave radiation *i.e* atmospheric radiation ($R_{atm\text{-}30}$), wind speed ($u_{30}$), wind direction ($u_{d\text{-}30mn}$), air temperature ($T_{a\text{-}30}$) and relative humidity~~, rainfall~~ ($RH_{a\text{-}30}$) and barometric pressure ($P_{30}$) were recorded using an automated weather station installed in the study area (Figure 2~~). Hereafter, this weather station is~~), referred as the Ben Salem meteorological station (35° 33' 1.44" N; 9° 55' 18.11"E). Meteorological data were used either to force the SPARSE model or as input data in XLAS derived sensible and latent heat flux. The global incoming radiation was also used in the extrapolation method to scale instantaneous observed (sect. 3.3.2) and modeled (sect. 4.2) available energy as well as modeled sensible heat flux (sect. 4.2) to daily values.

In addition, ~~a~~an EC flux station ~~based on the eddy correlation method~~, referred as the Ben Salem flux station (few tens of meters away from the meteorological station) was installed from November 2012 to June 2013 in an irrigated wheat field~~. This station measuring continuously LE was used to perform the extrapolation of instantaneous energy balance components at daily time scale.~~ (Figure 2) measuring half hourly convective fluxes exchanged between the surface and the atmosphere ($H_{BS\text{-}30}$ and $LE_{BS\text{-}30}$) combined with measurements of the net radiation $Rn_{BS\text{-}30}$ and the soil heat flux $G_{BS\text{-}30}$. Net radiation and soil heat flux measurements were transferred to the meteorological station from June 2013 till June 2015. Since, there are no Rn and G measurements in the two water towers EC stations, $Rn_{BS}$ and $G_{BS}$ measurements were among the inputs data to derive sensible and latent heat fluxes from the XLAS measurements. In addition, measured available energy ($AE_{BS}=Rn_{BS}-G_{BS}$) and $H_{BS}$ were used to calibrate the extrapolation relationship of the available energy and the sensible heat flux, respectively (sect. 3.3.2 and 4.2).

**Mis en forme :** Police :+Corps, Couleur de police : Bleu foncé

**Mis en forme :** Non Exposant/ Indice

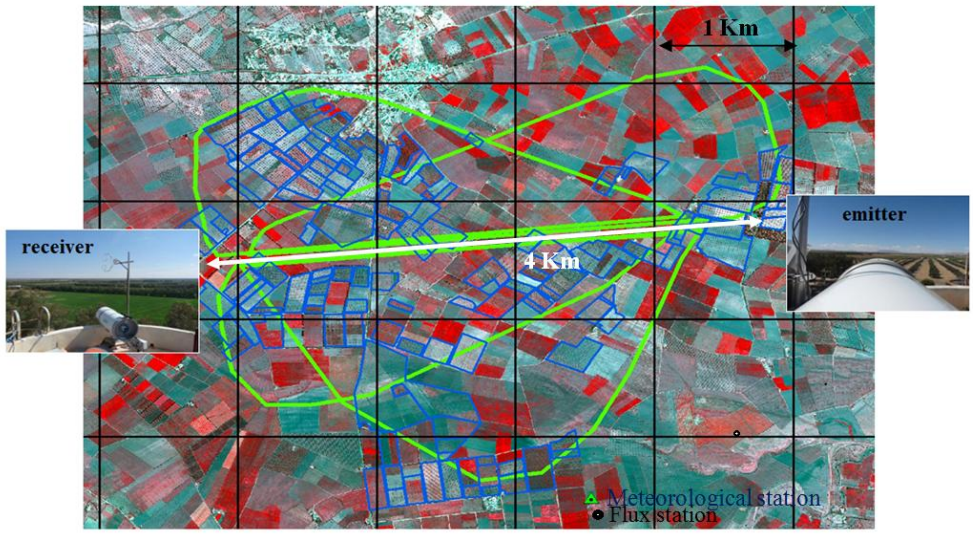


Mis en forme

Remotely sensed data were acquired for the study period (1st September 2012 to 30th June 2015) at the resolution of the MODIS sensor at 1 km, embarked on board of the satellites Terra (overpass time around 10:30 local solar time) and Aqua (overpass time around 13:30 local solar time). Downloaded MODIS products were (*i*) MOD11A1 and MYD11A1 for Terra and Aqua, respectively (land surface temperature LST, surface emissivity ε and viewing angle ϕ), (*ii*) MOD13A2 and MYD13A2 for Terra and Aqua, respectively (NDVI) and (*iii*) MCD43B1, MCD43B2 and MCD43B3 (albedo α). These MODIS data provided in sinusoidal projection were reprojected in UTM using the MODIS Reprojection Tool. Then, sub-images of 10 km × 8 km centered on the XLAS transect (Figure 1) were extracted. The daily MODIS LST and viewing angle, 8-day MODIS albedo, and 16-day MODIS NDVI contain some missing or unreliable data; hence, days with missing data (35% of all dates) in MODIS pixels regarding the scintillometer footprint (see later footprint computation in sect.3.2) were excluded. Albedo products (MCD43) are available every 8 days; the day of interest is the central date. Both Terra and Aqua data are used in the generation of this product, providing the highest probability for quality input data and designating it as a combined product. Moreover, the 1km/16days NDVI products (MOD13A2/MYD13A2) are available every 16 days and separately for Terra and Aqua. Algorithms generating this product operate on a per-pixel basis and require multiple daily observations to generate a composite NDVI value that will represent the full period (16 days). For both products, data are linearly interpolated over the available dates in order to get daily estimates. For each pixel, the quality index supplied with each product is used to select the best data.

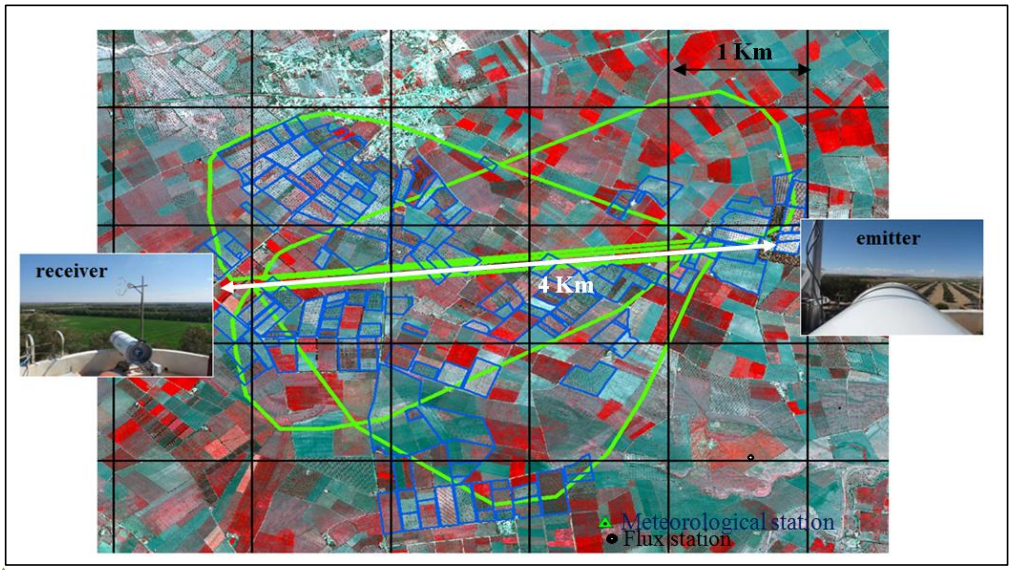


**Figure 2 : XLAS ~~Set~~set-up ~~(~~: XLAS transect (white), for which the emitter and the receiver ~~locations and~~ are located at the extremity of each white arrow, half-hourly XLAS footprint ~~in~~for selected typical wind conditions (green), MODIS grid (black), ~~trees plots~~orchards (blue) and the location of the Ben Salem meteorological and ~~the wheat field~~ flux ~~station. This figure illustrates~~stations. Background is a three ~~colour~~color (red, green, blue) composite of SPOT5 bands 3~~, 2 and 1~~ (NIR), 2 (VIS-red) and 1(VIS-green) acquired on 9th April 2013 and showing in red the cereal plots.**

## 3 Extra Large aperture scintillometer~~:~~ (XLAS): data processing

### 3.1 Scintillometer derived fluxes

Scintillometer ~~is~~measurements are based on the scintillation ~~method. Fluxes~~theory; fluxes of sensible heat and momentum cause atmospheric turbulence close to the ground, and ~~creates~~create, with surface evaporation, refractive index fluctuations due mainly to air temperature and humidity fluctuations (Hill et al., 1980). The fluctuations intensity of refractive index is directly linked to sensible and latent heat fluxes.

The light beam emitted by the XLAS transmitter towards the receiver is dispersed by the atmospheric turbulence. The scintillations representing the intensity fluctuations are analyzed at the XLAS receiver and are expressed as the structure parameter of the refractive index of air integrated along the optical path $C_{n^2}$ ~~[~~($m^{-2/3}$~~]~~) ~~(Lagouarde et al., 2002a; Wang et al., 1978)~~(Tatarskii, 1961). The sensitivity of the scintillometer to $C_{n^2}$ along the ~~bean~~beam is not uniform and follows a bell-shape curve~~. As transmitter and receiver apertures are equal,~~ due to the ~~curve is symmetrical. As a result~~ symmetry of the ~~scintillometer~~devices. This means that the measured flux is more sensitive to ~~turbulences, hence to fluxes, in the middle of its path~~sources located towards the transect centre and is less affected by those close to the transect extremities.

In order to compute the XLAS sensible heat flux~~,~~ $C_n^2$ was converted to the structure parameter of temperature turbulence $C_T^2$ ~~[K$^2$ m~~($K^2 m^{-2/3}$~~]~~, by introducing the Bowen ratio (ratio between sensible and latent heat fluxes), hereafter referred to as β, which is a temperature /humidity correlation factor. Moreover, the height of the scintillometer beam above the surface varies along the path. In our study site, the terrain is very flat leading to little beam height variation across the landscape, except for what is induced by the different roughness of the

**Mis en forme :** Couleur de police : Automatique

**Mis en forme :** Police :Non Gras

**Mis en forme :** Couleur de police : Automatique

**Mis en forme :** Couleur de police : Automatique

**Code de champ modifié**

**Mis en forme :** Police :+Titres CS

**Mis en forme :** Police :+Titres CS

**Mis en forme :** Police :10 pt

**Mis en forme :** Corps de texte, Justifié, Interligne : 1.5 ligne

**Mis en forme :** Police :10 pt

**Mis en forme :** Police :10 pt

**Mis en forme :** Police :10 pt

**Mis en forme :** Police :10 pt

**Mis en forme :** Police :10 pt

individual fields. Since the interspaces between trees are large, the effective roughness of the orchards is not significantly different from that of annual crops fields. Consequently, $C_n^2$ and therefore $C_T^2$ are not only averaged horizontally but vertically as well.

At visible wavelengths, the refractive index is more sensitive to temperature than humidity fluctuations. Then, we can relate the $C_{n^2}$ to $C_{T^2}$ ~~:~~as follows:

$$C_{n^2} \approx \left(\frac{-0.78 \times 10^{-6} \times P}{T^2}\right)^2 = \left(\frac{-0.78 \times 10^{-6} \times P}{T^2}\right)^2 C_{T^2}\left(1 + \frac{0.03}{\beta}\right)^2 \quad (1)$$

with T is the air temperature (°K) and P is the atmospheric pressure (Pa).

Green and Hayashi (1998) proposed another method to compute theXLAS sensible heat fluxflux (H_XLAS) assuming full energy budget closure and using an iterative process without the need of the Bowen ratioβ as an input parameter. This method is called the "β-closure method" (BCM, This method is called the "β-closure method" (BCM, Solignac et al., 2009;Twine et al., 2000). . In the calculation algorithm, β is estimated iteratively with the BCM method, as described in Solignac et al. (2009) with initial guess using $Rn_{BS}$ and $G_{BS}$ from the Ben Salem flux station and initial $u_*$ coming from the western water tower EC station.

Then, the similarity relationship proposed by (Andreas, 1988) is used to relate the $C_{T^2}$ to the temperature scale $T_*$ in unstable atmospheric conditions as follows:

$$\frac{C_{T^2}(z_{LAS} - d)^{\frac{2}{3}}}{T_*^2} = 4.9 \times \left(1 - 6.1 \times \left(\frac{z_{LAS} - d}{L_O}\right)^{-\frac{2}{3}}\right)\left(1 - 6.1\left(\frac{z_{LAS} - d}{L_O}\right)^{-\frac{2}{3}}\right) \quad (2)$$

andAnd for stable atmospheric conditions:

$$\frac{C_{T^2}(z_{LAS} - d)^{\frac{2}{3}}}{T_*^2} = 4.9 \times \left(1 + 2.2 \times \left(\frac{z_{LAS} - d}{L_O}\right)^{\frac{2}{3}}\right)\left(1 + 2.2\left(\frac{z_{LAS} - d}{L_O}\right)^{\frac{2}{3}}\right) \quad (3)$$

where $L_O$ (m) is the Obukhov length , $Z_{LAS}$ (m) is the scintillometer effective height, and d (m) is the displacement height, which corresponds to 2/3 of the averaged vegetation height $z_v$ (see Sect. 4.1).

From $T_*$ and the friction velocity, $u_*$, $u_*$ (computed based on an iteration approach in the BCM method), the sensible heat flux can be derived as follows:

$$H = -\rho c_p T_* u_* \quad (4)$$

where $\rho$ (kg mkgm$^{-3}$) is the density of air and $c_p$ (J KgJkg$^{-1}$K$^{-1}$ K$^{-1}$) is) the specific heat of air at constant pressure.

XLAS sensible heat flux ( H_XLAS) was computed at a half hourly time step. Before flux computation, a strict filtering was applied to the XLAS data to remove outliers depending on weak demod signal. Negative night-time data were set to zero and daytime flux missing data (one to three 30mn 30 mn-data) were gap filled using

Mis en forme : Police :10 pt

Mis en forme : Police :10 pt

Mis en forme : Police :10 pt, Condensé de 0.2 pt

Mis en forme : Police :10 pt

Mis en forme : Police :10 pt, Condensé de 0.2 pt

Mis en forme : Police :10 pt

Mis en forme : Police :10 pt

Mis en forme : Police :10 pt

Mis en forme : Police :10 pt

simple interpolation. ~~Flux anomalies in early morning (circa sunrise) and late afternoon (circa sunset) were corrected on the basis of the ratio between sensible heat flux and half hourly incoming solar radiation measurements (Rg) using Ben Salem meteo station.~~ Furthermore, half hourly H_XLAS aberrant values ~~of XLAS sensible heat flux~~due to measurement errors and values higher than 400 $Wm^{-2}$, arising from measurement saturation, were ruled out~~.~~ (3% of the total measurement throughout the experiment duration). Finally, daily H_XLAS was computed as the average of the half hourly H_XLAS.

### 3.2 XLAS footprint computation

The footprint of a flux measurement defines the spatial context of the measurement and the source area that influences the sensors. In case of inhomogeneous surfaces like patches of various land covers and moisture variability due to irrigation, the measured signal is dependent on the fraction of the surface having the strongest influence on the sensor and thus on the footprint size and location. Footprint models (Horst and Weil, 1992; Leclerc and Thurtell, 1990) have been developed to determine what area is contributing to the heat fluxes ~~to the sensors~~ as well as the relative weight of each particular cell inside the footprint limits. Contributions of upwind locations to the measured flux depend on the height of the vegetation, height of the instrumentation, wind speed, wind direction, and atmospheric stability conditions (Chávez et al., 2005).

According to the model of (Horst and Weil, 1992), for one-point measurement system, the footprint function $f$ relates the spatial distribution of surface fluxes, $F_0(x,y)$ *to* the measured flux at height $z_m$, $F(x,y,z_m)$, as follows:

$$F(x,y,z_m) = \int_{-\infty}^{\infty}\int_{-\infty}^{x} F_0(x',y')f(x-x',y-y',z_m)dx'dy' \quad (5)$$

The footprint function $f$ is computed as:

$$\bar{f}^y(x,z_m) \simeq \frac{d\bar{z}}{dx} = \frac{d\bar{z}}{dx}\frac{z_m}{\bar{z}^2}\frac{\bar{u}(z_m)}{\bar{u}(c\bar{z})}Ae^{-(z_m/b\bar{z})^r}e^{-(z_m/b\bar{z})^r} \quad (6)$$

~~Where~~where $\bar{u}(z)$ ~~is~~ the mean wind speed profile and $\bar{z}$ ~~is~~ the mean plume height for diffusion from a surface source. The variables *A*, *b* and *c* are scale factors and r a scale factor of the Gamma function. In the case of a scintillometer measurement, the footprint function has to be combined with the spatial weighting function *W(x)* of the scintillometer to account for the sensor integration along its path. Thus, the sensible heat flux footprint mainly depends on the scintillometer effective height $z_{LAS}$ (Hartogensis et al., 2003), which includes the topography below the path and the transmitter and receiver heights, the wind direction and the Obukhov length $L_O$, which characterizes the atmospheric stability (Solignac et al., 2009). In a subsequent step, daily footprints were computed as a weighted sum of the half hourly footprints by the XLAS sensible heat flux.

~~In a subsequent step, daily footprints were computed based on the half hourly footprints.~~

In fact, there is an issue with the MODIS pixel heterogeneity and notably the distribution of the land use classes at the intersection between the square pixel and the XLAS footprint (Bai et al., 2015). Hence, in order to provide a first guess on these relative heterogeneities, land use classes within each MODIS pixel of the 10 km × 8 km sub-image were studied based on the land use map of the 2013-2014 season (Chahbi, 2016). The average footprint of all half hourly footprints for the whole study period was computed and overlaid on the MODIS grid in order to identify the MODIS pixels partially or totally covered by footprint (Figure 3).

Mis en forme : Police :+Corps
Mis en forme : Police :+Corps
Mis en forme : Police :+Corps
Mis en forme : Couleur de police : Automatique
Mis en forme : Couleur de police : Automatique
Mis en forme : Couleur de police : Automatique
Mis en forme : Couleur de police : Automatique
Mis en forme : Couleur de police : Automatique
Mis en forme : Police :+Titres CS

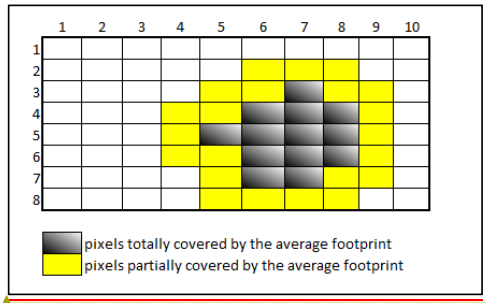


**Figure 3 : MODIS pixels partially or totally covered by XLAS source area**

The percentage of land use classes was computed for i) the part of each pixel that lies within the footprint, and ii) the complementary part of the pixel located outside of the footprint (Figure 4). Results show that difference in percentages of each land use classes for the pixel fractions located within or outside the footprint is low with 1.8%, 1.7%, 1.0% and 3.5% for cereals, market gardening, trees and bare soil, respectively. Moreover, the major part of the area above transect is covered by fallow and orchards. The land use classes' partition inside the 13 MODIS pixels totally covered by the average footprint is comparable.

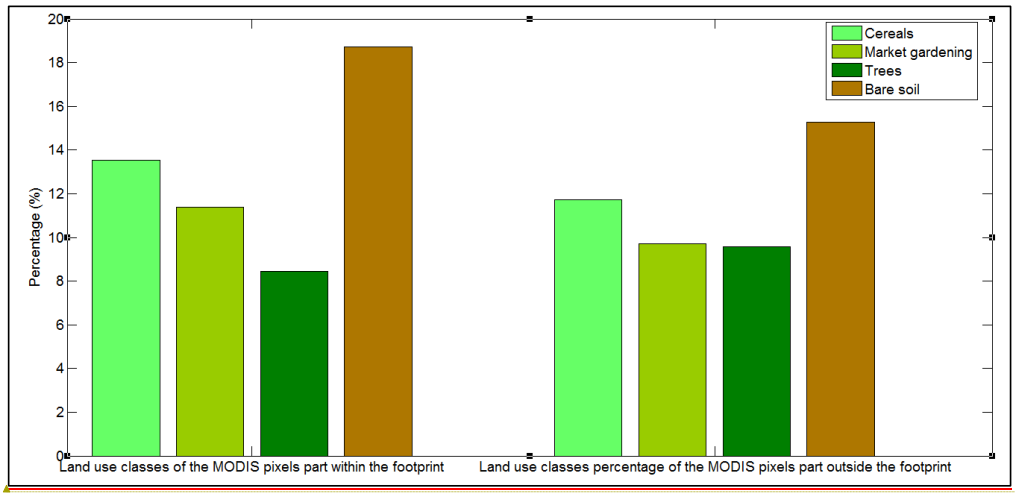


**Figure 4: Land use classes' percentage of the MODIS pixels within or outside the footprint**

### 3.3 XLAS derived latent heat flux

Instantaneous (LE_residual_XLAS$_{t\text{-}FP}$) and daily (LE_residual_XLAS$_{day\text{-}FP}$) XLAS derived latent heat flux (*i.e.* residual latent heat flux) of the XLAS upwind area were computed using the energy budget closure of the XLAS measured sensible heat flux (H_XLAS) with additional estimations of remotely sensed net surface radiation Rn ~~combined with~~and soil heat flux G, as available energy (AE=Rn-G), as follows:

$$LE\_residual\_XLAS_{t-FP} = AE_{t-FP} - ~~H\_XLAS_t~~ H\_XLAS_t \quad (7)$$

$$LE\_residual\_XLAS_{day-FP} = AE_{day-FP} - H\_XLAS_{day} \quad (8)$$

H_XLAS$_t$ ~~is~~and H_XLAS$_{day}$ are respectively the ~~scintillometer sensible heat flux~~instantaneous and daily measured H at the time of the satellite overpass interpolated from the half hourly fluxes measurements. ~~Daily H (H_XLAS$_{day}$) was computed as the average of the half hourly XLAS measured H.~~ Daily available energy within

Mis en forme : Police :(Par défaut) +Titres CS, Police de script complexe :+Titres CS

Mis en forme : Police :(Par défaut) +Titres CS, Police de script complexe :+Titres CS

Mis en forme : Police :Italique

the footprint ($AE_{day-FP}$) was computed from instantaneous available energy ($AE_{t-FP}$) as detailed in Sect. 3.3.1 and Sect. ~~3.3.2.~~ 3.3.2. The subscripts "30", "day" and "t" refer to half hourly, daily and instantaneous (at the time of Terra and Aqua overpasses) variables, respectively; while the subscript "FP" means that the footprint is taken into account *i.e.* instantaneous or the daily (depending on time scale) footprint was multiplied by the variable.

### 3.3.1 Instantaneous available energy

Net surface radiation is the balance of energy between incoming and outgoing shortwave and longwave radiation fluxes at the land-atmosphere interface. ~~Remote~~Remotely sensed surface radiative budget components provide unparalleled spatial and temporal information, thus several studies have attempted to estimate net radiation by combining remote sensing observations with surface and atmospheric data. Net radiation equation can be written as follows:

$$Rn = (1 - \alpha)Rg + \varepsilon_s \text{ ~~* } R_{atm}R_{atm} - \varepsilon_s \text{ ~~* } \sigma \text{ ~~* } LST^4LST^4 \quad (9)$$

where Rg ~~is~~ the incoming shortwave radiation ($W.m^{-2}$), $R_{atm}$ ~~is~~ the incoming longwave radiation ($W.m^{-2}$), $\varepsilon_s$ ~~is~~ the surface emissivity, $\sigma$ ~~is~~ Stefan-Boltzmann coefficient ($W.m^{-2}.K^4$) , $\alpha$ ~~is~~ the albedo, and LST ~~is~~the land-surface temperature (°K).

The soil heat flux G depends on the soil type and water content as well as the vegetation type (Allen et al., 2005).The direct estimation of G by remote sensing data is not possible (Allen et al., 2011), however, empirical relations ~~could~~can estimate the fraction $\xi$=G/Rn as a function of soil and vegetation characteristics using satellite image data, such as the LAI, NDVI, α and LST. ~~In order to estimate the~~ Generally, G~~/Rn ratio, several methods have been tested for various types~~ represents 5-20% of ~~surfaces at different locations (Bastiaanssen, 1995; Burba et al., 1999; Choudhury et al., 1987; Jackson et al., 1987; Kustas and Daughtry, 1990; Kustas et al., 1993; Ma et al., 2002; Payero et al., 2001).~~

Rn during daylight hours ~~Danelichen~~(Kalma et al. ~~(2014~~., 2008) ~~evaluated the parameterization of these different models in three sites in Mato Grosso state in Brazil and found that the model proposed by Bastiaanssen (2005) showed the best performance for all sites, followed by the model from Choudhury et al. (1987) and Jackson et al. (1987). Hence to estimate G, we tested three methods:~~

. In order to estimate the G/Rn ratio, several methods have been tested for various types of surfaces at different locations. The most common methods parameterize $\xi$ as a constant for the entire day or at satellite overpass time ~~Bastiaanssen (2005)~~(Ventura et al., 1999) ~~:~~

, according to NDVI (Jackson et al., 1987; Kustas and Daughtry, 1990), LAI (Choudhury et al., 1987; Kustas et al., 1993; Tasumi et al., 2005), vegetation fraction (fc ) (Su, 2002), LST and α (Bastiaanssen, 1995), or only LST (Santanello Jr and Friedl, 2003). These empirical methods are suitable for specific conditions; therefore, estimating G, especially in this type of environment where NDVI values are low and thus G/Rn values are large, is a critical issue. The approach adopted here was drawn on Danelichen et al. (2014) who evaluated the parameterization of these different models in three sites in Mato Grosso state in Brazil and found that the model proposed by (Bastiaanssen, 1995) showed the best performance for all sites, followed by the model from Choudhury et al. (1987) and Jackson et al. (1987):

Bastiaanssen (1995):

Code de champ modifié

Code de champ modifié

Code de champ modifié

$G = Rn \times (LST - 273.16) \times (0.0038 + 0.0074\alpha) \times ((LST - 273.16)(0.0038 + 0.0074\alpha)(1 - 0.98NDVI^4)$ (10)

Choudhury et al. (1987):

$G = Rn \times 0.4 \times (\exp(-0.5LAI)) 4Rn(\exp(-0.5LAI))$ (11)

Jackson et al. (1987)

$G = Rn \times 0.583 \times (\exp(-2.13NDVI)) 583Rn(\exp(-2.13NDVI))$ (12)

Code de champ modifié

Hence, these three methods were tested for the Ben Salem flux station measurements, by comparing the measured $G_{BS\text{-}t}$ and the computed G using measured $Rn_{BS\text{-}t}$, $LST_{BS\text{-}t}$, $\alpha_{BS}$, $NDVI_{BS}$ and $LAI_{BS}$ at Terra and Aqua overpass time (results not shown). The best results are issued from Bastiaanssen (1995) method with a Root Mean Square Error (RMSE) of 0.09 (average value of the two satellites overpass time) followed by Jackson et al. (1987) and Choudhury et al. (1987) with RMSE values of 0.15 and 0.2, respectively. Moreover, daily measured $G_{BS\text{-}day}$ was computed and a G accumulation is generally found as it has been already mentioned by (Clothier et al., 1986) who showed that G is neither constant nor negligible on diurnal timescales, and can constitute as much as 50% of Rn over sparsely vegetated area. Since G estimation was the most uncertain variable, the three above methods were tested to compute the distributed remotely sensed AE. The Ben Salem meteorological station was used to provide $Rg_t$ and $R_{atm\text{-}t}$. Remote sensing variables α, LST, $\varepsilon_s$ and NDVI came from MODIS products. Remotely sensed LAI was computed from the MODIS NDVI using a single equation (Clevers, 1989) for all crops in the study area:

$$LAI = -\frac{1}{k} ln\left(\frac{NDVI_\infty - NDVI}{NDVI_\infty - NDVI_{soil}}\right) \quad (13)$$

The calibration of this relationship was done over the Yaqui irrigated perimeter (Mexico) during the 2007-2008 growing season using hemispherical LAI measured in all the studied fields (Chirouze et al., 2014). Calibration results gave the asymptotical values of NDVI, $NDVI_\infty$ = 0.97 and $NDVI_{soil}$ = 0.05, as well as the extinction factor k=1.13. As this relationship was calibrated over a heterogeneous land surface but on herbaceous vegetation only, its relevance for trees was checked. ~~Remote sensing variables α, LST, $\varepsilon_s$, LAI and NDVI were calculated at the resolution of the sensor (MODIS, 1 km resolution). The Ben Salem meteo station was used to provide Rg and $R_{atm}$. MODIS Available Energy $AE_t$ was computed for a 10 km × 8 km sub image centered on the XLAS transect at Terra MODIS and Aqua MODIS overpass time, using the three methods estimating G. Since, the measured heat fluxes $H\_XLAS_t$ represents only the weighted contribution of the fluxes from the upwind area to the tower (footprint)~~For that purpose, clump-LAI measurements on an olive tree, as well as allometric measurements *i.e.* mean distance between trees and mean crown size done using Pleiades satellite data (Mougenot et al., 2014;Touhami, 2013) were obtained. Clump LAI is the value of the LAI of an isolated element of vegetation (tree, shrub...); if this element occupies a fraction cover f and is surrounded by bare soil, then the clump LAI value is equal to the area average LAI divided by f. Hence, we checked that the pixels with tree dominant cover show LAI values close to what was expected (of the order of 0.3 to 0.4 given the interrow distance of 12 m on average).

Remote sensed available energy was computed for the 10 km × 8 km MODIS sub-images at Terra-MODIS and Aqua-MODIS overpass time, using the three methods estimating G. Since the measured heat fluxes $H\_XLAS_t$

represent only the weighted contribution of the fluxes from the upwind area to the tower (footprint), then instantaneous footprint at the time of Terra and Aqua overpass were selected among the two half hour preceding and following the satellite's time of overpass (lowest time interval) and then was multiplied by the instantaneous remote sensed available energy $AE_t$ to get the available energy of the upwind area $AE_{t\text{-}FP}$.

### 3.3.2 Daily available energy

Most methods using TIR domain data rely on once-a-day acquisitions, late morning (such as Terra-MODIS overpass time) or early afternoon (such as Aqua-MODIS overpass time). Thus, they provide a single instantaneous estimate of energy budget components~~, since the diurnal cycle of the energy budget is not recorded.~~. In order to obtain daily AE from these instantaneous measurements ~~(Eq. (13) and Eq. (14))~~ and to reconstruct hourly variations of AE, we considered that its evolution was proportional to another variable whose diurnal evolution can be easily known. ~~Here the global solar incoming radiation Rg was used to scale AE from instantaneous to daily values as follows:~~

The extrapolation from an instantaneous flux estimate to a daytime flux assumes that the surface energy budget is "self-preserving" *i.e.* the relative partitioning among components of the budget remains constant throughout the day. However, many studies (Brutsaert and Sugita, 1992; Gurney and Hsu, 1990; Sugita and Brutsaert, 1990) showed that the self-preservation method gives day-time latent heat estimates that are smaller than observed values by 5-10%. Moreover, (Anderson et al., 1997) found that the evaporative fraction computed from instantaneous measured fluxes tends to underestimate the daytime average by about 10%, hence, a corrected parameterization was used and a coefficient=1.1 was applied. Similarly, Delogu et al. (2012) found an overestimation of about 10% between estimated and measured daily component of the available energy thus, a coefficient =0.9 was applied. The corrected parameterization proposed by Delogu et al. (2012) was tested, but this coefficient did not give consistent results, therefore, the extrapolation relationship was calibrated in order to get accurate daily results of AE .

Thereby, the applied extrapolation method was tested using *in situ* Ben Salem flux station measurements. The incoming short wavelengths radiation was used to scale available energy from instantaneous to daily values; but only for clear sky days for which MODIS images can be acquired and remote sensing data used to compute AE are available. Clear sky days were selected based on the ratio of daily measured incoming short wavelengths radiation $Rg_{day}$ to the theoretical clear sky radiation Rso as proposed by the FAO-56 method (Allen et al., 1998). A day was defined as clear if the measured $Rg_{day}$ is higher than 85 % of the theoretical clear sky radiation at the satellite overpass time (Delogu et al., 2012).

Daily measured available energy $AE_{BS\text{-}day}$ computed as the average of half-hourly measured $AE_{BS\text{-}30}$, was compared to daily available energy ($AE_{BS\text{-}day\text{-}Terra}$ and $AE_{BS\text{-}day\text{-}Aqua}$) computed using the extrapolation method from instantaneous measured $AE_{BS\text{-}t\text{-}Terra}$ and $AE_{BS\text{-}t\text{-}Aqua}$ at Terra and Aqua overpass time, respectively (Equation 14).

~~$AE_{day_{Terra}} = a_{Terra} \times Rg_{day} \frac{AE_{t_{Terra}}}{Rg_t} + b_{Terra} AE_{BS-day-Terra}$~~

$$= a_{Terra} Rg_{day} \frac{AE_{BS-t-Terra}}{Rg_{t-Terra}} + b_{Terra}$$ ~~(13)~~(14)

Mis en forme : Interligne : simple
Tableau mis en forme
Cellules fusionnées
Mis en forme : Police :(Par défaut) +Corps, 10 pt, Gras, Police de script complexe :Arial
Mis en forme : Police :(Par défaut) +Corps, 10 pt, Police de script complexe :Arial

$AE_{day_{Aqua}} = a_{Aqua} \times Rg_{day} \frac{AE_{t_{Aqua}}}{Rg_{t}} + b_{Aqua}$ $AE_{BS-day-Aqua} = a_{Aqua} Rg_{day} \frac{AE_{BS-t-Aqua}}{Rg_{t-Aqua}} + b_{Aqua}$ (14)

where $Rg_t$ and $Rg_{day}$ are respectively the instantaneous and daily global measured incoming solar short wavelengths radiation.

A bias was found when assuming $a_{Terra}=a_{Aqua}=1$ and $b_{Terra}=b_{Aqua}=0$; hence basing on in the Ben Salem meteorological station; $Rg_{t\text{-}Terra}$ and $Rg_{t\text{-}Aqua}$ are the instantaneous incoming short wavelengths radiations measured at Terra and Aqua overpass time, respectively and $AE_{BS\text{-}t\text{-}Terra}$ and $AE_{BS\text{-}t\text{-}Aqua}$ are the instantaneous measured available energy in the Ben Salem flux station Rn, at Terra and G measurements, Aqua overpass time. Results gave an overestimation of about 15 %. The corrected parameterizations of AE (a and b) were computed and used Table 1), needed to remove this bias (see Sect. 6.1). Consequently, the bias between measured ($AE_{BS\text{-}day}$) and computed AE ($AE_{BS\text{-}day\text{-}Terra}$ and $AE_{BS\text{-}day\text{-}Aqua}$), were applied to compute daily remotely sensed AE ($AE_{day}$) from instantaneous AE ($AE_i$) following the extrapolation method shown in equation 14.

**Table 1: Corrected parameterizations of available energy was computed for the 10 km × 8 km sub-image at the time of Terra-MODIS ($AE_{day_{Terra}}$) and Aqua-MODIS ($AE_{day_{Aqua}}$) overpass, diurnal reconstitution**

| | | |
|---|---|---|
| Terra | $a_{Terra}$ | 0.85 |
| | $b_{Terra}$ | -19.81 |
| Aqua | $a_{Aqua}$ | 0.87 |
| | $b_{Aqua}$ | -18.94 |

Then $AE_{day}$ was multiplied by the weighting coefficients ranging from zero and then was weighted by one of the corresponding daily footprint to get the daily available energy of the upwind area $AE_{day\text{-}FP}$.

Finally, estimates of Terra MODIS and Aqua MODIS observed daily LE (LE residual $XLAS_{day\text{-}FP}$) were obtained based on the three methods used to compute the soil heat flux G. G.

## 4 SPARSE model

### 4.1 Energy fluxes derived from SPARSE model

The SPARSE dual-source model solves the energy budgets of the soil and the vegetation. Here we use the "layer approach", for which the resistance network relating the soil and vegetation heat sources to a main reference level through a common aerodynamic level use a series electrical branching. Main unknowns are the component temperatures, *i.e.* the temperature of the soil ($T_s$) and that of the vegetation ($T_v$). temperatures. Totals at the reference height, (the measurement height of the meteorological forcing), as well as the longwave radiation budget, are also solved so that altogether a system of five equations can be built:

$$\begin{cases} H = H_s + H_v \\ LE = LE_s + LE_v \\ R_{ns} = G + H_s + LE_s \\ R_{nv} = H_v + LE_v \\ \sigma T_{rad}^4 = R_{atm} - R_{as} - R_{av} \end{cases} \quad \begin{cases} H = H_s + H_v \\ LE = LE_s + LE_v \\ R_{ns} = G + H_s + LE_s \\ R_{nv} = H_v + LE_v \\ \sigma T_{rad}^4 = R_{atm} - R_{as} - R_{av} \end{cases} \quad \text{(15) (15)}$$

where $R_{atm}$ is the atmospheric radiation (W/m Wm$^{-2}$), Ra is the net component longwave radiation (W/m Wm$^{-2}$) and $T_{rad}$ is the $T_{rd}$ the radiative surface temperature (°K) as observed by the satellite; indexes "s" and "v" designate the soil and the vegetation, respectively.

The first two (Eq. (15)) express the continuity of the latent and sensible heat fluxes from the sources to the aerodynamic level through to the reference level, the third and the fourth (Eq. (15)) are the soil and vegetation

**Mis en forme :** Police :(Par défaut) +Corps, 10 pt, Police de script complexe :Arial
**Mis en forme :** Interligne : simple
**Mis en forme :** Police :Gras, Police de script complexe :Arial
**Mis en forme :** Centré
**Mis en forme :** Couleur de police : Texte 1
**Mis en forme :** Couleur de police : Texte 1
**Mis en forme :** Couleur de police : Texte 1
**Mis en forme :** Couleur de police : Texte 1
**Mis en forme :** Couleur de police : Texte 1
**Mis en forme :** Couleur de police : Texte 1
**Mis en forme :** Police :Italique
**Mis en forme :** Police :+Corps

energy budgets, and the fifth (Eq. (15)) relates the radiative surface temperature $T_{rad}$ derived from observed LST to $T_s$ and $T_v$.

The SPARSE model system of equations is fully described in Boulet et al~~.~~ (2015). SPARSE is similar to the TSEB model (Kustas and Norman, 1999) but includes ~~classical~~the expressions of the aerodynamic resistances of (Choudhury and Monteith~~,~~ (1988~~;~~) and Shuttleworth and Gurney~~,~~ (1990)~~.~~

~~System (15) is solved iteratively~~. This system can be solved in a forward mode for which the surface temperature is an output (prescribed conditions), and an inverse mode when the surface temperature is an input derived from satellite observations or *in situ* measurements in the thermal infra-red domain (retrieval conditions). Figure 5 illustrates a diagram showing the flowchart of the model algorithm. System (15) is solved step-by-step by following similar guidelines as in the TSEB model: the first step assumes that the vegetation transpiration ($LE_v$) is maximum, and evaporation ($LE_s$) is computed. If this soil latent heat flux ($LE_s$) is ~~negative~~below a minimum positive threshold for vegetation stress detection of 30 $Wm^{-2}$, the hypothesis that the vegetation is unstressed is no longer valid. In that case, the vegetation is assumed to suffer from water stress and the soil surface is assumed to be already long dry. Then, $LE_s$ is set to ~~a minimum~~30 $Wm^{-2}$. This value ~~of 30 W.m$^{-2}$ so that one~~ accounts for the small but non ~~neglectable~~negligible vapor flow reaching the surface (Boulet et al., 1997). The system is then solved for vegetation latent heat flux ($LE_v$). If $LE_v$ is also negative, both $LE_s$ and $LE_v$ values are set to zero, whatever the value of $T_{rad}$. The system of equation can also be solved for $T_s$ and $T_v$ only if the efficiencies representing stress levels (dependent on surface soil moisture for the evaporation, and root zone soil moisture for the transpiration) are known. In that case the sole first four equations are solved. This prescribed mode allows computing all the fluxes in known limiting soil moisture levels (very dry, e.g. fully stressed, and wet enough, e.g. potential). It limits unrealistically high values of component fluxes, latent heat flux values above the potential rates or sensible heat flux values above that of a non evaporating surface. The potential evaporation and transpiration rates used later on are computed using this prescribed mode with minimum surface resistance to evaporation and transpiration, respectively.

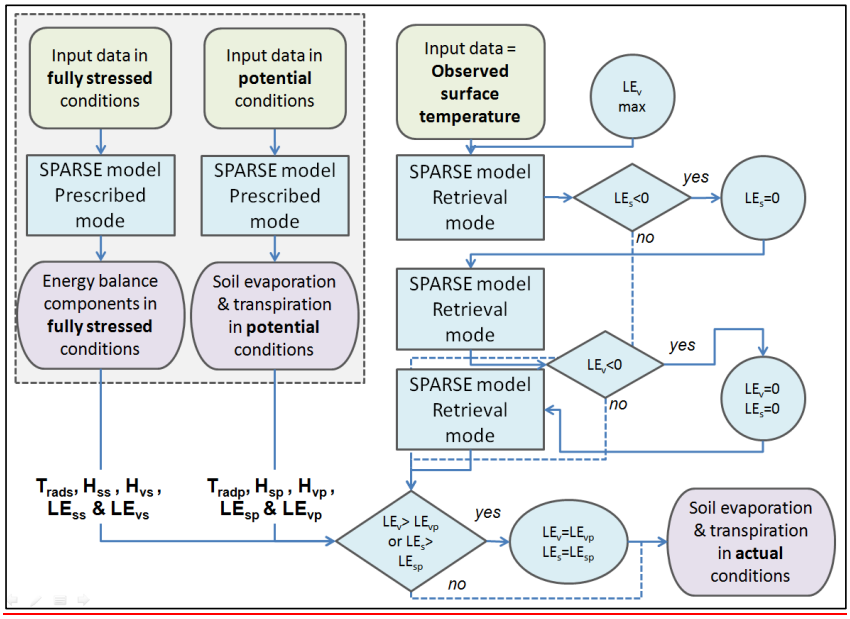


Mis en forme : Police :+Corps
Mis en forme : Police :+Corps
Mis en forme : Police :+Corps
Mis en forme : Police :+Corps
Code de champ modifié
Mis en forme : Police :+Corps
Mis en forme : Police :+Corps
Mis en forme : Police :+Corps
Mis en forme : Police :+Corps
Mis en forme : Police :+Corps
Mis en forme : Police :+Corps
Mis en forme : Police :+Corps

**Figure 5: Flowchart of the SPARSE algorithm; $T_{rads}$, $H_{ss}$ , $H_{vs}$ $LE_{ss}$ and $LE_{vs}$ are radiative surface temperature, soil sensible heat flux, vegetation sensible heat flux, soil latent heat flux and vegetation latent heat flux in fully stressed conditions, respectively; $T_{radp}$, $H_{sp}$, $H_{vp}$, $LE_{sp}$ and $LE_{vp}$ are radiative surface temperature, soil sensible heat flux , vegetation sensible heat flux, soil latent heat flux and vegetation latent heat flux in potential conditions, respectively.**

Some of the model parameters were remotely sensed data while others were taken from the bibliography or measured *in situ*.

Remotely sensed data fed into SPARSE are~~: land surface temperature (~~ LST~~), surface emissivity (~~ ε~~) and viewing angle (~~ ϕ~~) (MOD11A1/ MYD11A1 for Terra and Aqua, respectively),~~ NDVI ~~(MOD13A2/MYD13A2 for Terra and Aqua, respectively) and albedo (α) (MCD43B1, MCD43B2, MCD43B3). These data were acquired for the study period (1st September 2012 to 30th June 2015) at the resolution of the MODIS sensor at 1 km, embarked on board of the satellites Terra (overpass time around 10:30 local solar time) and Aqua (overpass time around 13:30 local solar time).

~~MODIS data provided in sinusoidal projection was reprojected in UTM using the MODIS Reprojection Tool (MRT). Then the sub images of 10 km× 8 km over the study zone (Figure 1) were extracted. Since the MODIS pixels in our study area are considered to include the same land use (mainly arboriculture with some annual crops), the footprint of the MODIS pixel resulting from the variation in the size of the ground area that is detected (variation in the view zenith angles) as well as to the MODIS gridding process (Peng et al., 2015) were not reconstructed. The daily MODIS LST and viewing angle, 8-day MODIS albedo, and 16-day MODIS NDVI contain some missing or unreliable data; hence, days with missing data in MODIS pixels regarding the scintillometer footprint were excluded. Temporal interpolation of albedo and NDVI data were done to get daily remote sensing data.~~

~~A single equation (Clevers, 1989) was used to compute remotely sensed leaf area index (~~ LAI~~) from the NDVI of all crops in the study area:~~

~~$$LAI = -\frac{1}{k} ln\left(\frac{NDVI_{\infty} - NDVI}{NDVI_{\infty} - NDVI_{soil}}\right)$$~~ ~~(16)~~

and α. ~~The calibration of this relationship was done over the Yaqui irrigated perimeter (Mexico) during the 2007-2008 growing season using hemispherical LAI measured in all the studied fields (Chirouze et al., 2014). Calibration results gave the asymptotical values of NDVI, $NDVI_{\infty}$ = 0.97 and $NDVI_{soil}$ = 0.05, as well as the extinction factor~~ k1.13. ~~As this relationship was calibrated over a heterogeneous land surface but on herbaceous vegetation only, its relevance for trees was checked. For that purpose, clump LAI measurements on an olive tree, as well as allometric measurements (mean distance between trees and mean crown size done using Pleiades satellite data (Mougenot et al., 2014;Touhami, 2013)) were obtained. We checked that the pixels with tree dominant cover show LAI values close to what was expected (of the order of 0.3 to 0.4 given the interrow distance of 12 m on average).~~

A grid of the vegetation height ($z_v$) was also necessary as input in the SPARSE model; for herbaceous crops, vegetation height was interpolated with the help of NDVI time series between fixed minimum (0.05 m) and maximum (0.8 m) values, while for trees, the roughness length ($z_{om}$) was linked to the allometric measurements (mentioned before) and computed as a function of canopy area index, drag coefficient and canopy height using the drag partition approach proposed by ~~(~~Raupach~~,~~ (1994) for tall sparse vegetative environments. Then, since SPARSE deals with vegetation height and not roughness length, the same simple rule of the thumb as the one used in SPARSE was used to reconstruct $z_v$ for the tree cover types ($z_v$=$z_{om}$/0.13). In a final step, to get spatial vegetation height, $z_v$ was averaged over the MODIS pixels.~~ *In situ* parameters used in SPARSE were mainly

meteorological data: Rg, $R_{atm}$, Ta, Ha and u. No calibration was performed on the model parameters shown in Table 2.

~~In situ parameters used in SPARSE were mainly meteorological data: incoming solar radiation (Rg), incoming atmospheric radiation ($R_{atm}$), air temperature (Ta), air humidity (Ha) and wind speed (u).~~

~~No calibration was performed on the model parameters shown in Table 1.~~

**Table 2~~1~~. SPARSE parameters**

| | Definition | Value | Data Sources |
|---|---|---|---|
| ***Remote sensing parameters*** | | | |
| NDVI | Normalized Difference Vegetation Index | | Satellite imagery |
| Trad (K) | Radiative surface temperature (K) | | Satellite imagery |
| α | Albedo | | Satellite imagery |
| ε | Emissivity | | Satellite imagery |
| Φ (rad) | View zenith angle | | Satellite imagery |
| ***Meteorological parameters*** | | | |
| $R_g$ (~~W.m~~$Wm^{-2}$) | Incoming solar radiation | | *In situ* data |
| $R_{atm}$ (~~W.m~~$Wm^{-2}$) | Incoming atmospheric radiation | | *In situ* data |
| $T_a$ (K) | Air temperature at reference level | | *In situ* data |
| $RH_a$ (%) | Air relative humidity | | *In situ* data |
| $u_a$ (~~m.s~~$ms^{-1}$) | Horizontal wind speed at reference level | | *In situ* data |
| ***Fixed parameters*** | | | |
| $z_a$ (m) | Atmospheric forcing height | 2.32 | *In situ* data |
| $z_v$ (m) | Vegetation height | | Derived from land cover |
| $\beta_{pot}$ | Evapotranspiration efficiency in full potential conditions | 1.000 | |
| $\beta_{stress}$ | Evapotranspiration efficiency in fully stressed conditions | 0.001 | |
| $r_{stmin}$ (~~s.m~~$sm^{-1}$) | Minimum stomatal resistance | 100 | ~~Bibliography~~ (Boulet et al., 2015) |
| *w* (m) | Leaf width | 0.05 | ~~Bibliography~~ (Braud et al., 1995) |
| $\varepsilon_v$ | Vegetation emissivity | 0.98 | ~~Bibliography~~ (Braud et al., 1995) |
| $\alpha_v$ | Vegetation albedo | 0.25 | Estimation |
| ***Constants*** | | | |
| $\rho_{cp}$ ($J.kg^{-1}.K^{-1}$) | Product of air density and specific heat | 1170 | ~~Bibliography~~ (Braud et al., 1995) |
| σ ($W.m^{-2}.k^4$) | Stefan–Boltzmann constant | $5.66.\ 10^{-8}$ | ~~Bibliography~~ (Braud et al., 1995) |
| γ ($Pa.K^{-1}$) | Psychrometric constant | 0.66 | ~~Bibliography~~ (Braud et al., 1995) |
| $z_{om,s}$(m) | Equivalent roughness length of the underlying bare soil in the absence of vegetation | $5.10^{-3}$ | ~~Bibliography~~ (Braud et al., 1995) |

Tableau mis en forme

Mis en forme : Police :Italique

Mis en forme : Police :Italique

Tableau mis en forme

Mis en forme : Police :Italique

Mis en forme : Police :Italique

Mis en forme : Police :Italique

Mis en forme : Police :Italique

Tableau mis en forme

| | | | |
|---|---|---|---|
| $n_{SW}$ | Coefficient in $r_{av}$ (Aerodynamic resistance between the vegetation and the aerodynamic level) | 2.5 | ~~Bibliography~~ (Boulet et al., 2015) |
| $\xi$ | Ratio between soil heat flux G and available net radiation on the bare soil $Rn_s$ | 0.4 | ~~Bibliography~~ (Braud et al., 1995) |

The retrieval and prescribed modes of the SPARSE ~~was~~model were run for the 10 km × 8 km sub-~~image~~images at the time of Terra ~~MODIS~~ and Aqua ~~MODIS overpass. Then,~~ overpasses, to get instantaneous ~~modelled~~modeled fluxes ~~were~~$H\_SPARSE_t$, $LE\_SPARSE_t$ and $AE\_SPARSE_t$ as well as sensible heat flux ($H_{s\text{-}t}$ =$H_{ss\text{-}t}$ +$H_{vs\text{-}t}$) in fully stressed conditions and latent heat ($LE_{p\text{-}t}$ =$LE_{sp\text{-}t}$ +$LE_{vp\text{-}t}$) and sensible heat ($H_{p\text{-}t}$ =$H_{sp\text{-}t}$ +$H_{vp\text{-}t}$) fluxes in potential conditions. Modeled values were then multiplied by the nearest half hourly footprint to the satellite overpass time, in order to get fluxes corresponding to the upwind area ~~(~~: $H\_SPARSE_{t\text{-}FP}$, $LE\_SPARSE_{t\text{-}FP}$ ~~and~~, $AE\_SPARSE_{t\text{-}FP}$~~). In a subsequent step, SPARSE model was run at a half hourly time step using the half hourly meteorological measurements and assuming that the remote sensed MODIS data are invariant during the same day,~~ $H_{s\text{-}t\text{-}FP}$, $H_{p\text{-}t\text{-}FP}$ and $LE_{p\text{-}t\text{-}FP}$.

In a subsequent step, the prescribed mode of SPARSE model at potential conditions was run at a half hourly time step using the half hourly meteorological measurements to get half hourly latent heat flux at potential conditions $LE_{p\text{-}30}$. This potential LE weighted by the corresponding half hourly footprint ($LE_{p\text{-}30\text{-}FP}$) is used later when computing daily LE based on the stress factor method (section 4.2).

### 4.2 Reconstruction of daily ~~modelled~~modeled ET from instantaneous latent heat flux

Daily ET is usually required for applications in hydrology or agronomy for instance, whereas most SEB methods provide a single instantaneous latent heat flux because the energy budget is only computed at the satellite overpass time (Delogu et al., 2012). In order to scale daily ET from one instantaneous ~~measurement,~~estimate, there are various methods relying on the preservation, during the day, of the ratio of the latent heat flux to a scale factor having known diurnal evolution~~, have been developed. The global solar incoming radiation Rg, the net radiation Rn, the available energy or a maximum ET rate are generally used as scale factors. Chávez et al. (2008) , Colaizzi et al. (2005) and Van Niel et al. (2011) tested several extrapolation methods to estimate daily ET. The most common methods use as scaling factors the available energy or the potential ET. The first method assumes a constant diurnal evaporative fraction (EF) which is defined as the ratio of the latent heat flux (LE) to the available energy (Rn-G) at the land surface (Eq. (17)). The second one assumes a constant stress factor (SF) which is defined as the complementary part to 1 of the ratio between the simulated (actual conditions) and the potential (theoretical value for an unstressed surface i.e. potential ET) latent heat fluxes (LEpot (Eq. (18)). Potential ET is usually computed using a reference calculation such as the FAO-56 (Allen et al., 1998) method or derived from a surface energy balance model (e.g. Lhommel, 1997)~~. Either the stress factor SF (Eq. (16)) or the evaporative fraction EF (Eq. (17)) are assumed invariant during the same day, the diurnal modeled fluxes are accounted for by recovering the diurnal course of either potential ET or available energy.

~~$EF = \frac{LE}{Rn-G}$~~ $SF = 1 - \frac{LE\_SPARSE_{t-FP}}{LE_{p-t-FP}}$ ~~(17)~~ (16)

~~$SF = 1 - \frac{LE}{LEpot}$~~ $EF = \frac{LE\_SPARSE_{t-FP}}{AE\_SPARSE_{Ft-P}}$ (~~14~~18)

~~Besides, daily ET can also be estimated using the residual method, after computing the daily H, Rn and G (same approach as for the XLAS derived LE detailed in Sect. 3.3).~~

**Tableau mis en forme**

**Mis en forme :** Espace Après : 0 pt

**Mis en forme :** Police :Times New Roman

**Mis en forme :** Police :Times New Roman

**Mis en forme :** Police :Times New Roman

**Mis en forme :** Police :9 pt

**Mis en forme :** Anglais (États-Unis)

**Mis en forme :** Police :+Titres CS, Couleur de police : Automatique

**Mis en forme :** Police :+Titres CS

**Tableau mis en forme**

**Mis en forme :** Police :11 pt, Police de script complexe :Arial

**Mis en forme :** Justifié

**Mis en forme :** Police :11 pt, Police de script complexe :Arial

~~All daily ET estimates were done for the 10 km × 8 km sub-image ($LE\_SPARSE_{day}$) and then were weighted by the corresponding daily footprint to get the daily ET of the upwind area ($LE\_SPARSE_{day-FP}$).~~

***Stress Factor (SF) method***

Assuming that the stress factor is constant during the day, the daily modeled ET ($LE\_SPARSE_{day-FP}$) can be expressed as the product of the instantaneous estimate of SF at the satellite overpass time and the daily potential evapotranspiration :

$$\boldsymbol{LE\_SPARSE_{day-FP} = (1 - SF) LE_{p-day-FP}} \quad (15)$$

$LE_{p\text{-}day\text{-}FP}$ was calculated as the sum of the half hourly modeled latent heat fluxes at potential conditions $LE_{p\text{-}30\text{-}FP}$.

~~**4.2.1**~~ ***Evaporative Fraction method***

~~Under clear sky days, EF self preservation was revised by several studies. Hoedjes et al. (2008) showed that EF is almost constant during daytime under dry conditions whereas it follows a concave up shape under wet conditions. Hence, EF depends strongly on soil moisture as well as canopy fraction cover, but, it is nearly unrelated to solar radiation and wind speed, as shown by Gentine et al. (2007).~~

~~Consequently, the~~The daily modeled ET ~~total (i.e.~~ ($LE\_SPARSE_{day-FP}$) can be expressed as the product of the instantaneous estimate of EF at the satellite overpass time and the daily modeled available energy ~~$AE\_SPARSE_{day}$~~:

~~$$\boldsymbol{LE\_SPARSE_{day} = EF \times AE\_SPARSE_{day} LE\_SPARSE_{day-FP}} \quad (19)$$~~

$$\boldsymbol{= EF \times AE\_SPARSE_{day-FP}} \quad (19)$$

~~Daily cumulative available energy~~ $AE\_SPARSE_{day}$ was computed from instantaneous modeled available energy ($AE\_SPARSE_t$) ~~at the two satellite overpass times~~ using the same approach detailed in Sect. 3.3.2 ~~(Eq. (13)~~ and ~~Eq.~~applying equation (14~~)). Instantaneous estimates of Rn and G with the SPARSE model were used.~~

~~**4.2.2 Stress Factor (SF) method**~~

~~Assuming that the stress factor (SF) is constant during the day, the daily ET (LE). AE_~~$SPARSE_{day}$~~) can be expressed as the product of the instantaneous estimate of SF at the satellite overpass time and~~ was weighted by the corresponding daily footprint to get the daily ~~potential evapotranspiration $LEpot_{day}$ :~~modeled AE of the upwind area $AE\_SPARSE_{day-FP}$.

~~$$\boldsymbol{LE\_SPARSE_{day} = (1 - SF) \times LEpot_{day}} \quad (20)$$~~

~~$LEpot_{day}$ was calculated as the sum of the half hourly modelled latent heat fluxes at potential conditions. The SF method is more complex than the EF method since inputs for the SF method have to be computed from a potential evapotranspiration model while inputs used for EF method can be derived from remote sensing.~~

~~**4.2.3**~~ ***Residual method***

~~Daily modelled latent heat flux~~Besides, daily modeled ET ($LE\_$~~residual~~$\_SPARSE_{day-FP}$) was also estimated as a residual term of the surface energy budget using daily ~~modelled~~modeled sensible heat flux ($H\_SPARSE_{day-FP}$) and available energy ($AE\_SPARSE_{day}$~~) totals~~$_{FP}$) as ~~shown in Eq. (21).~~ follows:

**Mis en forme :** Police :Italique
**Mis en forme :** Sans numérotation ni puces
**Mis en forme :** Police :10 pt, Police de script complexe :Arial
**Mis en forme :** Police :Italique
**Mis en forme :** Sans numérotation ni puces
**Mis en forme :** Police :+Titres
**Mis en forme :** Police :+Titres

~~LE_residual_SPARSE$_{day}$~~ (21)(20)

~~$= AE\_SPARSE_{day}$~~

~~$- H\_SPARSE_{day}$~~$LE\_SPARSE_{day-FP}$

$= AE\_SPARSE_{day-FP} - H\_SPARSE_{day-FP}$

$H\_SPARSE_{day}$ was computed from ~~modelled instantaneous H~~modeled sensible heat flux ($H\_SPARSE_t$) following the same extrapolation method used for the available energy (see Sect. 3.3.2~~);~~). The corrected parameterizations of H were got from the comparison of daily measured sensible heat flux $H_{BS\text{-}day}$ computed as the average of half-hourly measured $H_{BS\text{-}30}$ and daily sensible heat flux ($H_{BS\text{-}day\text{-}Terra}$ and $H_{BS\text{-}day\text{-}Aqua}$) computed using the extrapolation method from instantaneous measured $H_{BS\text{-}t\text{-}Terra}$ and $H_{BS\text{-}t\text{-}Aqua}$ at Terra and Aqua overpass time, respectively (Equation 21).

~~$H\_SPARSE_{day_{Aqua}} = a'_{Terra} \times Rg_{day} \frac{H\_SPARSE_{t_{Aqua}}}{Rg_t} + b'_{Terra} H_{BS-day-Terra}$~~

$= a'_{Terra} Rg_{day} \frac{H_{BS-t-Terra}}{Rg_{t-Terra}} + b'_{Terra}$ (22)(21)

~~$H\_SPARSE_{day_{Terra}} = a'_{Aqua} \times Rg_{day} \frac{H\_SPARSE_{t_{Terra}}}{Rg_t} + b'_{Aqua}$~~

$H_{BS-day-Aqua} = a'_{Aqua} Rg_{day} \frac{H_{BS-t-Aqua}}{Rg_{t-Aqua}} + b'_{Aqua}$ (23)

where ~~$Rg_t$~~$H_{BS\text{-}t\text{-}Terra}$ and ~~$Rg_{day}$~~$H_{BS\text{-}t\text{-}Aqua}$ are ~~respectively~~ the instantaneous measured sensible heat flux in the Ben Salem flux station.

Therefore, the corrected parameterizations of H (Table 3), needed to remove the bias between measured ($H_{BS\text{-}day}$) and computed H ($H_{BS\text{-}day\text{-}Terra}$ and $AE_{BS\text{-}day\text{-}Aqua}$), were applied to compute daily ~~global incoming solar radiation.~~ modeled H ( $H\_SPARSE_{day}$) from instantaneous modeled H ($H\_SPARSE_t$) following the extrapolation method shown in equation 21. Finally, $H\_SPARSE_{day}$ was weighted by the corresponding daily footprint to get the daily modeled H of the upwind area $H\_SPARSE_{day\text{-}FP}$.

**Table 3: Corrected parameterizations of sensible heat flux for the diurnal reconstitution**

| | | |
|---|---|---|
| Terra | $a'_{Terra}$ | 1.02 |
| | $b'_{Terra}$ | -17.31 |
| Aqua | $a'_{Aqua}$ | 1.00 |
| | $b'_{Aqua}$ | -14.83 |

## 5 Water stress estimates

Water stress estimation is crucial to ~~deduct~~deduce the root zone soil moisture level using remote sensing data, (Hain et al., 2009). Water stress results in a drop of actual ~~evaporation~~evapotranspiration below the potential rate. Its intensity is usually represented by a stress factor ~~(SF)~~ as defined in Sect. 4.2, ranging between 0 (unstressed surface) and 1 (fully stressed surface).

~~Values~~Modeled values of SF at the time of Terra and Aqua overpass ($SF_{mod}$) have been computed from modeled potential LE ~~generated with the SPARSE model in prescribed conditions ($\beta s = \beta v = 1$). It is thus possible to relate $SF_{mod}$ to a combination of radiative temperatures~~($LE_{p\text{-}t\text{-}FP}$) as follows:

~~$SF_{mod} = 1 - \frac{LE}{LE_{pot}} = \frac{LST - Trad_{pot}}{Trad_{stress} - Trad_{pot}} \frac{LE\_SPARSE_{t-FP}}{LE_{p-t-FP}}$~~ (16)(24)



Mis en forme : Police :10 pt, Police de script complexe :Arial

Mis en forme : Centré, Interligne : simple

Tableau mis en forme

Cellules fusionnées

Mis en forme : Police :(Par défaut) +Corps, 10 pt, Gras, Police de script complexe :Arial

Mis en forme : Police :(Par défaut) +Corps, 10 pt, Police de script complexe :Arial

Mis en forme : Centré, Interligne : simple

Mis en forme : Centré

Mis en forme : Police :(Par défaut) Times New Roman, Gras, Police de script complexe :Arial

Mis en forme : Police :(Par défaut) +Corps, 10 pt, Police de script complexe :Arial

Mis en forme : Indice

Tableau mis en forme

Mis en forme : Police :11 pt

Mis en forme : Police :11 pt

Mis en forme : Police :11 pt

Mis en forme : Police :11 pt

where LE_SPARSE$_{t\text{-}FP}$ and ~~LE$_{pot}$~~LE$_{p\text{-}tFP}$ are the ~~simulated~~modeled latent heat fluxes in actual and potential conditions, respectively~~, and Trad$_{stress}$ and Trad$_{pot}$ are simulated radiative temperature in actual and potential conditions, respectively; and LST is the MODIS land surface temperature~~.

Furthermore, surface water stress factor derived from XLAS measurement, named SF$_{obs}$, at the time of Terra and Aqua overpass was computed as follows (Su, 2002):

$$SF_{obs} = \frac{H\_XLAS_t - H_{pot}}{H_{stress} - H_{pot}} \frac{H\_XLAS_t - H_{p-t-FP}}{H_{s-t-FP} - H_{p-t-FP}} \quad (17\sout{25})$$

where ~~H$_{stress}$~~H$_{s\text{-}t\text{-}FP}$ and ~~H$_{pot}$~~H$_{p\text{-}t\text{-}FP}$ are the ~~simulated~~modeled sensible heat flux in actual and potential conditions, respectively; and H_XLAS$_t$ is the XLAS sensible heat flux at the satellite overpass time.

## 6 Results and discussion

~~**6.1 Reconstruction of daily available energy and sensible heat flux**~~

~~For the sake of validation, daily AE computed from half hourly in situ data measured in the Ben Salem flux station (from November 2012 to June 2013) were compared to daily AE$_{day}$ estimated from instantaneous AE$_t$ using the scaling method based on Rg at both Terra-MODIS and Aqua-MODIS time overpass (see Sect. 3.3.2).~~

~~This comparison was achieved only for clear sky days for which MODIS images can be acquired and remote sensing data used to compute AE are available. In order to select clear sky days, the ratio of the incoming solar radiation Rg to the theoretical clear sky radiation Rso as proposed by the FAO-56 method (Allen et al., 1998) was computed. A day was defined as clear if the measured Rg is higher than 85 % of the theoretical clear sky radiation at the satellite overpass time (Delogu et al., 2012).~~

~~An overestimation of about 15% is found between measured and estimated daily available energy (Figure 3); and the coefficients a$_{Terra}$, b$_{Terra}$, a$_{Aqua}$ and b$_{Aqua}$ (Table 2) were applied to remove this bias.~~

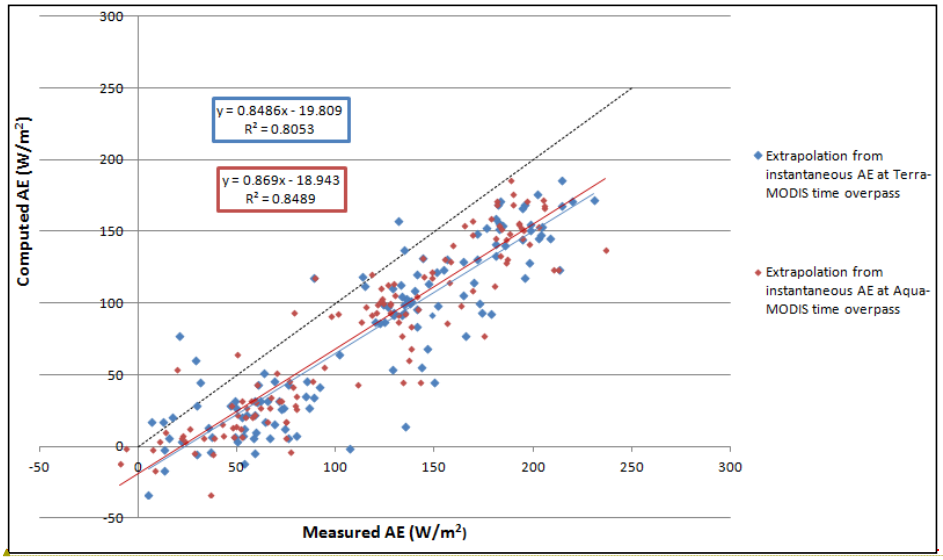


~~**Figure 3: Comparison of daily AE observed at Ben Salem flux station (2012-2013) and daily AE estimated using the scaling method based on Rg.**~~

**Mis en forme :** Indice

**Mis en forme :** Police :11 pt

**Mis en forme :** Police :11 pt

**Mis en forme :** Police :11 pt

**Mis en forme :** Police :11 pt

**Mis en forme :** Police :Italique, Police de script complexe :Italique

~~Using the same approach, figure 4 shows the comparison of daily H observed at Ben Salem flux station (2012-2013) and daily H estimated using the scaling method based on Rg. The coefficients $a'_{Terra}$, $b'_{Terra}$, $a'_{Aqua}$ and $b'_{Aqua}$ (Table 2) were applied to remove the bias between measured and estimated daily H.~~

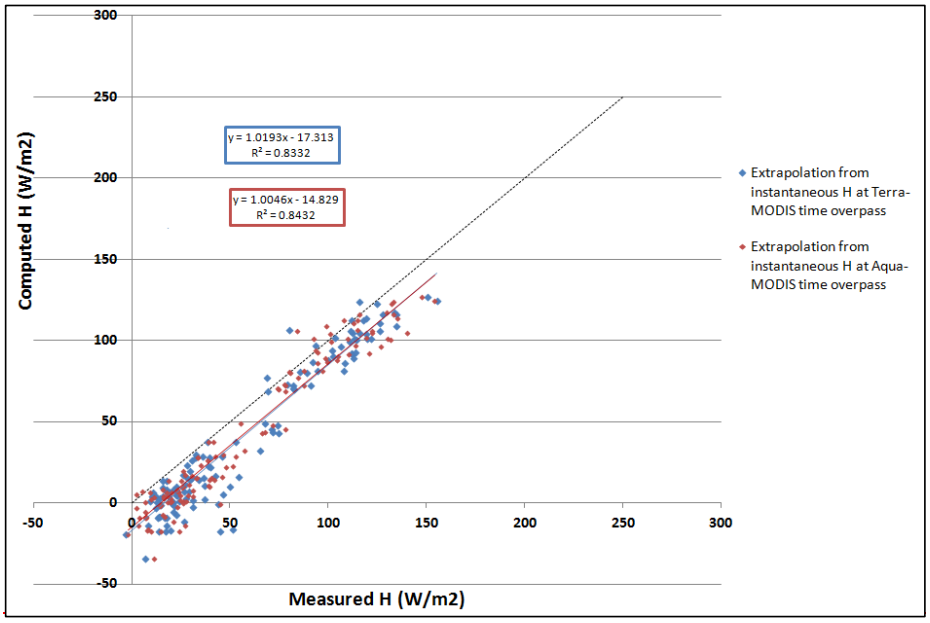


~~**Figure 4: Comparison of daily H observed at Ben Salem flux station (2012-2013) and daily H estimated using the scaling method based on Rg.**~~

~~**Table 2: Corrected parameterizations of AE and H**~~

| | | | |
|---|---|---|---|
| ~~Available energy (AE)~~ | ~~Terra~~ | ~~$a_{Terra}$~~ | ~~0.85~~ |
| | | ~~$b_{Terra}$~~ | ~~19.81~~ |
| | ~~Aqua~~ | ~~$a_{Aqua}$~~ | ~~0.87~~ |
| | | ~~$b_{Aqua}$~~ | ~~18.94~~ |
| ~~Sensible heat flux (H)~~ | ~~Terra~~ | ~~$a'_{Terra}$~~ | ~~1.02~~ |
| | | ~~$b'_{Terra}$~~ | ~~17.31~~ |
| | ~~Aqua~~ | ~~$a'_{Aqua}$~~ | ~~1.00~~ |
| | | ~~$b'_{Aqua}$~~ | ~~14.83~~ |

### ~~6.2~~6.1 XLAS and model derived instantaneous sensible heat fluxes

Our primary focus is the comparison between scintillometer measurements and the ~~modelled~~modeled sensible heat fluxes computed using the Terra and Aqua remotely sensed data. The scintillometer H at the time of the two satellites overpass ($H\_XLAS_t$) are interpolated from the half hourly H measurements ~~and are shown in figure 5.~~. Heat flux determination was possible for typically about 87% of the daytime measurements during the summer, availability of XLAS heat flux values was ~~less~~lower during the cold season due to poor visibility and/or stable stratification.

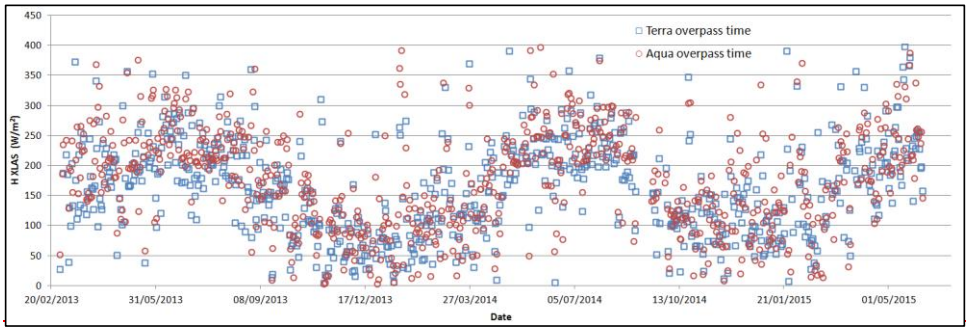


~~**Figure 5: Time series of XLAS measured sensible heat flux (H) at the time of Terra and Aqua overpass**~~

~~By convolving~~ SPARSE was weighted by the XLAS footprint ~~with the SPARSE derived H, we were~~in order to be able to compare the ~~modelled~~modeled values ($H\_SPARSE_{t\text{-}FP}$) with the XLAS measurements ($H\_XLAS_t$). Therefore, due to XLAS and remote sensing data availability, we got 175 ~~dots~~ and 118 ~~dots~~values for Terra and Aqua respectively. ~~As example~~ In order to highlight H inter-seasonality between the drier 2012-2013 and the wetter 2013-2014 seasons, we present ~~this comparison for~~ an example of two days ~~of special interest~~each in one season, DOY 2013-083 ~~and~~ shows H value ranging between 25 $Wm^{-2}$ and 757 $Wm^{-2}$ while DOY 2014-185 shows H value ranged between 128 $Wm^{-2}$ and 470 $Wm^{-2}$ (Figure 6). The colored area shows the ~~modelled~~modeled flux and the contours shows the surface source area contributing to ~~95% of~~ the scintillometer measurements. The ~~DOY 2013-083 corresponds to~~Day 2013-86 (24th March 2013) is chosen in the cold season while day 185-2014 (4th July 2014) is in the warm season to focus on land cover impact on LST and thus on modeled H, (trees and cereals in winter vs. only irrigated trees and market gardening in summer). Moreover, the first day experiences a ~~large footprint with a south~~strong southern wind while ~~the DOY 2014-185 corresponds to smaller upwind area with a north~~there is a light northern wind during the second day. Generally, a little number of MODIS pixels brings a high contribution to the signal; among them two are hot pixels (pixel with high LST and low NDVI) in which the land use is mainly arboriculture.

Prediction performance is assessed using ~~two widely used indicators: the root mean square error (~~RMSE~~)~~ and the coefficient of determination ($R^2$). Results for the sensible heat flux are illustrated in figure 7 and show good agreement between ~~modelled~~modeled and measured H at the time of satellites overpass. This is illustrated by linear regressions of $H\_SPARSE_{t\text{-}FP}$ = 1.065 $H\_XLAS_t$ -14.788 ($R^2$ = 0.6; RMSE = 57.89 ~~W.m~~$Wm^{-2}$) and ~~–~~ ~~H_SPARSE$_{t\text{-}FP}$ = 1.12 H_XLAS$_t$ -10.57 ($R^2$ = 0.63; RMSE = 53.85 W.m~~$Wm^{-2}$) for Terra and Aqua, respectively. This result is of great interest considering that the SPARSE model was run with no prior calibration. ~~–~~ However, we noted that bias is a function of the flux level and most outliers are recorded for H greater than 200 $Wm^{-2}$. This can be explained by (i) the XLAS measurement saturation (according to the "Kipp & Zonen LAS and XLAS instruction manual" (KIPP&ZONEN, 2007), for a path length of 4 km and a scintillometer height of 20 m, saturation measurement problem starts from H values higher than 300 $Wm^{-2}$), (ii) uncertainties on the correction of stability using the universal stability function and (iii) potential inconsistencies between the area average MODIS radiative temperature and the air temperature measured locally at the meteorological station.

Whereas there are several studies dealing with large aperture scintillometer (LAS) data whose measurements are compared to ~~modelled~~modeled fluxes, in the few studies dealing with extra large aperture scintillometer (XLAS)

**Mis en forme :** Police :+Titres CS

**Mis en forme :** Police :+Titres CS

**Mis en forme :** Police :+Titres CS

**Mis en forme :** Police :+Titres CS

**Mis en forme :** Police :+Titres CS

**Mis en forme :** Police :+Titres CS

data, the comparison is generally done with Eddy Covariance station measurements (Kohsiek et al., 2002; Moene et al., 2006). Indeed, our results are in agreement with those found by Marx et al. (2008) who compared LAS-derived and satellite-derived H (SEBAL was applied with NOAA-AVHRR images providing maps of surface energy fluxes at a 1 km × 1 km spatial resolution), and found that ~~modelled~~modeled H is underestimated with a RMSE of 39 ~~W.m~~$Wm^{-2}$ for the site Tamale and 104 ~~W.m~~$Wm^{-2}$ for the site Ejura. Moreover, Watts et al.(2000) compared the satellite (AVHRR radiometer) estimates of H to those from LAS over ~~a~~ semi-arid grassland in northwest Mexico during the summer of 1997. They found RMSE values of 31 ~~W.m~~$Wm^{-2}$ and 43 ~~W.m~~$Wm^{-2}$ for LAS path lengths of 300 m and 600 m respectively and showed that LAS measurements are less good than those derived from a 3D sonic anemometer. They also suggested longer LAS path length (greater than 1.1 km) since the LAS is rather insensitive to the surface near the receiver and the emitter.

Code de champ modifié

a)

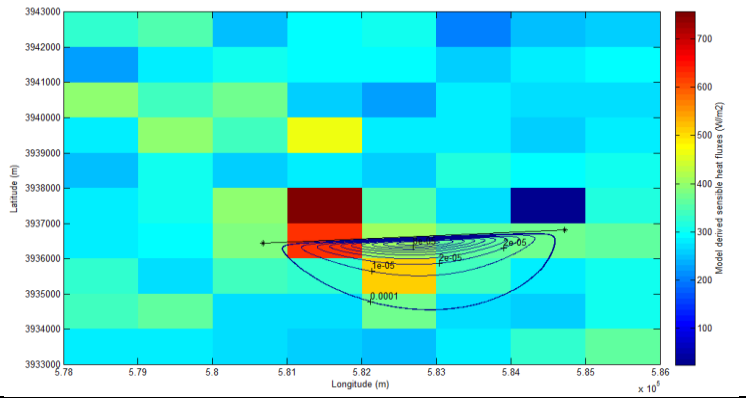


Tableau mis en forme

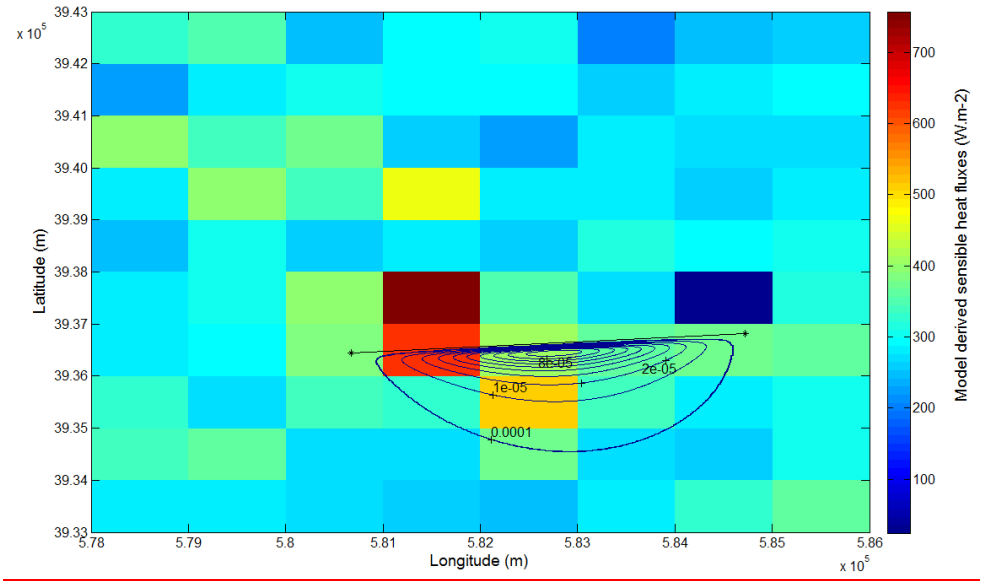


b)

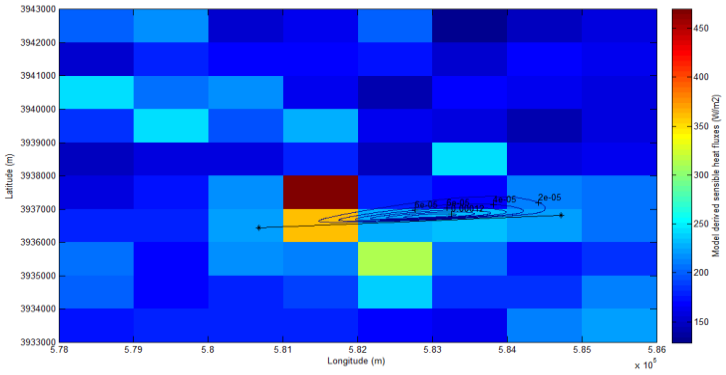


**Mis en forme :** Justifié

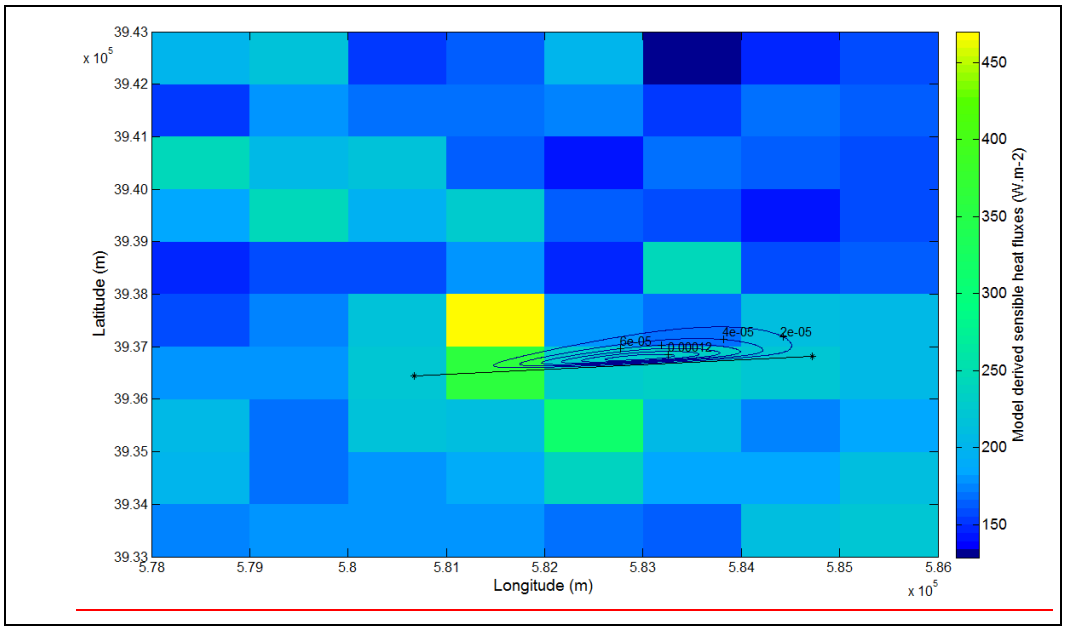


**Figure 6: Model derived sensible heat fluxes and footprints for (a) DOY 2013-~~083~~082 at Aqua time overpass and (b) DOY 2014-185 at Terra time overpass. The colored area shows the modeled flux and the contours shows the surface source area contributing to the scintillometer measurements.**

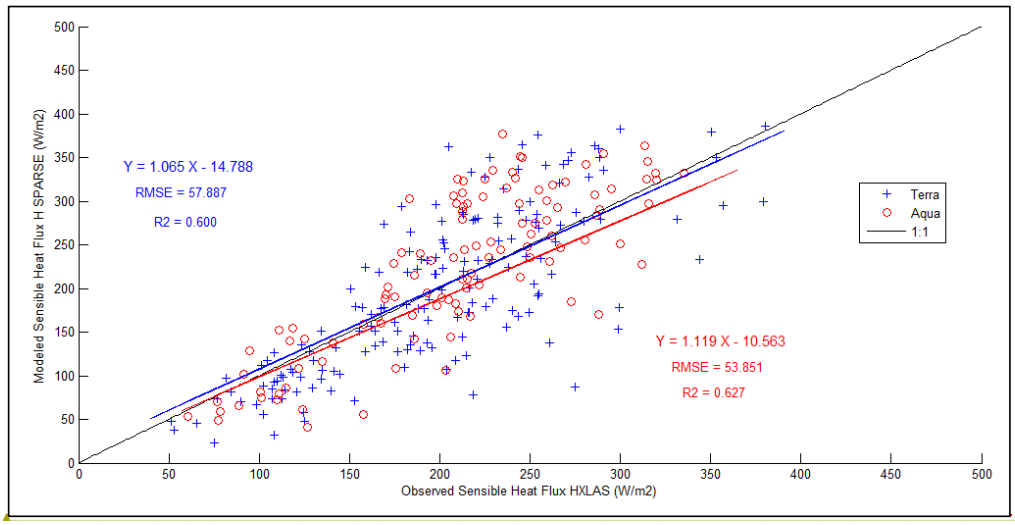


**Mis en forme :** Couleur de police : Automatique

**Mis en forme :** Couleur de police : Automatique

**Mis en forme :** Couleur de police : Rouge

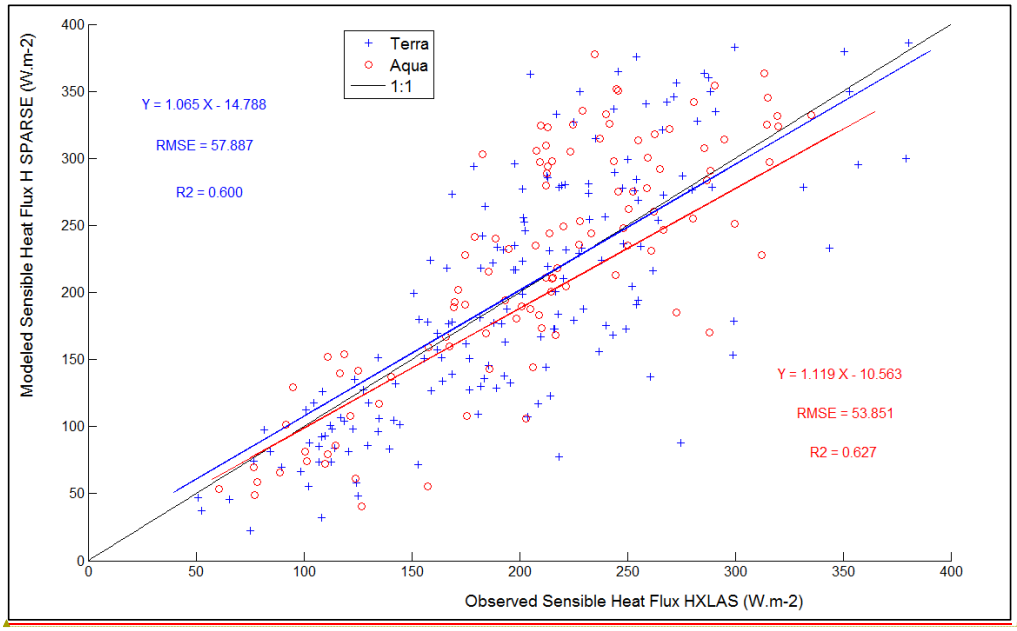


**Figure 7: ~~Modelled~~Modeled vs. observed sensible heat fluxes at Terra and Aqua time overpass**

### ~~6.3~~6.2 XLAS and model derived instantaneous latent heat fluxes

In a subsequent step, SPARSE derived LE ($LE\_SPARSE_{t\text{-}FP}$) was compared to observed LE ($LE\_residual\_XLAS_{t\text{-}FP}$). Results are illustrated in figure 8 showing a good agreement between ~~modelled~~modeled and observed LE. However, these results are less good than for the H results, as shown by the linear regressions: $LE\_SPARSE_{t\text{-}FP}$ =0.94 $LE\_residual\_XLAS_{t\text{-}FP}$ + 12.47 (RMSE = 47.20 ~~W.m~~$Wm^{-2}$) and $LE\_SPARSE_{t\text{-}FP}$ = 0.85 $LE\_residual\_XLAS_{t\text{-}FP}$ +11.51 (RMSE = 43.20 ~~W.m~~$Wm^{-2}$) for Terra and Aqua respectively, with an overall $R^2$ of 0.55 for both satellites. We note a greater scatter for latent heat flux than for the sensible heat flux (Figure 7), which can be explained by the fact that LE is here a residual term affected by estimation errors in both ~~estimated~~ AE and H. Despite this moderate discrepancy, the good agreement between both approaches indicates that the methodology adopted in SPARSE for estimating H and AE using MODIS imagery is appropriate for modeling latent heat fluxes.

**Mis en forme :** Couleur de police : Rouge

**Mis en forme :** Police :+Titres

**Mis en forme :** Police :+Titres

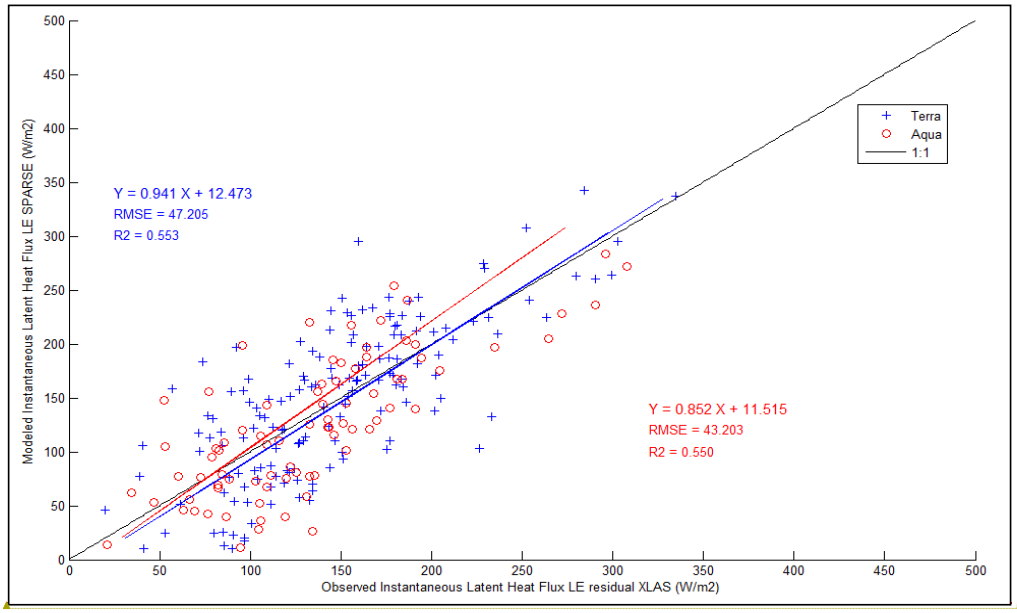


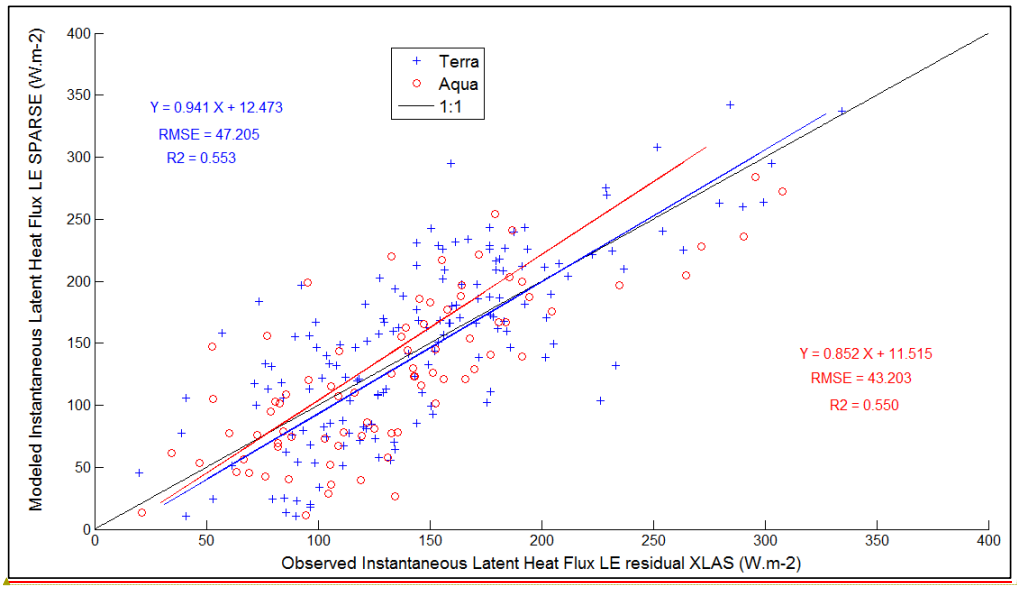


**Figure 8: ~~Modelled Vs. Observed~~Modeled vs. observed latent heat fluxes at Terra and Aqua time overpass**

## ~~6.4~~6.3 Water stress

The scattered values of the Stress Factor as shown in figure 9 are consistent with previous studies such as Boulet et al. (2015). SEB retrieval of stress is limited by the scale mismatch between the instantaneous estimate of the surface temperature during the satellite overpass (which can be influenced by high frequency turbulence) and the aggregated values of other forcing data which are derived from half hourly averages (Lagouarde et al., 2013; Lagouarde et al., 2015). However, general tendencies are well reproduced, with most points located within a 0.2 confidence interval (illustrated by dotted lines along the 1:1 line) as found by Boulet et al. (2015) at ~~plot~~field

**Mis en forme :** Police :Italique, Couleur de police : Couleur personnalisée(RVB(79;129;189)), Police de script complexe :10 pt, Gras, Italique

**Mis en forme :** Police :Italique, Couleur de police : Couleur personnalisée(RVB(79;129;189)), Police de script complexe :10 pt, Gras, Italique

scale, which is encouraging in a perspective of assimilating ET or SF in a water balance model for example. Moreover, it is noted that results include small LE and ~~LE$_{pot}$~~LE$_p$ values having the same order of magnitude as the measurement uncertainty itself. Most outliers having greater water stress (~1) correspond to high evaporation from bare soil since the dominant land use in the study area is arboriculture, but also, this could be due to saturation of scintillation which led to an underestimation of H XLAS measurements as pointed by Frehlich and Ochs (1990) and Kohsiek et al. (2002).

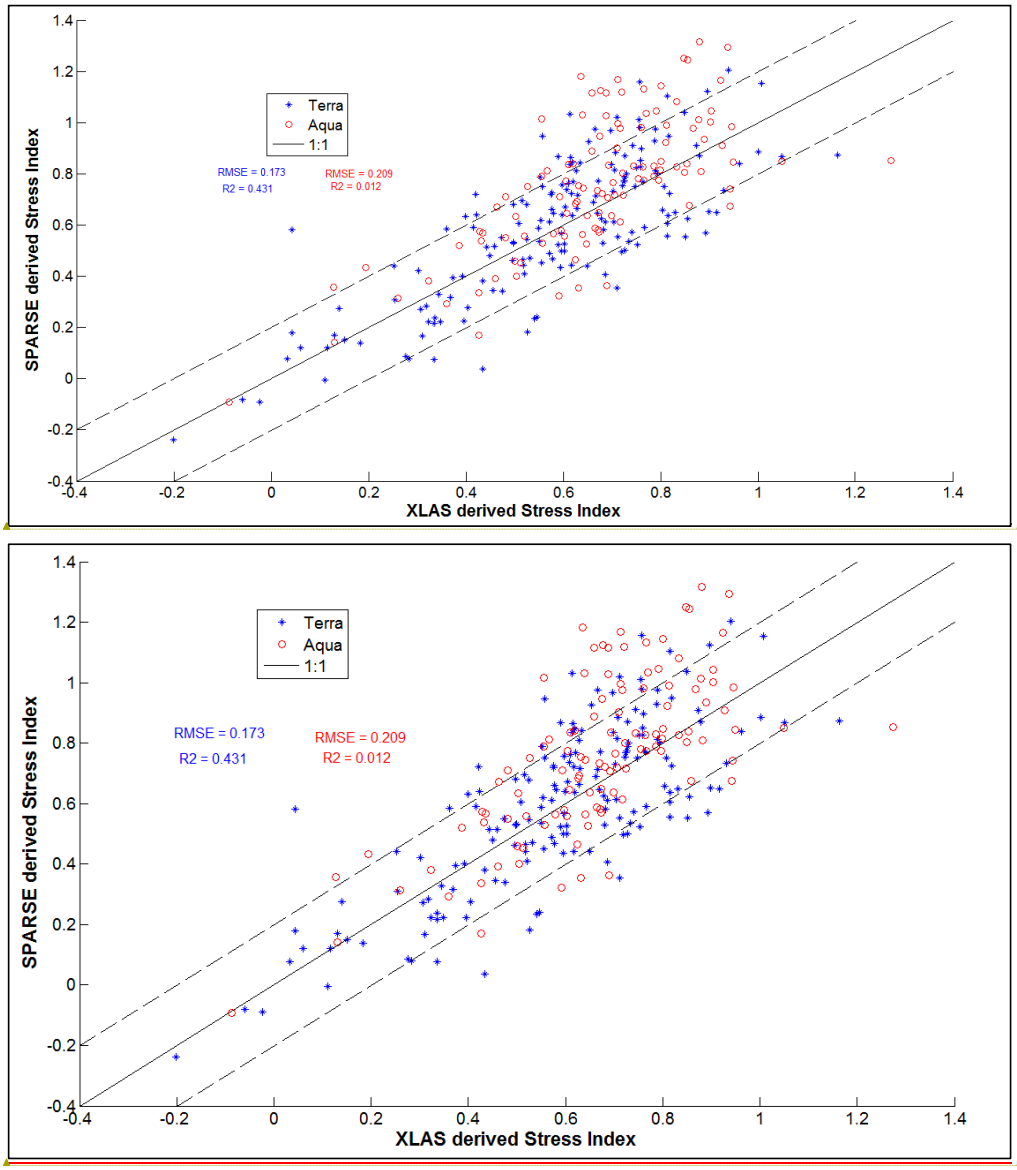


**Mis en forme :** Couleur de police : Rouge

Terra
Aqua
1:1
RMSE = 0.173
R2 = 0.431
RMSE = 0.209
R2 = 0.012
SPARSE derived Stress Index
XLAS derived Stress Index

**Mis en forme :** Couleur de police : Rouge

**Figure 9: ~~Modelled Vs~~Modeled vs. XLAS derived stress index SF at Terra and Aqua time overpass**

~~Modelled~~Modeled and observed stress index at Terra and Aqua time overpass show a consistent evolution with daily rainfall (Figure 10), although the ~~modelled~~modeled stress show a greater dispersion than the observed one.

During a rainy episode (or an eventual irrigation period), the surface temperature decreases towards the unstressed surface temperature, thus marking an unstressed state, and SF tends to 0. Conversely, after a long dry down, the water stress appears and the surface temperature increases towards the equilibrium surface temperature computed by SPARSE under stressed conditions, and SF tends towards 1. Besides, it is noted that ~~modelled~~modeled stress indexes computed on the basis of Aqua MODIS's LST are often greater than those computed used Terra MODIS's LST due to higher LST (higher global solar radiation) at the time of Terra overpass (around midday).

a)

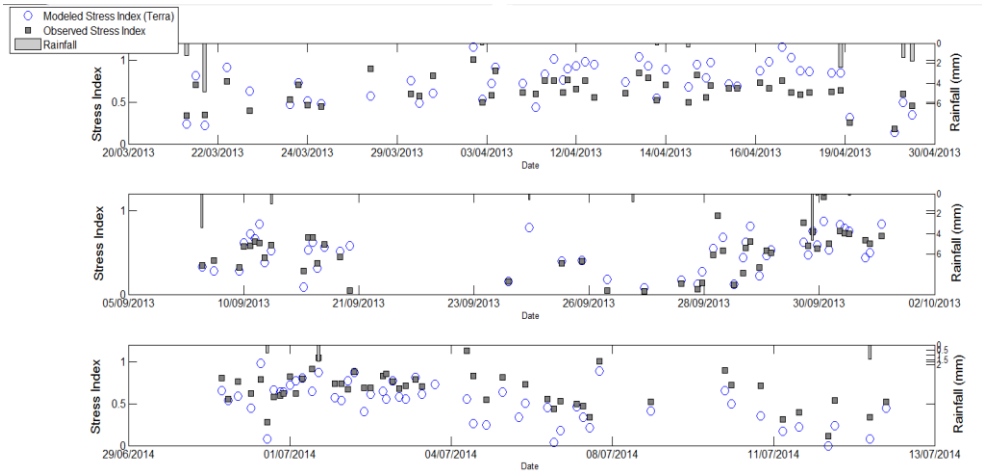


b)

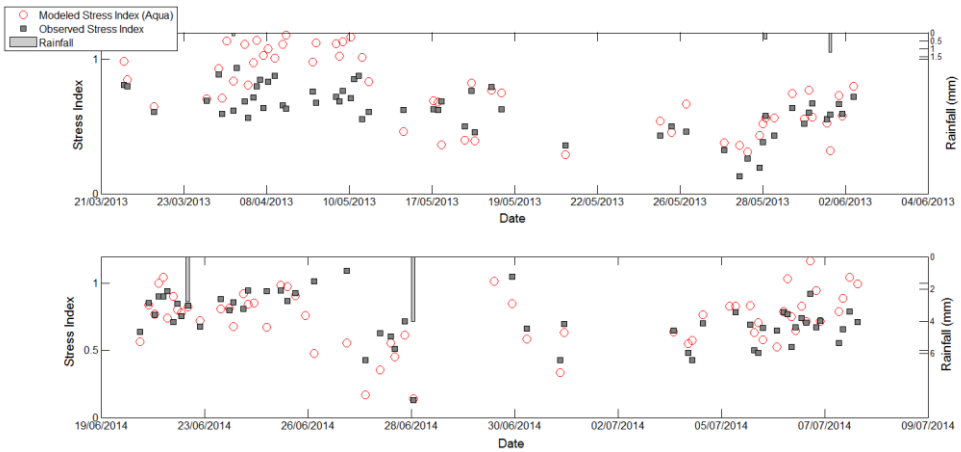


**Figure 10: ~~Modelled~~Modeled and observed ~~Stress~~stress index evolution at (a) Terra and (b) Aqua time overpass compared to daily rainfall**

### ~~6.5~~6.4 XLAS and model derived daily latent heat fluxes

Daily observed ET, *i.e.* LE_residual_XLAS$_{day\text{-}FP}$, was computed using the residual method; hence, six estimates of the daily observed ET were obtained by combining the two satellite ~~passes data~~datasets and three methods to compute G and thus AE (see Sect. 3.3). Only the residual method was used to estimate daily observed ET for two reasons; on the first hand, to reduce the computations approach since, already, three methods to compute AE have been tested and on the other hand, the application of the EF method was not possible because we do not ~~dispose of spatialized~~have a measured spatially distributed potential evapotranspiration (only point potential evapotranspiration data at the Ben Salem meteorological station are available). From daily observed ET estimates, minimum and maximum ET were selected for each day and minimum and maximum daily ET time series were interpolated between successive days based on the self preservation of the ratio of ~~the available energy (AE) to the global incoming radiation~~AE to Rg as scale factor (Figure 11).

In addition, three methods were used to compute SPARSE daily ET for the Terra and Aqua overpasses (see Sect. 4.2), providing six estimates of the daily ~~modelled~~modeled ET. For each day average ET was plotted (260 days) with error bars figuring minimum and maximum values, along with precipitation to understand the rainfall impact on the ET evolution (Figure 11).

Despite the uncertainty in reconstructing the daily ET from instantaneous ET, overall results show a good agreement between XLAS derived and SPARSE derived ET values with similar seasonal dynamics. Daily observed and ~~modelled~~modeled ET over the whole study period were both in the range of 0-4 ~~mm mm.day~~mmday$^{-1}$ with an RMSE of 0.7 mmday$^{-1}$ which is consistent with the land use present in the XLAS path: mainly trees ~~with~~spaced by a considerable fraction of bare soil~~.~~, and less herbaceous soil-covering crops (see Sect.3.2). As expected, ET rates decrease significantly during dry periods (summers) since arid conditions limit the latent heat flux in favor of sensible heat flux and increase immediately after rainfall events~~.~~ due to the high amount of water evaporated from soil. The rainfall peaks that occurred on 3$^{rd}$ September 2013 (about ~~10mm~~10 mm), 6$^{th}$ October 2013 (about 20 mm), 15$^{th}$ March 2014 (about 100 mm) and 22$^{nd}$ April 2014 (about 25 mm) are followed by well-reproduced ~~drydown (soil drying) events.~~ drydowns.

At seasonal scale, we note a good agreement between ~~modelled~~modeled and observed daily ET for the 2013-2014 and 2014-2015 seasons, especially when vegetation cover was more developed: from March to July 2014 and from March to Mai 2015; these periods correspond to cereals vegetation peak in some plots (March-April) and to market gardening crops (e.g. tomato, water melon, pepper~~…~~), etc.) cultivated generally from spring to the beginning of autumn in the interrow area of trees plots, which is a common farming practice in the Kairouan plain. However, the 2012-2013 season was dry compared with the two other ones, and less accurate results were obtained. Some points with little to null ET were recorded from May to July 2013 which can be explained by the very dry conditions and scattered vegetation cover with a considerable amount of bare soil. ~~Lower ET values are generally~~This behavior was not observed in the same period of 2014, because 2014 was a rainy year in comparison to 2013, therefore, even supposing that the farmers have the same attitude and cultivate the same crop types between the two years (which is not true in the context of our study area and farmers always change crop types), precipitations favor the growth of spontaneous vegetation over fallows which contribute to ET rise. On the other hand, since this year experiences more rain, farmers cultivate a larger part of the land and diversify the crop types; the vegetation cover is denser and contributes to an overall increase in ET. Overall, lower ET values are recorder in autumn (October and November) which correspond to evapotranspiration from trees only,

Mis en forme : Police :Italique

since the latest summer crops (market gardening crops) have been already harvested and the winter crops (mainly cereals) are not yet sown.

Moreover, it can be seen that occasionally SPARSE ~~model~~ overestimated ET. As example, three dates can be selected in August 2013 (15th, 25th and 29th August 2013) for which ~~modelled~~modeled ET were 3.30 mm, 3.80 mm and 2.80 mm while maximum observed ET were 2.0 mm, 2.40 mm and 1.20 mm, respectively; broader amplitude between ~~modelled~~modeled (4.00 mm) and observed ET (1.40 mm) was also recorded on the 18th of May 2013. SPARSE also overestimates ET throughout ten days in August 2014 with an average difference of 1.1 mm and a maximum difference of 1.60 mm recorded in 23rd August 2014. These discrepancies are always recorded under wet conditions (minimum stress factor) which show the difficulty in representing accurately the conditions close to the potential ET. This might be related to the theoretical limit of the model for low vegetation stress especially when coupled with low evaporation efficiencies (*i.e.* dry soil surface) as already reported by Boulet et al. (2015) for senescent vegetation. Average difference between SPARSE and XLAS derived LE estimates when both are available indicate that SPARSE can predict evapotranspiration with accuracies approaching 5% of that of the XLAS.

**Mis en forme :** Police :Italique

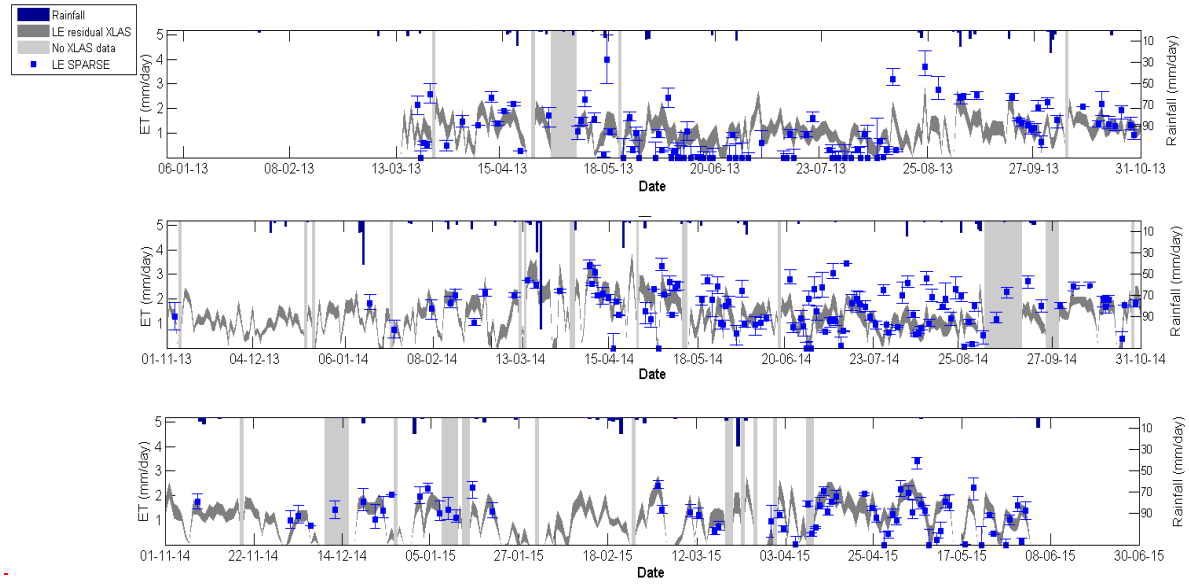
Rainfall
LE residual XLAS
No XLAS data
LE SPARSE
ET (mm/day)
Rainfall (mm/day)
Date
06-01-13
08-02-13
13-03-13
15-04-13
18-05-13
20-06-13
23-07-13
25-08-13
27-09-13
31-10-13
01-11-13
04-12-13
06-01-14
08-02-14
13-03-14
15-04-14
18-05-14
20-06-14
23-07-14
25-08-14
27-09-14
31-10-14
01-11-14
22-11-14
14-12-14
05-01-15
27-01-15
18-02-15
12-03-15
03-04-15
25-04-15
17-05-15
08-06-15
30-06-15

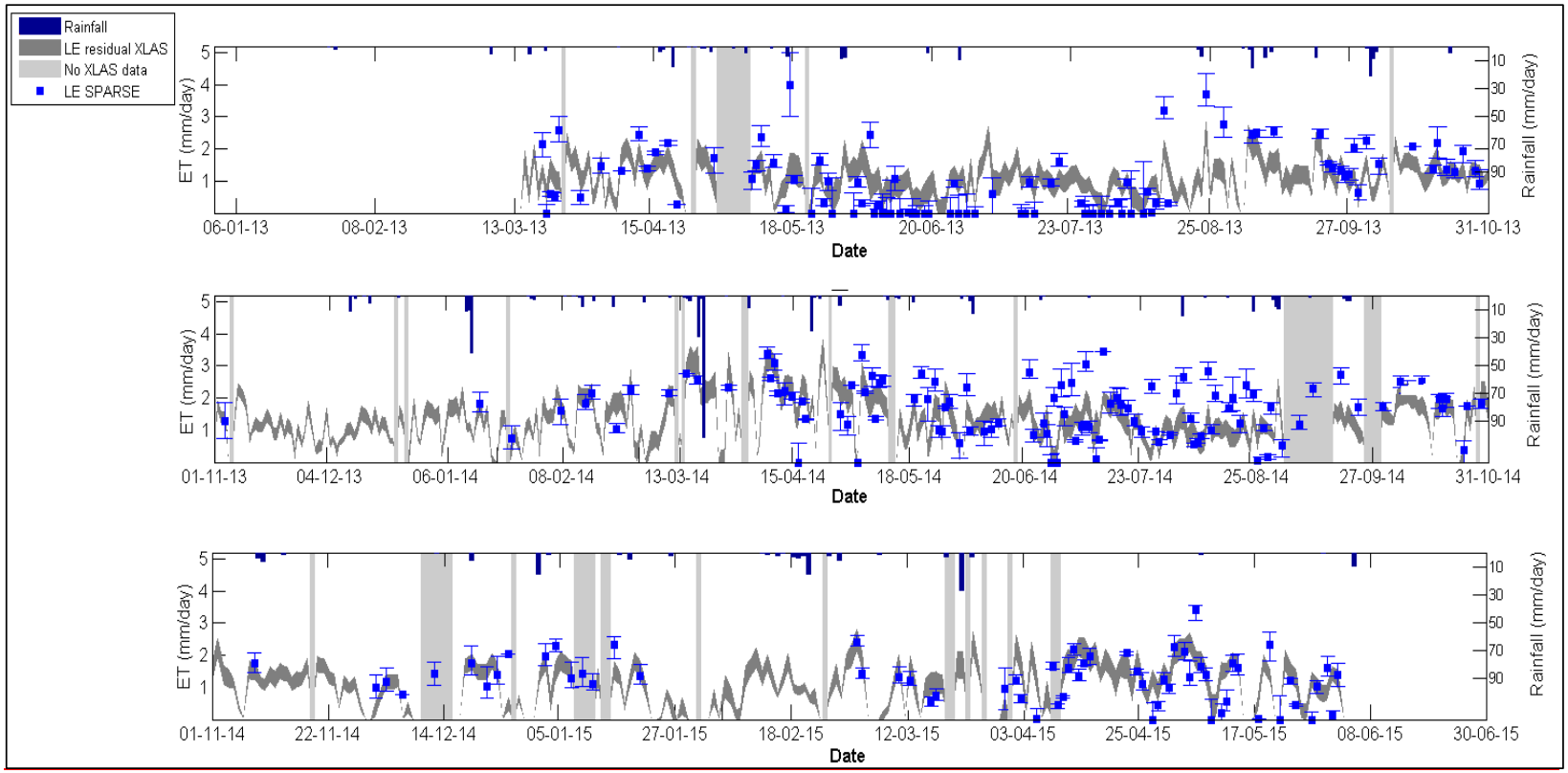


**Figure 11: ~~Modelled~~Modeled vs. observed daily latent heat fluxes. Dark grey color shows minimum and maximum daily observed LE. Light grey vertical bars show gaps in XLAS data. Error bars for the modeled ET show the minimum and the maximum daily ET resulting from the three methods used to compute daily ET from instantaneous modeled ET.**

**Mis en forme :** Couleur de police : Automatique

880

## 7 Conclusions

This study evaluated the performances of the SPARSE model forced by MODIS remote sensing products in an operational context (no model calibration) to estimate instantaneous and daily evapotranspiration. The validation protocol was based on an unprecedented dataset with an extra large aperture scintillometer. Indeed, up to our knowledge, this is the first work based on XLAS measurements acquired during more than 2 years, as compared to three months in previous works (Kohsiek et al., 2002; Moene et al., 2006). The estimates of the sensible heat flux derived from the SPARSE model are in close agreement with those obtained from the XLAS. These results indicate that the XLAS can be fruitfully used to validate large-scale sensible heat flux derived from remote sensing data (and residual latent heat flux), in particular for the results obtained at the satellite overpass time, providing a feasible alternative to local micrometeorological techniques for measuring the sensible heat flux and validating satellite-derived estimates (*i.e.* eddy correlation). Furthermore, the extrapolation from instantaneous to daily evapotranspiration is less obvious and three methods were tested based on the stress index, the evaporative fraction and the residual approach. The daily latent heat fluxes derived from the XLAS agreed rather well with those ~~modelled~~modeled using SPARSE model, which shows the potential of the SPARSE model in water consumption monitoring over heterogeneous landscape in semi-arid conditions, and especially to locate areas most affected by water stress. ~~Even though overall results are encouraging, further work is needed to better valorize the XLAS dataset and~~ However, the precision in ET prediction with the SPARSE model is restricted by several assumptions and uncertainties. For instance, the instantaneous remote sensing data and mainly LST which is paramount in stress coefficient computation are assumed to be reliable. Moreover, there is an issue with the MODIS pixel heterogeneity and notably the distribution of components at the intersection between the square pixel and the XLAS footprint. Uncertainties are also due to half hourly forcing (meteorological and flux data) and XLAS data as well as to the extrapolation method from instantaneous to daily results. Furthermore, the empirical estimation methods of soil heat flux G (three methods were tested) as well as the possible daily heat accumulation lead to possible errors in available energy estimation and in turn in residual LE estimation.

Even if overall results are encouraging, further work is needed to improve results by i) being most efficient in the SPARSE model application using calibrated input data specific to our study area, especially input parameters to which the model is particularly sensitive such as the mean leaf width and the minimum stomatal resistance ~~and~~, ii) taking into account the heterogeneity of the 1km MODIS pixel by applying MODIS footprint, which is determined by the sensor's observation geometry~~.~~ and (iii) using a Land Surface Model applied at the field scale (Etchanchu et al., 2017) to analyze the scaling properties from the field to the footprint of the XLAS and the MODIS pixels similarly.

Finally, in a future work, we plan to take advantage of the complementarities between the Soil Water Balance and Surface Energy Balance approaches (*i.e.* continuous but uncertain estimates using SWB due to poor soil water content control on one hand and sensitivity of SEB to the actual water stress on the other hand) to implement an assimilation scheme of the remotely sensed surface temperature into ~~SVAT~~land surface models. In fact, in order to provide further information about distributed soil water status over the studied areas, the TIR-derived evapotranspiration products could be assimilated directly either in ~~SVAT~~land surface or hydrological models.

Mis en forme : Police :Italique

Mis en forme : Police :Times New Roman, 10 pt

Mis en forme : Police par défaut

Mis en forme : Police :Italique

**Author contribution:**

Sameh Saadi: data processing, data analysis and results interpretation.
Gilles Boulet: data analysis and results interpretation.
Malik Bahir: SPARSE inputs and XLAS data processing and analysis.
Aurore Brut: XLAS data processing and analysis.
Bernard Mougenot and Zohra Lili Chabaane: site management.
Pascal Fanise: site instrumentation.
Vincent Simonneaux and Zohra Lili-Chabaane contributed with ideas and discussions.

**Competing interests:**

The authors declare that they have no conflict of interest.

**Acknowledgements**

The authors are thankful to the GDAs of Ben Salem I and Ben Salem II which enabled the scintillometer set-up and access above the two water towers. Funding from the CNES/TOSCA program for the EVA2IRT project, from the MISTRALS/SICMED program for the ReSAMEd project, from the ORFEO/CNES Program for Pléiades images (© CNES 2012, Distribution Airbus DS, all rights reserved), and from the ANR/TRANSMED program for the AMETHYST project (ANR-12-TMED-0006-01) as well as the mobility support from PHC Maghreb program (N° 32592VE) are gratefully acknowledged,. This work has benefited also from the financial support of the ARTS program ("Allocations de recherche pour une thèse au Sud") of IRD (Institut de Recherche pour le Développement).

**References**

~~Allen, R., Irmak, A., Trezza, R., Hendrickx, J. M., Bastiaanssen, W., and Kjaersgaard, J.: Satellite-based ET estimation in agriculture using SEBAL and METRIC, Hydrological Processes, 25, 4011-4027, 2011.~~

~~Allen, R. G., Pereira, L. S., Raes, D., and Smith, M.: Crop evapotranspiration-Guidelines for computing crop water requirements-FAO Irrigation and drainage paper 56, FAO, Rome, 300, D05109, 1998.~~

~~Allen, R. G., Tasumi, M., and Trezza, R.: AIP Conf. Proc., 852, 127, 2005.~~

~~Allen, R. G., Tasumi, M., and Trezza, R.: J. Irrig. Drain. Eng., 133, 395, 2007.~~

~~Amri, R., Zribi, M., Lili-Chabaane, Z., Szczypta, C., Calvet, J. C., and Boulet, G.: FAO-56 dual model combined with multi-sensor remote sensing for regional evapotranspiration estimations, Remote Sensing, 6, 5387-5406, 2014.~~

~~Anderson, M. C., Kustas, W. P., Norman, J. M., Hain, C. R., Mecikalski, J. R., Schultz, L., González-Dugo, M. P., Cammalleri, C., d'Urso, G., Pimstein, A., and Gao, F.: Mapping daily evapotranspiration at field to~~

continental scales using geostationary and polar orbiting satellite imagery, Hydrol. Earth Syst. Sci., 15, 223-239, 10.5194/hess-15-223-2011, 2011.

Andreas, E. L.: Atmospheric stability from scintillation measurements, Applied optics, 27, 2241-2246, 1988.

Bai, J., Liu, S., and Mao, D.: Area-averaged evapotranspiration fluxes measured from large aperture scintillometer in the Hai River basin, River Basin Research And Planning Approach, edited by: Zhang, H., Zhao, R., and Zhoa, H., Orient ACAD Forum, Marrickville, Australia, 2009, 331-340,

Bastiaanssen, W. G. M.: Regionalization of surface flux densities and moisture indicators in composite terrain; a remote sensing approach under clear skies in mediterranean climates, SC-DLO, Wageningen, 1995.

Bastiaanssen, W. G. M.: J. Irrig. Drain. Eng., 131, 85, 2005.

Bastiaanssen, W. G. M., Allen, R. G., Droogers, P., D'Urso, G., and Steduto, P.: Twenty five years modeling irrigated and drained soils: State of the art, Agricultural Water Management, 92, 111-125, http://dx.doi.org/10.1016/j.agwat.2007.05.013, 2007.

Bisht, G., Venturini, V., Islam, S., and Jiang, L.: Estimation of the net radiation using MODIS (Moderate Resolution Imaging Spectroradiometer) data for clear sky days, Remote Sensing of Environment, 97, 52-67, https://doi.org/10.1016/j.rse.2005.03.014, 2005.

Boulet, G., Braud, I., and Vauclin, M.: Study of the mechanisms of evaporation under arid conditions using a detailed model of the soil-atmosphere continuum. Application to the EFEDA-I experiment, Journal of Hydrology, 193, 114-141, https://doi.org/10.1016/S0022-1694(96)03148-4, 1997.

Boulet, G., Chehbouni, A., Gentine, P., Duchemin, B., Ezzahar, J., and Hadria, R.: Monitoring water stress using time series of observed to unstressed surface temperature difference, Agricultural and Forest Meteorology, 146, 159-172, https://doi.org/10.1016/j.agrformet.2007.05.012, 2007.

Boulet, G., Mougenot, B., Lhomme, J. P., Fanise, P., Lili-Chabaane, Z., Olioso, A., Bahir, M., Rivalland, V., Jarlan, L., Merlin, O., Coudert, B., Er-Raki, S., and Lagouarde, J. P.: The SPARSE model for the prediction of water stress and evapotranspiration components from thermal infra-red data and its evaluation over irrigated and rainfed wheat, Hydrol. Earth Syst. Sci., 19, 4653-4672, 10.5194/hess-19-4653-2015, 2015.

Bounoua, L., Zhang, P., Thome, K., Masek, J., Safia, A., Imhoff, M. L., and Wolfe, R. E.: Mapping Biophysical Parameters for Land Surface Modeling over the Continental US Using MODIS and Landsat, Dataset Papers in Science, 2015, 11, 10.1155/2015/564279, 2015.

Braud, I., Dantas-Antonino, A. C., Vauclin, M., Thony, J. L., and Ruelle, P.: A simple soil-plant-atmosphere transfer model (SiSPAT) development and field verification, Journal of Hydrology, 166, 213-250, http://dx.doi.org/10.1016/0022-1694(94)05085-C, 1995.

Brunsell, N. A., Ham, J. M., and Arnold, K. A.: Validating remotely sensed land surface fluxes in heterogeneous terrain with large aperture scintillometry, International Journal of Remote Sensing, 32, 6295-6314, 10.1080/01431161.2010.508058, 2011.

Burba, G. G., Verma, S. B., and Kim, J.: Surface energy fluxes of Phragmites australis in a prairie wetland, Agricultural and Forest Meteorology, 94, 31-51, https://doi.org/10.1016/S0168-1923(99)00007-6, 1999.

Calera, A., Campos, I., Osann, A., D'Urso, G., and Menenti, M.: Remote Sensing for Crop Water Management: From ET Modelling to Services for the End Users, Sensors, 17, 1104, 2017.

Chávez, J., Neale, C. M. U., Hipps, L. E., Prueger, J. H., and Kustas, W. P.: Comparing Aircraft-Based Remotely Sensed Energy Balance Fluxes with Eddy Covariance Tower Data Using Heat Flux Source Area Functions, Journal of Hydrometeorology, 6, 923-940, 10.1175/jhm467.1, 2005.

Chávez, J. L., Neale, C. M. U., Prueger, J. H., and Kustas, W. P.: Daily evapotranspiration estimates from extrapolating instantaneous airborne remote sensing ET values, Irrigation Science, 27, 67-81, 10.1007/s00271-008-0122-3, 2008.

Chehbouni, A., Watts, C., Lagouarde, J. P., Kerr, Y. H., Rodriguez, J. C., Bonnefond, J. M., Santiago, F., Dedieu, G., Goodrich, D. C., and Unkrich, C.: Estimation of heat and momentum fluxes over complex terrain using a large aperture scintillometer, Agricultural and Forest Meteorology, 105, 215-226, https://doi.org/10.1016/S0168-1923(00)00187-8, 2000.

Chirouze, J., Boulet, G., Jarlan, L., Fieuzal, R., Rodriguez, J. C., Ezzahar, J., Er-Raki, S., Bigeard, G., Merlin, O., Garatuza-Payan, J., Watts, C., and Chehbouni, G.: Intercomparison of four remote-sensing-based energy balance methods to retrieve surface evapotranspiration and water stress of irrigated fields in semi-arid climate, Hydrol. Earth Syst. Sci., 18, 1165-1188, 10.5194/hess-18-1165-2014, 2014.

Choudhury, B., and Monteith, J.: A four-layer model for the heat budget of homogeneous land surfaces, Quarterly Journal of the Royal Meteorological Society, 114, 373-398, 1988.

Choudhury, B. J., Idso, S. B., and Reginato, R. J.: Analysis of an empirical model for soil heat flux under a growing wheat crop for estimating evaporation by an infrared-temperature based energy balance equation, Agricultural and Forest Meteorology, 39, 283-297, http://dx.doi.org/10.1016/0168-1923(87)90021-9, 1987.

Clevers, J. G. P. W.: Application of a weighted infrared-red vegetation index for estimating leaf Area Index by Correcting for Soil Moisture, Remote Sensing of Environment, 29, 25-37, http://dx.doi.org/10.1016/0034-4257(89)90076-X, 1989.

Colaizzi, P. D., Evett, S. R., Howell, T. A., and Tolk, J. A.: Comparison of Five Models to Scale Daily Evapotranspiration from One-Time-of-Day Measurements, 10.13031/2013.18885, 2005.

Cragoa, R., and Brutsaert, W.: Daytime evaporation and the self-preservation of the evaporative fraction and the Bowen ratio, Journal of Hydrology, 178, 241-255, http://dx.doi.org/10.1016/0022-1694(95)02803-X, 1996.

Danelichen, V. H. d. M., Biudes, M. S., Souza, M. C., Machado, N. G., Silva, B. B. d., and Nogueira, J. d. S.: Estimation of soil heat flux in a neotropical Wetland region using remote sensing techniques, Revista Brasileira de Meteorologia, 29, 469-482, 2014.

De Bruin, H. A. R., and Wang, J.: Scintillometry: a review. Researchgate, 2017.

Delogu, E., Boulet, G., Olioso, A., Coudert, B., Chirouze, J., Ceschia, E., Le Dantec, V., Marloie, O., Chehbouni, G., and Lagouarde, J. P.: Reconstruction of temporal variations of evapotranspiration using instantaneous estimates at the time of satellite overpass, Hydrol. Earth Syst. Sci., 16, 2995-3010, 10.5194/hess-16-2995-2012, 2012.

Ezzahar, J., Chehbouni, A., Hoedjes, J., Ramier, D., Boulain, N., Boubkraoui, S., Cappelaere, B., Descroix, L., Mougenot, B., and Timouk, F.: Combining scintillometer measurements and an aggregation scheme to estimate area-averaged latent heat flux during the AMMA experiment, Journal of Hydrology, 375, 217-226, http://dx.doi.org/10.1016/j.jhydrol.2009.01.010, 2009.

Feddes, R. A., Kowalik, P. J., and Zaradny, H.: Simulation of Field Water Use and Crop Yield, Wiley, 1978.

Frehlich, R. G., and Ochs, G. R.: Effects of saturation on the optical scintillometer, Applied optics, 29, 548-553, 1990.

Gentine, P., Entekhabi, D., Chehbouni, A., Boulet, G., and Duchemin, B.: Analysis of evaporative fraction diurnal behaviour, Agricultural and Forest Meteorology, 143, 13-29, https://doi.org/10.1016/j.agrformet.2006.11.002, 2007.

Giorgi, F., and Avissar, R.: Representation of heterogeneity effects in earth system modeling: Experience from land surface modeling, Reviews of Geophysics, 35, 413-437, 1997.

Glenn, E. P., Huete, A. R., Nagler, P. L., Hirschboeck, K. K., and Brown, P.: Integrating remote sensing and ground methods to estimate evapotranspiration, Critical Reviews in Plant Sciences, 26, 139-168, 2007.

Green, A. E., and Hayashi, Y.: Use of the scintillometer technique over a rice paddy, Journal of Agricultural Meteorology, 54, 225-234, 1998.

Hain, C. R., Mecikalski, J. R., and Anderson, M. C.: Retrieval of an Available Water-Based Soil Moisture Proxy from Thermal Infrared Remote Sensing. Part I: Methodology and Validation, Journal of Hydrometeorology, 10, 665-683, 10.1175/2008jhm1024.1, 2009.

Hartogensis, O. K., Watts, C. J., Rodriguez, J. C., and Bruin, H. A. R. D.: Derivation of an Effective Height for Scintillometers: La Poza Experiment in Northwest Mexico, Journal of Hydrometeorology, 4, 915-928, 10.1175/1525-7541(2003)004<0915:doaehf>2.0.co;2, 2003.

Hemakumara, H. M., Chandrapala, L., and Moene, A. F.: Evapotranspiration fluxes over mixed vegetation areas measured from large aperture scintillometer, Agricultural Water Management, 58, 109-122, http://doi.org/10.1016/S0378-3774(02)00131-2, 2003.

Hill, R., Clifford, S. F., and Lawrence, R. S.: Refractive-index and absorption fluctuations in the infrared caused by temperature, humidity, and pressure fluctuations, JOSA, 70, 1192-1205, 1980.

Hoedjes, J. C. B., Chehbouni, A., Jacob, F., Ezzahar, J., and Boulet, G.: Deriving daily evapotranspiration from remotely sensed instantaneous evaporative fraction over olive orchard in semi-arid Morocco, Journal of Hydrology, 354, 53-64, https://doi.org/10.1016/j.jhydrol.2008.02.016, 2008.

Horst, T., and Weil, J.: Footprint estimation for scalar flux measurements in the atmospheric surface layer, Boundary-Layer Meteorology, 59, 279-296, 1992.

Hunink, J., Eekhout, J., Vente, J., Contreras, S., Droogers, P., and Baille, A.: Hydrological Modelling using Satellite-Based Crop Coefficients: A Comparison of Methods at the Basin Scale, Remote Sensing, 9, 174, 2017.

Jackson, R. D., Moran, M. S., Gay, L. W., and Raymond, L. H.: Evaluating evaporation from field crops using airborne radiometry and ground-based meteorological data, Irrigation Science, 8, 81-90, 10.1007/bf00259473, 1987.

Jacobs, J. M., Myers, D. A., Anderson, M. C., and Diak, G. R.: GOES surface insolation to estimate wetlands evapotranspiration, Journal of Hydrology, 266, 53-65, https://doi.org/10.1016/S0022-1694(02)00117-8, 2002.

Kalma, J. D., McVicar, T. R., and McCabe, M. F.: Estimating land surface evaporation: A review of methods using remotely sensed surface temperature data, Surveys in Geophysics, 29, 421-469, 2008.

Kohsiek, W., Meijninger, W. M. L., Moene, A. F., Heusinkveld, B. G., Hartogensis, O. K., Hillen, W. C. A. M., and De Bruin, H. A. R.: An Extra Large Aperture Scintillometer For Long Range Applications, Boundary Layer Meteorology, 105, 119-127, 10.1023/a:1019600908144, 2002.

Kohsiek, W., Meijninger, W. M. L., Debruin, H. A. R., and Beyrich, F.: Saturation of the Large Aperture Scintillometer, Boundary Layer Meteorology, 121, 111-126, 10.1007/s10546-005-9031-7, 2006.

Kustas, W., and Anderson, M.: Advances in thermal infrared remote sensing for land surface modeling, Agricultural and Forest Meteorology, 149, 2071-2081, 2009.

Kustas, W. P., and Daughtry, C. S. T.: Estimation of the soil heat flux/net radiation ratio from spectral data, Agricultural and Forest Meteorology, 49, 205-223, http://dx.doi.org/10.1016/0168-1923(90)90033-3, 1990.

Kustas, W. P., Daughtry, C. S. T., and Van Oevelen, P. J.: Analytical treatment of the relationships between soil heat flux/net radiation ratio and vegetation indices, Remote Sensing of Environment, 46, 319-330, http://dx.doi.org/10.1016/0034-4257(93)90052-Y, 1993.

Kustas, W. P., and Norman, J. M.: Evaluation of soil and vegetation heat flux predictions using a simple two-source model with radiometric temperatures for partial canopy cover, Agricultural and Forest Meteorology, 94, 13-29, https://doi.org/10.1016/S0168-1923(99)00005-2, 1999.

Lagouarde, J. P., Bonnefond, J. M., Kerr, Y. H., McAneney, K. J., and Irvine, M.: Integrated Sensible Heat Flux Measurements of a Two-Surface Composite Landscape using Scintillometry, Boundary-Layer Meteorology, 105, 5-35, 10.1023/a:1019631428921, 2002a.

Lagouarde, J. P., Jacob, F., Gu, X. F., Olioso, A., Bonnefond, J. M., Kerr, Y., Mcaneney, K. J., and Irvine, M.: Spatialization of sensible heat flux over a heterogeneous landscape, Agronomie-Sciences des Productions Vegetales et de l'Environnement, 22, 627-634, 2002b.

Lagouarde, J. P., Bach, M., Sobrino, J. A., Boulet, G., Briottet, X., Cherchali, S., Coudert, B., Dadou, I., Dedieu, G., and Gamet, P.: The MISTIGRI thermal infrared project: scientific objectives and mission specifications, International journal of remote sensing, 34, 3437-3466, 2013.

Lagouarde, J. P., Irvine, M., and Dupont, S.: Atmospheric turbulence induced errors on measurements of surface temperature from space, Remote Sensing of Environment, 168, 40-53, https://doi.org/10.1016/j.rse.2015.06.018, 2015.

Leclerc, M. Y., and Thurtell, G. W.: Footprint prediction of scalar fluxes using a Markovian analysis, Boundary-Layer Meteorology, 52, 247-258, 10.1007/bf00122089, 1990.

Leduc, C., Calvez, R., Beji, R., Nazoumou, Y., Lacombe, G., and Aouadi, C.: Evolution de la ressource en eau dans la vallée du Merguellil (Tunisie centrale), Séminaire sur la modernisation de l'agriculture irriguée, 2004, 10 p.,

Lhommel, J. P.: Towards a rational definition of potential evaporation, Hydrology and Earth System Sciences Discussions, 1, 257-264, 1997.

Li, Z. L., Tang, R., Wan, Z., Bi, Y., Zhou, C., Tang, B., Yan, G., and Zhang, X.: A review of current methodologies for regional evapotranspiration estimation from remotely sensed data, Sensors, 9, 3801-3853, 2009.

Liou, Y. A., and Kar, S.: Evapotranspiration Estimation with Remote Sensing and Various Surface Energy Balance Algorithms - A Review, Energies, 7, 2821, 2014.

Mis en forme : Anglais (États-Unis)

Ma, Y., Su, Z., Li, Z., Koike, T., and Menenti, M.: Determination of regional net radiation and soil heat flux over a heterogeneous landscape of the Tibetan Plateau, Hydrological Processes, 16, 2963-2971, 2002.

Marx, A., Kunstmann, H., Schüttemeyer, D., and Moene, A. F.: Uncertainty analysis for satellite derived sensible heat fluxes and scintillometer measurements over Savannah environment and comparison to mesoscale meteorological simulation results, Agricultural and Forest Meteorology, 148, 656-667, https://doi.org/10.1016/j.agrformet.2007.11.009, 2008.

Mauser, W., and Schädlich, S.: Modelling the spatial distribution of evapotranspiration on different scales using remote sensing data, Journal of Hydrology, 212, 250-267, 1998.

Meijninger, W. M. L., Hartogensis, O. K., Kohsiek, W., Hoedjes, J. C. B., Zuurbier, R. M., and De Bruin, H. A. R.: Determination of Area-Averaged Sensible Heat Fluxes with a Large Aperture Scintillometer over a Heterogeneous Surface—Flevoland Field Experiment, Boundary-Layer Meteorology, 105, 37-62, 10.1023/a:1019647732027, 2002.

Minacapilli, M., and Ciraolo, G.: Evaluating actual evapotranspiration by means of multi platform remote sensing data: a case study in Sicily, 2007.

Minacapilli, M., Agnese, C., Blanda, F., Cammalleri, C., Ciraolo, G., D'Urso, G., Iovino, M., Pumo, D., Provenzano, G., and Rallo, G.: Estimation of actual evapotranspiration of Mediterranean perennial crops by means of remote-sensing-based surface energy balance models, Hydrology and Earth System Sciences, 13, 1061-1074, 2009.

Mira, M., Olioso, A., Gallego-Elvira, B., Courault, D., Garrigues, S., Marloie, O., Hagolle, O., Guillevic, P., and Boulet, G.: Uncertainty assessment of surface net radiation derived from Landsat images, Remote Sensing of Environment, 175, 251-270, 2016.

Moene, A. F., Meijninger, W., Kohsiek, W., Gioli, B., Miglietta, F., and Bosveld, F.: Validation of fluxes of an extra-large aperture scintillometer at Cabauw using sky-arrow aircraft flux measurements, Proceedings of 17th symposium on boundary layers and turbulence. American Meteorological Society, San Diego, CA, 2006, 22-25,

Mougenot, B., Touhami, N., Lili Chabaane, Z., Boulet, G., Simonneaux, V., and Zribi, M.: Trees detection for water resources management in irrigated and rainfed arid and semi arid agricultural areas, Pléiades Days, Toulouse, April 1-3, 2014, 2014.

Mutziger, A. J., Burt, C. M., Howes, D. J., and Allen, R. G.: Comparison of measured and FAO-56 modeled evaporation from bare soil, Journal of irrigation and drainage engineering, 131, 59-72, 2005.

Nichols, W. E., and Cuenca, R. H.: Evaluation of the evaporative fraction for parameterization of the surface energy balance, Water Resources Research, 29, 3681-3690, 10.1029/93wr01958, 1993.

Odi-Lara, M., Campos, I., Neale, C., Ortega-Farías, S., Poblete-Echeverría, C., Balbontín, C., and Calera, A.: Estimating Evapotranspiration of an Apple Orchard Using a Remote Sensing-Based Soil Water Balance, Remote Sensing, 8, 253, 2016.

Oki, T., and Kanae, S.: Global Hydrological Cycles and World Water Resources, Science, 313, 1068-1072, 10.1126/science.1128845, 2006.

Payero, J. O., Neale, C. M. U., and Wright, J. L.: Estimating Diurnal Variation of Soil Heat Flux for Alfalfa and Grass, Proceedings of the 2001 ASAE Annual Meeting Sacramento, California, 10.13031/2013.5546, 2001.

Peng, J., Liu, Q., Wang, L., Liu, Q., Fan, W., Lu, M., and Wen, J.: Characterizing the Pixel Footprint of Satellite Albedo Products Derived from MODIS Reflectance in the Heihe River Basin, China, Remote Sensing, 7, 6886, 2015.

Pereira, L. S., Oweis, T., and Zairi, A.: Irrigation management under water scarcity, Agricultural water management, 57, 175-206, 2002.

Poussin, J. C., Imache, A., Beji, R., Le Grusse, P., and Benmihoub, A.: Exploring regional irrigation water demand using typologies of farms and production units: An example from Tunisia, Agricultural Water Management, 95, 973-983, https://doi.org/10.1016/j.agwat.2008.04.001, 2008.

Pradelcix, L., Roux, P., Bouarfa, S., Jaouani, B., Lili-Chabaane, Z., and Bellon-Maurel, V.: Environmental Impacts of Contrasted Groundwater Pumping Systems Assessed by Life Cycle Assessment Methodology: Contribution to the Water Energy Nexus Study, Irrigation and Drainage, 64, 124-138, 2015.

Raupach, M. R.: Simplified expressions for vegetation roughness length and zero-plane displacement as functions of canopy height and area index, Boundary Layer Meteorology, 71, 211-216, 10.1007/bf00709229, 1994.

Saadi, S., Simonneaux, V., Boulet, G., Raimbault, B., Mougenot, B., Fanise, P., Ayari, H., and Lili Chabaane, Z.: Monitoring Irrigation Consumption Using High Resolution NDVI Image Time Series: Calibration and Validation in the Kairouan Plain (Tunisia), Remote Sensing, 7, 13005, 2015.

Samain, B., Simons, G. W., Voogt, M. P., Defloor, W., Bink, N. J., and Pauwels, V.: Consistency between hydrological model, large aperture scintillometer and remote sensing based evapotranspiration estimates for a heterogeneous catchment, Hydrology and Earth System Sciences, 16, 2095-2107, 2012.

Schmid, H. P.: Footprint modeling for vegetation atmosphere exchange studies: a review and perspective, Agricultural and Forest Meteorology, 113, 159-183, https://doi.org/10.1016/S0168-1923(02)00107-7, 2002.

Shuttleworth, W. J., Gurney, R. J., Hsu, A. Y., and Ormsby, J. P.: FIFE: The Variation in Energy Partition at Surface Flux Sites, 1989.

Shuttleworth, W. J., and Gurney, R. J.: The theoretical relationship between foliage temperature and canopy resistance in sparse crops, Quarterly Journal of the Royal Meteorological Society, 116, 497-519, 1990.

Solignac, P. A., Brut, A., Selves, J. L., Béteille, J. P., Gastellu-Etchegorry, J. P., Keravec, P., Béziat, P., and Ceschia, E.: Uncertainty analysis of computational methods for deriving sensible heat flux values from scintillometer measurements, Atmos. Meas. Tech., 2, 741-753, 10.5194/amt-2-741-2009, 2009.

Su, Z.: The Surface Energy Balance System (SEBS) for estimation of turbulent heat fluxes, Hydrology and Earth System Sciences Discussions, 6, 85-100, 2002.

Torres, E. A., and Calera, A.: Bare soil evaporation under high evaporation demand: a proposed modification to the FAO-56 model, Hydrological Sciences Journal-Journal des Sciences Hydrologiques, 55, 303-315, 2010.

Touhami, N.: Détection des arbres par imagerie Très Haute Résolution Spatiale sur la plaine de Kairouan Engineer, Institut National Agronomqiue de Tunisie, Tunis, 78 pp., 2013.

Tucker, C. J.: A comparison of satellite sensor bands for vegetation monitoring, 1978.

Mis en forme : Anglais (États-Unis)

~~Twine, T. E., Kustas, W., Norman, J., Cook, D., Houser, P., Meyers, T., Prueger, J., Starks, P., and Wesely, M.: Correcting eddy-covariance flux underestimates over a grassland, Agricultural and Forest Meteorology, 103, 279-300, 2000.~~

~~Van Niel, T. G., McVicar, T. R., Roderick, M. L., van Dijk, A. I. J. M., Renzullo, L. J., and van Gorsel, E.: Correcting for systematic error in satellite-derived latent heat flux due to assumptions in temporal scaling: Assessment from flux tower observations, Journal of Hydrology, 409, 140-148, https://doi.org/10.1016/j.jhydrol.2011.08.011, 2011.~~

~~Wang, T. i., Ochs, G. R., and Clifford, S. F.: A saturation-resistant optical scintillometer to measure Cn2†, Journal of the Optical Society of America, 68, 334-338, 10.1364/josa.68.000334, 1978.~~

~~Watts, C. J., Chehbouni, A., Rodriguez, J. C., Kerr, Y. H., Hartogensis, O., and de Bruin, H. A. R.: Comparison of sensible heat flux estimates using AVHRR with scintillometer measurements over semi-arid grassland in northwest Mexico, Agricultural and Forest Meteorology, 105, 81-89, http://doi.org/10.1016/S0168-1923(00)00188-X, 2000.~~

~~Xie, Y., Sha, Z., and Yu, M.: Remote sensing imagery in vegetation mapping: a review, Journal of Plant Ecology, 1, 9-23, 2008.~~

~~Zribi, M., Chahbi, A., Shabou, M., Lili-Chabaane, Z., Duchemin, B., Baghdadi, N., Amri, R., and Chehbouni, A.: Soil surface moisture estimation over a semi-arid region using ENVISAT ASAR radar data for soil evaporation evaluation, Hydrology and Earth System Sciences Discussions, 15, 345-358, 2011.~~

Allen, R. G., Pereira, L. S., Raes, D., and Smith, M.: Crop evapotranspiration-Guidelines for computing crop water requirements-FAO Irrigation and drainage paper 56, FAO, Rome, 300, D05109, 1998.

Allen, R., Irmak, A., Trezza, R., Hendrickx, J. M., Bastiaanssen, W., and Kjaersgaard, J.: Satellite-based ET estimation in agriculture using SEBAL and METRIC, Hydrological Processes, 25, 4011-4027, 2011.

Amri, R., Zribi, M., Lili-Chabaane, Z., Szczypta, C., Calvet, J. C., and Boulet, G.: FAO-56 dual model combined with multi-sensor remote sensing for regional evapotranspiration estimations, Remote Sensing, 6, 5387-5406, 2014.

Anderson, M. C., Kustas, W. P., Norman, J. M., Hain, C. R., Mecikalski, J. R., Schultz, L., González-Dugo, M. P., Cammalleri, C., d'Urso, G., Pimstein, A., and Gao, F.: Mapping daily evapotranspiration at field to continental scales using geostationary and polar orbiting satellite imagery, Hydrol. Earth Syst. Sci., 15, 223-239, 10.5194/hess-15-223-2011, 2011.

Anderson, M., Norman, J., Diak, G., Kustas, W., and Mecikalski, J.: A two-source time-integrated model for estimating surface fluxes using thermal infrared remote sensing, Remote sensing of environment, 60, 195-216, 1997.

Andreas, E. L.: Atmospheric stability from scintillation measurements, Applied optics, 27, 2241-2246, 1988.

Bai, J., Jia, L., Liu, S., Xu, Z., Hu, G., Zhu, M., and Song, L.: Characterizing the footprint of eddy covariance system and large aperture scintillometer measurements to validate satellite-based surface fluxes, IEEE Geoscience and Remote Sensing Letters, 12, 943-947, 2015.

Bastiaanssen, W. G. M., Allen, R. G., Droogers, P., D'Urso, G., and Steduto, P.: Twenty-five years modeling irrigated and drained soils: State of the art, Agricultural Water Management, 92, 111-125, http://dx.doi.org/10.1016/j.agwat.2007.05.013, 2007.

Bastiaanssen, W. G. M.: Regionalization of surface flux densities and moisture indicators in composite terrain; a remote sensing approach under clear skies in mediterranean climates, SC-DLO, Wageningen, 1995.

Boulet, G., Braud, I., and Vauclin, M.: Study of the mechanisms of evaporation under arid conditions using a detailed model of the soil–atmosphere continuum. Application to the EFEDA I experiment, Journal of Hydrology, 193, 114-141, https://doi.org/10.1016/S0022-1694(96)03148-4, 1997.

Boulet, G., Chehbouni, A., Gentine, P., Duchemin, B., Ezzahar, J., and Hadria, R.: Monitoring water stress using time series of observed to unstressed surface temperature difference, Agricultural and Forest Meteorology, 146, 159-172, https://doi.org/10.1016/j.agrformet.2007.05.012, 2007.

Boulet, G., Mougenot, B., Lhomme, J. P., Fanise, P., Lili-Chabaane, Z., Olioso, A., Bahir, M., Rivalland, V., Jarlan, L., Merlin, O., Coudert, B., Er-Raki, S., and Lagouarde, J. P.: The SPARSE model for the prediction of water stress and evapotranspiration components from thermal infra-red data and its evaluation over irrigated and rainfed wheat, Hydrol. Earth Syst. Sci., 19, 4653-4672, 10.5194/hess-19-4653-2015, 2015.

Bounoua, L., Zhang, P., Thome, K., Masek, J., Safia, A., Imhoff, M. L., and Wolfe, R. E.: Mapping Biophysical Parameters for Land Surface Modeling over the Continental US Using MODIS and Landsat, Dataset Papers in Science, 2015, 11, 10.1155/2015/564279, 2015.

Braud, I., Dantas-Antonino, A. C., Vauclin, M., Thony, J. L., and Ruelle, P.: A simple soil-plant-atmosphere transfer model (SiSPAT) development and field verification, Journal of Hydrology, 166, 213-250, http://dx.doi.org/10.1016/0022-1694(94)05085-C, 1995.

Brunsell, N. A., Ham, J. M., and Arnold, K. A.: Validating remotely sensed land surface fluxes in heterogeneous terrain with large aperture scintillometry, International Journal of Remote Sensing, 32, 6295-6314, 10.1080/01431161.2010.508058, 2011.

Brutsaert, W., and Sugita, M.: Application of self-preservation in the diurnal evolution of the surface energy budget to determine daily evaporation, Journal of Geophysical Research: Atmospheres, 97, 18377-18382, 1992.

Calera, A., Campos, I., Osann, A., D'Urso, G., and Menenti, M.: Remote Sensing for Crop Water Management: From ET Modelling to Services for the End Users, Sensors, 17, 1104, 2017.

Chahbi, A., Zribi, M., Saadi, S., Simonneaux, V., Lili Chabaane, Z. : Classification et caractérisation de la couverture végétale dans un milieu semi aride en utilisant des images SPOT 5, Deuxième Workshop AMETHYST, 11 Février 2016, Marrakech, Maroc, 2016,

Chávez, J., Neale, C. M. U., Hipps, L. E., Prueger, J. H., and Kustas, W. P.: Comparing Aircraft-Based Remotely Sensed Energy Balance Fluxes with Eddy Covariance Tower Data Using Heat Flux Source Area Functions, Journal of Hydrometeorology, 6, 923-940, 10.1175/jhm467.1, 2005.

Chirouze, J., Boulet, G., Jarlan, L., Fieuzal, R., Rodriguez, J. C., Ezzahar, J., Er-Raki, S., Bigeard, G., Merlin, O., Garatuza-Payan, J., Watts, C., and Chehbouni, G.: Intercomparison of four remote-sensing-based energy balance methods to retrieve surface evapotranspiration and water stress of irrigated fields in semi-arid climate, Hydrol. Earth Syst. Sci., 18, 1165-1188, 10.5194/hess-18-1165-2014, 2014.

Choudhury, B. J., Idso, S. B., and Reginato, R. J.: Analysis of an empirical model for soil heat flux under a growing wheat crop for estimating evaporation by an infrared-temperature based energy balance equation, Agricultural and Forest Meteorology, 39, 283-297, http://dx.doi.org/10.1016/0168-1923(87)90021-9, 1987.

Choudhury, B., and Monteith, J.: A four-layer model for the heat budget of homogeneous land surfaces, Quarterly Journal of the Royal Meteorological Society, 114, 373-398, 1988.

Clevers, J. G. P. W.: Application of a weighted infrared-red vegetation index for estimating leaf Area Index by Correcting for Soil Moisture, Remote Sensing of Environment, 29, 25-37, http://dx.doi.org/10.1016/0034-4257(89)90076-X, 1989.

Clothier, B., Clawson, K., Pinter, P., Moran, M., Reginato, R. J., and Jackson, R.: Estimation of soil heat flux from net radiation during the growth of alfalfa, agricultural and forest meteorology, 37, 319-329, 1986.

Danelichen, V. H. d. M., Biudes, M. S., Souza, M. C., Machado, N. G., Silva, B. B. d., and Nogueira, J. d. S.: Estimation of soil heat flux in a neotropical Wetland region using remote sensing techniques, Revista Brasileira de Meteorologia, 29, 469-482, 2014.

Delogu, E., Boulet, G., Olioso, A., Coudert, B., Chirouze, J., Ceschia, E., Le Dantec, V., Marloie, O., Chehbouni, G., and Lagouarde, J. P.: Reconstruction of temporal variations of evapotranspiration using

instantaneous estimates at the time of satellite overpass, Hydrol. Earth Syst. Sci., 16, 2995-3010, 10.5194/hess-16-2995-2012, 2012.

Etchanchu, J., Rivalland, V., Gascoin, S., Cros, J., Brut, A., and Boulet, G.: Effects of multi-temporal high-resolution remote sensing products on simulated hydrometeorological variables in a cultivated area (southwestern France), Hydrol. Earth Syst. Sci. Discuss., 2017, 1-23, 10.5194/hess-2016-661, 2017.

Feddes, R. A., Kowalik, P. J., and Zaradny, H.: Simulation of Field Water Use and Crop Yield, Wiley, 1978.

Frehlich, R. G., and Ochs, G. R.: Effects of saturation on the optical scintillometer, Applied optics, 29, 548-553, 1990.

Giorgi, F., and Avissar, R.: Representation of heterogeneity effects in earth system modeling: Experience from land surface modeling, Reviews of Geophysics, 35, 413-437, 1997.

Giorgi, F., and Lionello, P.: Climate change projections for the Mediterranean region, Global and planetary change, 63, 90-104, 2008.

Glenn, E. P., Huete, A. R., Nagler, P. L., Hirschboeck, K. K., and Brown, P.: Integrating remote sensing and ground methods to estimate evapotranspiration, Critical Reviews in Plant Sciences, 26, 139-168, 2007.

Green, A. E., and Hayashi, Y.: Use of the scintillometer technique over a rice paddy, Journal of Agricultural Meteorology, 54, 225-234, 1998.

Gurney, R., and Hsu, A.: Relating evaporative fraction to remotely sensed data at the FIFE site, 1990.

Hain, C. R., Mecikalski, J. R., and Anderson, M. C.: Retrieval of an Available Water-Based Soil Moisture Proxy from Thermal Infrared Remote Sensing. Part I: Methodology and Validation, Journal of Hydrometeorology, 10, 665-683, 10.1175/2008jhm1024.1, 2009.

Hartogensis, O. K., Watts, C. J., Rodriguez, J.-C., and Bruin, H. A. R. D.: Derivation of an Effective Height for Scintillometers: La Poza Experiment in Northwest Mexico, Journal of Hydrometeorology, 4, 915-928, 10.1175/1525-7541(2003)004<0915:doaehf>2.0.co;2, 2003.

Hemakumara, H. M., Chandrapala, L., and Moene, A. F.: Evapotranspiration fluxes over mixed vegetation areas measured from large aperture scintillometer, Agricultural Water Management, 58, 109-122, http://doi.org/10.1016/S0378-3774(02)00131-2, 2003.

Horst, T., and Weil, J.: Footprint estimation for scalar flux measurements in the atmospheric surface layer, Boundary-Layer Meteorology, 59, 279-296, 1992.

Hunink, J., Eekhout, J., Vente, J., Contreras, S., Droogers, P., and Baille, A.: Hydrological Modelling using Satellite-Based Crop Coefficients: A Comparison of Methods at the Basin Scale, Remote Sensing, 9, 174, 2017.

Jackson, R. D., Moran, M. S., Gay, L. W., and Raymond, L. H.: Evaluating evaporation from field crops using airborne radiometry and ground-based meteorological data, Irrigation Science, 8, 81-90, 10.1007/bf00259473, 1987.

Kalma, J. D., McVicar, T. R., and McCabe, M. F.: Estimating land surface evaporation: A review of methods using remotely sensed surface temperature data, Surveys in Geophysics, 29, 421-469, 2008.

Kohsiek, W., Meijninger, W. M. L., Moene, A. F., Heusinkveld, B. G., Hartogensis, O. K., Hillen, W. C. A. M., and De Bruin, H. A. R.: An Extra Large Aperture Scintillometer For Long Range Applications, Boundary-Layer Meteorology, 105, 119-127, 10.1023/a:1019600908144, 2002.

Kroes, J. G., J.C. van Dam, R.P. Bartholomeus, P. Groenendijk, M. Heinen, R.F.A. Hendriks, H.M. Mulder, I. Supit, P.E.V. van Walsum: SWAP version 4; Theory description and user manual. Report 2780. Wageningen, Wageningen Environmental Research.Available at: http://library.wur.nl/WebQuery/wurpubs/fulltext/416321, 2017.

Kustas, W. P., and Daughtry, C. S. T.: Estimation of the soil heat flux/net radiation ratio from spectral data, Agricultural and Forest Meteorology, 49, 205-223, http://dx.doi.org/10.1016/0168-1923(90)90033-3, 1990.

Kustas, W. P., and Norman, J. M.: Evaluation of soil and vegetation heat flux predictions using a simple two-source model with radiometric temperatures for partial canopy cover, Agricultural and Forest Meteorology, 94, 13-29, https://doi.org/10.1016/S0168-1923(99)00005-2, 1999.

Kustas, W. P., Daughtry, C. S. T., and Van Oevelen, P. J.: Analytical treatment of the relationships between soil heat flux/net radiation ratio and vegetation indices, Remote Sensing of Environment, 46, 319-330, http://dx.doi.org/10.1016/0034-4257(93)90052-Y, 1993.

Kustas, W., and Anderson, M.: Advances in thermal infrared remote sensing for land surface modeling, Agricultural and Forest Meteorology, 149, 2071-2081, 2009.

Lagouarde, J.-P., Bach, M., Sobrino, J. A., Boulet, G., Briottet, X., Cherchali, S., Coudert, B., Dadou, I., Dedieu, G., and Gamet, P.: The MISTIGRI thermal infrared project: scientific objectives and mission specifications, International journal of remote sensing, 34, 3437-3466, 2013.

Lagouarde, J.-P., Irvine, M., and Dupont, S.: Atmospheric turbulence induced errors on measurements of surface temperature from space, Remote Sensing of Environment, 168, 40-53, https://doi.org/10.1016/j.rse.2015.06.018, 2015.

Lagouarde, J.-P., Jacob, F., Gu, X. F., Olioso, A., Bonnefond, J.-M., Kerr, Y., Mcaneney, K. J., and Irvine, M.: Spatialization of sensible heat flux over a heterogeneous landscape, Agronomie-Sciences des Productions Vegetales et de l'Environnement, 22, 627-634, 2002.

LAS and X-LAS instruction manual: http://www.kippzonen.fr/Download/244/LAS-and-X-LAS-Scintillometers-Manual?ShowInfo=true, access: 7th December, 2007.

Leclerc, M. Y., and Thurtell, G. W.: Footprint prediction of scalar fluxes using a Markovian analysis, Boundary-Layer Meteorology, 52, 247-258, 10.1007/bf00122089, 1990.

Leduc, C., Calvez, R., Beji, R., Nazoumou, Y., Lacombe, G., and Aouadi, C.: Evolution de la ressource en eau dans la vallée du Merguellil (Tunisie centrale), Séminaire sur la modernisation de l'agriculture irriguée, 2004, 10 p.,

Li, Z.-L., Tang, R., Wan, Z., Bi, Y., Zhou, C., Tang, B., Yan, G., and Zhang, X.: A review of current methodologies for regional evapotranspiration estimation from remotely sensed data, Sensors, 9, 3801-3853, 2009.

Liou, Y.-A., and Kar, S.: Evapotranspiration Estimation with Remote Sensing and Various Surface Energy Balance Algorithms—A Review, Energies, 7, 2821, 2014.

Marx, A., Kunstmann, H., Schüttemeyer, D., and Moene, A. F.: Uncertainty analysis for satellite derived sensible heat fluxes and scintillometer measurements over Savannah environment and comparison to mesoscale meteorological simulation results, Agricultural and Forest Meteorology, 148, 656-667, https://doi.org/10.1016/j.agrformet.2007.11.009, 2008.

Mauser, W., and Schädlich, S.: Modelling the spatial distribution of evapotranspiration on different scales using remote sensing data, Journal of Hydrology, 212, 250-267, 1998.

Meijninger, W. M. L., Hartogensis, O. K., Kohsiek, W., Hoedjes, J. C. B., Zuurbier, R. M., and De Bruin, H. A. R.: Determination of Area-Averaged Sensible Heat Fluxes with a Large Aperture Scintillometer over a Heterogeneous Surface – Flevoland Field Experiment, Boundary-Layer Meteorology, 105, 37-62, 10.1023/a:1019647732027, 2002.

Minacapilli, M., Agnese, C., Blanda, F., Cammalleri, C., Ciraolo, G., D'Urso, G., Iovino, M., Pumo, D., Provenzano, G., and Rallo, G.: Estimation of actual evapotranspiration of Mediterranean perennial crops by means of remote-sensing based surface energy balance models, Hydrology and Earth System Sciences, 13, 1061-1074, 2009.

Minacapilli, M., Ciraolo, G., D Urso, G., and Cammalleri, C.: Evaluating actual evapotranspiration by means of multi-platform remote sensing data: a case study in Sicily, IAHS PUBLICATION, 316, 207., 2007.

Moene, A. F., Meijninger, W., Kohsiek, W., Gioli, B., Miglietta, F., and Bosveld, F.: Validation of fluxes of an extra large aperture scintillometer at Cabauw using sky arrow aircraft flux measurements, Proceedings of 17th symposium on boundary layers and turbulence. American Meteorological Society, San Diego, CA, 2006, 22-25,

Monin, A., and Obukhov, A.: Basic laws of turbulent mixing in the surface layer of the atmosphere, Contrib. Geophys. Inst. Acad. Sci. USSR, 151, e187, 1954.

Mougenot, B., Touhami, N., Lili Chabaane, Z., Boulet, G., Simonneaux, V., and Zribi, M.: Trees detection for water resources management in irrigated and rainfed arid and semi-arid agricultural areas, Pléiades Days, Toulouse, April 1-3, 2014, 2014.

Mutziger, A. J., Burt, C. M., Howes, D. J., and Allen, R. G.: Comparison of measured and FAO-56 modeled evaporation from bare soil, Journal of irrigation and drainage engineering, 131, 59-72, 2005.

Odi-Lara, M., Campos, I., Neale, C., Ortega-Farías, S., Poblete-Echeverría, C., Balbontín, C., and Calera, A.: Estimating Evapotranspiration of an Apple Orchard Using a Remote Sensing-Based Soil Water Balance, Remote Sensing, 8, 253, 2016.

Oki, T., and Kanae, S.: Global Hydrological Cycles and World Water Resources, Science, 313, 1068-1072, 10.1126/science.1128845, 2006.

Pereira, L. S., Oweis, T., and Zairi, A.: Irrigation management under water scarcity, Agricultural water management, 57, 175-206, 2002.

Poussin, J. C., Imache, A., Beji, R., Le Grusse, P., and Benmihoub, A.: Exploring regional irrigation water demand using typologies of farms and production units: An example from Tunisia, Agricultural Water Management, 95, 973-983, https://doi.org/10.1016/j.agwat.2008.04.001, 2008.

Pradeleix, L., Roux, P., Bouarfa, S., Jaouani, B., Lili-Chabaane, Z., and Bellon-Maurel, V.: Environmental Impacts of Contrasted Groundwater Pumping Systems Assessed by Life Cycle Assessment Methodology: Contribution to the Water–Energy Nexus Study, Irrigation and Drainage, 64, 124-138, 2015.

Raupach, M. R.: Simplified expressions for vegetation roughness length and zero-plane displacement as functions of canopy height and area index, Boundary-Layer Meteorology, 71, 211-216, 10.1007/bf00709229, 1994.

Saadi, S., Simonneaux, V., Boulet, G., Raimbault, B., Mougenot, B., Fanise, P., Ayari, H., and Lili-Chabaane, Z.: Monitoring Irrigation Consumption Using High Resolution NDVI Image Time Series: Calibration and Validation in the Kairouan Plain (Tunisia), Remote Sensing, 7, 13005, 2015.

Samain, B., Simons, G. W., Voogt, M. P., Defloor, W., Bink, N.-J., and Pauwels, V.: Consistency between hydrological model, large aperture scintillometer and remote sensing based evapotranspiration estimates for a heterogeneous catchment, Hydrology and Earth System Sciences, 16, 2095-2107, 2012.

Santanello Jr, J. A., and Friedl, M. A.: Diurnal covariation in soil heat flux and net radiation, Journal of Applied Meteorology, 42, 851-862, 2003.

Shuttleworth, W. J., and Gurney, R. J.: The theoretical relationship between foliage temperature and canopy resistance in sparse crops, Quarterly Journal of the Royal Meteorological Society, 116, 497-519, 1990.

Simonneaux, V., Lepage, M., Helson, D., Metral, J., Thomas, S., Duchemin, B., Cherkaoui, M., Kharrou, H., Berjami, B., and Chehbouni, A.: Estimation spatialisée de l'évapotranspiration des cultures irriguées par télédétection: application à la gestion de l'irrigation dans la plaine du Haouz (Marrakech, Maroc), Science et changements planétaires/Sécheresse, 20, 123-130, 2009.

Solignac, P. A., Brut, A., Selves, J. L., Béteille, J. P., Gastellu-Etchegorry, J. P., Keravec, P., Béziat, P., and Ceschia, E.: Uncertainty analysis of computational methods for deriving sensible heat flux values from scintillometer measurements, Atmos. Meas. Tech., 2, 741-753, 10.5194/amt-2-741-2009, 2009.

Steduto, P., Hsiao, T. C., Raes, D., and Fereres, E.: AquaCrop—The FAO crop model to simulate yield response to water: I. Concepts and underlying principles, Agronomy Journal, 101, 426-437, 2009.

Stöckle, C. O., Donatelli, M., and Nelson, R.: CropSyst, a cropping systems simulation model, European journal of agronomy, 18, 289-307, 2003.

Su, Z.: The Surface Energy Balance System (SEBS) for estimation of turbulent heat fluxes, Hydrology and Earth System Sciences Discussions, 6, 85-100, 2002.

Sugita, M., and Brutsaert, W.: Regional surface fluxes from remotely sensed skin temperature and lower boundary layer measurements, Water Resources Research, 26, 2937-2944, 1990.

Tasumi, M., Trezza, R., Allen, R. G., and Wright, J. L.: Operational aspects of satellite-based energy balance models for irrigated crops in the semi-arid US, Irrigation and Drainage Systems, 19, 355-376, 2005.

Tatarskii, V. I.: Wave propagation in turbulent medium, Wave Propagation in Turbulent Medium, by Valerian Ilich Tatarskii. Translated by RA Silverman. 285pp. Published by McGraw-Hill, 1961., 1961.

Torres, E. A., and Calera, A.: Bare soil evaporation under high evaporation demand: a proposed modification to the FAO-56 model, Hydrological Sciences Journal–Journal des Sciences Hydrologiques, 55, 303-315, 2010.

Touhami, N.: Détection des arbres par imagerie Très Haute Résolution Spatiale sur la plaine de Kairouan Engineer, Institut National Agronomqiue de Tunisie, Tunis, 78 pp., 2013.

Tucker, C. J.: A comparison of satellite sensor bands for vegetation monitoring, 1978.

Twine, T. E., Kustas, W., Norman, J., Cook, D., Houser, P., Meyers, T., Prueger, J., Starks, P., and Wesely, M.: Correcting eddy-covariance flux underestimates over a grassland, Agricultural and Forest Meteorology, 103, 279-300, 2000.

Ventura, F., Spano, D., Duce, P., and Snyder, R.: An evaluation of common evapotranspiration equations, Irrigation Science, 18, 163-170, 1999.

Xie, Y., Sha, Z., and Yu, M.: Remote sensing imagery in vegetation mapping: a review, Journal of Plant Ecology, 1, 9-23, 2008.

Zribi, M., Chahbi, A., Shabou, M., Lili-Chabaane, Z., Duchemin, B., Baghdadi, N., Amri, R., and Chehbouni, A.: Soil surface moisture estimation over a semi-arid region using ENVISAT ASAR radar data for soil evaporation evaluation, Hydrology and Earth System Sciences Discussions, 15, 345-358, 2011.

**Mis en forme :** Police :+Titres, 10 pt, Non Gras

**Mis en forme :** Espace Avant : 6 pt, Après : 6 pt